

**Diaphanous-related formins: characterization of mouse
mDia1, and ForA/dDia3
from *Dictyostelium discoideum* amoebae**

**Dissertation
der Fakultät für Biologie der
Ludwig-Maximilians-Universität
München**

vorgelegt von

Nagendran Ramalingam

München, August 2009

Ehrenwörtliche Versicherung

Diese Dissertation wurde selbständig und ohne unerlaubte Hilfsmittel angefertigt.

München, August 2009

Nagendran Ramalingam

Erstgutachter: Prof. Dr. Michael Schleicher

Zweitgutachter: Prof. Dr. Dirk Eick

Eingereicht am: 12.08.2009

Tag der mündlichen Prüfung: 29.09.2009

Meeting abstracts:

Ramalingam, N., Breitsprecher, D., Faix, J. and Schleicher, M. (2008) Differential regulation of mDia formins by phospholipids. The American Society for Cell Biology, San Francisco, USA, *Mol. Biol. Cell*, **19 (suppl)**, S-L94.

Ramalingam, N., Rohlfs, M., Faix, J. and Schleicher, M. (2007) ForA regulates the integrity of the cortical actin cytoskeleton. The American Society for Cell Biology, Washington DC, USA, *Mol. Biol. Cell*, **18 (suppl)**, 418, B353.

Ramalingam, N., Rohlfs, M., Faix, J. and Schleicher, M. (2007) ForA is a Diaphanous-related formin required for directed cell motility in *Dictyostelium discoideum*. The American Society for Cell Biology, Dijon, France, *Dynamic interplay between cytoskeletal and membrane systems*, **Abstract: 17**.

Ramalingam, N., Faix, J. and Schleicher, M. (2006) ForA is a Diaphanous-related formin required for phototaxis and normal development of *Dictyostelium* cells. The American Society for Cell Biology, San Diego, USA, *Mol. Biol. Cell*, **17 (suppl)**, 839, B102.

Ramalingam, N., Schleicher, M. and Faix, J. (2005) dDia3 is a membrane-associated Diaphanous-related formin involved in growth of *Dictyostelium discoideum* cells. German Society for Cell Biology, Heidelberg, Germany, *Eur. J. Cell Biol*, **84S1 (suppl. 55)**, S4-7.

Publications:

Joseph, J.M., Fey, P., Ramalingam, N., Liu, X.I., Rohlfs, M., Noegel, A.A., Mueller-Taubenberger, A., Gloeckner, G. and Schleicher, M. (2008) The actinome of *Dictyostelium discoideum* in comparison to actins and actin-related protein from other organisms. *PLoS One*, **3**, e2654.

Arasada, R., Son, H., Ramalingam, N., Eichinger, L., Schleicher, M., Rohlfs, M. (2006) Characterization of the Ste20-like kinase Krs1 of *Dictyostelium discoideum*. *Eur J Cell Biol*, **85**, 1059-68.

The experimental parts of the work presented here were carried out in the laboratory of Prof. Dr. Michael Schleicher from November 2003 to May 2009 at the Institute for Cell Biology, Ludwig-Maximilians-University, Munich.

Table of contents

Summary.....	1
Zusammenfassung.....	3
1 Introduction.....	5
1.1 The actin cytoskeleton	5
1.2 Actin-binding proteins	7
1.3 Formins	9
1.4 <i>Dictyostelium discoideum</i> as a model system.....	11
1.5 Goals of the thesis.....	13
2 Materials and Methods.....	14
2.1 Materials	14
2.1.1 Computer programs	14
2.1.2 Instruments.....	15
2.1.3 Reagents.....	15
2.1.4 Media	17
2.1.5 Bacterial strains and <i>D. discoideum</i> cell lines	17
2.1.6 Parental and recombinant plasmids	18
2.2 Methods.....	21
2.2.1 Molecular biology.....	21
2.2.2 Biochemistry	21
2.2.3 Cell biology methods	26
2.2.4 Yeast-two hybrid assay.....	27
3 Results.....	30
3.1 Characterization of the mDia1-phospholipid interaction.....	30
3.1.1 mDia1 is a Diaphanous-related formin (DRF) from <i>Mus musculus</i>	30
3.1.2 Domain structure of mDia1	30
3.1.3 BR is the N-terminal phospholipid-binding region in mDia1	30
3.1.4 BR alone is sufficient for phospholipid interaction	32
3.1.5 The first two poly-basic clusters are important for lipid-binding.....	33
3.1.6 The N-terminal BR interacts specifically with PS.....	33
3.1.7 mDia1 N-terminus clusters PS and PIP ₂	35

3.1.8	mDia1 N-terminus inserts into the plasma membrane.....	36
3.1.9	BR is essential for plasma membrane targeting of mDia1	37
3.1.10	PIP ₂ -BR interaction does not influence the activity of mDia1	40
3.1.11	PIP ₂ negatively regulates the activity of mDia1	41
3.1.12	Potential phospholipid-binding sites at the C-termini of formins.....	46
3.1.13	DAD relieves the PIP ₂ -mediated inhibition of mDia1 activity.....	46
3.1.14	mDia1FH1FH2DAD is inhibited also by unilamellar PIP ₂ vesicles	47
3.1.15	The C-terminal region of mDia1 harbors at least two PIP ₂ -binding sites.....	49
3.1.16	mDia1FH1FH2DAD clusters PIP ₂ and inserts into the plasma membrane.....	51
3.2	Characterization of ForA	53
3.2.1	Formins from <i>D. discoideum</i>	53
3.2.2	Domain architecture of ForA	55
3.2.3	ForA interaction with actin	56
3.2.4	ForA interacts with profilin I	57
3.2.5	Generation of a ForA null mutant.....	58
3.2.6	ForA null mutant development is largely unaffected	59
3.2.7	ForA is essential for directed cell migration of slugs during phototaxis.	60
3.2.8	ForA null mutant cells show reduced random motility	63
3.2.9	ForA null mutant cells are prone to membrane blebbing	63
3.2.10	ForA induced blebbing is myosin II dependent.....	66
3.2.11	Subcellular localization of GFP-ForA and GFP-ForAΔC2	68
3.2.12	Subcellular localization of constitutively active ForA.....	68
3.2.13	The C2 domain is also not required for localizing constitutively active ForA..	71
3.2.14	GBD-FH3 harbors the localization signal.....	72
3.2.15	GFP-ForA N-terminus overexpression leads to an altered phenotype	74
3.2.16	ForA localization is myosin II independent.....	74
3.2.17	Putative binding partners of ForA.....	75
3.3	Characterization of dDia3	77
3.3.1	dDia3 is a DRF from <i>Dictyostelium discoideum</i>	77
3.3.2	Recombinant dDia3 nucleates and caps actin filaments	79
3.3.3	dDia3 interacts with all three profilin isoforms	79

3.3.4	Characterization of dDia3 null mutant cells	80
3.3.5	Subcellular localization of GFP-dDia3	80
3.3.6	Subcellular localization of constitutively active dDia3	82
4	Discussion	83
4.1	mDia1	83
4.2	ForA	87
5	References	90
6	List of figures	100
7	Abbreviations	102
	Acknowledgements	103
	Curriculum Vitae	104

Summary

Dynamics in the non-muscle actin cytoskeleton are well controlled by an array of actin-binding proteins. Especially an efficient appearance of newly formed microfilaments is an essential feature for numerous cellular activities, including cell migration, cytokinesis, phagocytosis and others. The two major classes of ubiquitous proteins that nucleate actin polymerization are specific actin-related proteins (Arp2/3) and formins. The multi-domain and tightly regulated formins (Diaphanous-related formins, 'DRF') not only nucleate linear actin filaments de novo, but stay associated with the fast growing end while allowing the insertional incorporation of actin monomers. Binding of GTP bound Rho GTPases to the GTPase-binding domain (GBD) triggers the activation of formin by disrupting an intra-molecular hairpin interaction. Although in recent years this regulation was plausibly explained, the molecular principles for e.g. the interaction with membranes, peculiar subcellular localizations, or additional regulatory mechanisms remained a mystery. To unravel such novel molecular interactions, the mouse DRF **mDia1** and the formins **ForA** and **dDia3** from *Dictyostelium discoideum* amoebae have been investigated in more detail.

A thorough analysis of the mouse formin **mDia1** led to the discovery of two phospholipid-binding regions that directly interacted in vitro with phosphatidylinositol-4,5-bisphosphate (PIP₂) and phosphatidylserine (PS). The molecular structures for this interaction are clusters of basic residues in the N-terminal Basic Region (BR) and at the C-terminus. Most interestingly, both lipid-binding regions are distinguishable in their activities. The N-terminal site is required for anchoring mDia1 in the membrane, whereas the C-terminal site confers a regulatory signal and arrests actin assembly as long as PIP₂ is bound. These in formins absolutely novel activities allow now a large number of experimental approaches to understand the signaling pathways of the most powerful actin nucleators.

In addition, the two *D. discoideum* DRFs ForA and dDia3 have been investigated by molecular genetics, cell biological and biochemical techniques. **dDia3** resembles in its nucleating activity and its accumulation in filopodia tips the already published dDia2, but it is not as specific in the formin/profilin interaction and carries at its N-terminus a putative lipid-binding protein kinase C conserved region 1 (C1). **ForA** harbors at its N-terminus also a protein kinase C

conserved region, the C2 domain which was shown to interact with various phospholipids including PIP₂. In contrast to mDia1, the deletion of the putative lipid-binding domain of ForA did not alter the localization below the plasma membrane suggesting that additional signals are required to target the protein to the cortical region. In order to identify the cellular function of ForA, a null mutant was generated by disrupting the *forA* gene. Besides increased blebbing that is indicative for a perturbation of the cortical actin cytoskeleton, the null mutant also displayed strong defects in cell migration. Random motility of single cells was decreased and during the multicellular stage of development there was a complete failure of slug motility towards light. Normal phototaxis could be rescued by ectopic expression of a GFP-tagged ForA construct. Taken together, these data suggest that ForA is involved in the generation of actin filaments needed for stabilization of the cortical actin cytoskeleton which in turn is required for the coordinated cell movement of *D. discoideum* amoebae.

Zusammenfassung

Die Dynamik des Aktin Zytoskeletts in Nicht-Muskelzellen ist durch eine Anzahl Aktin-bindender Proteine genau reguliert. Insbesondere eine effiziente Ausbildung neuer Mikrofilamente ist essentiell für zahlreiche Aktivitäten einer Zelle, z.B. Zellbewegung, Zytokinese, Phagozytose usw.. Für die Nukleation der Aktin Polymerisation sind die 'actin-related proteins' Arp2/3 und die Formine die zwei wichtigsten ubiquitären Proteinklassen. Die aus mehreren Domänen bestehenden und streng regulierten Formine (sog. Diaphanous-related formins, DRF) können nicht nur lineare Aktinfilamente de novo nukleieren, sondern bleiben mit dem schnell wachsenden Ende assoziiert und erlauben eine ständige Insertion neuer Aktin Monomere. Durch die Bindung aktiver Rho GTPasen an die GTPase-Bindedomäne (GBD) wird das Formin aus einer intramolekularen Haarnadel-Struktur aufgefaltet und aktiviert. Diese Art der Regulation ist in den letzten Jahren ausführlich untersucht worden, andere wichtige molekulare Befunde, wie z.B. die Interaktion mit Membranen, besondere subzelluläre Lokalisierungen, zusätzliche regulatorische Mechanismen, sind aber immer noch unklar. Zur Aufklärung solcher für Formine neuartigen molekularen Interaktionen wurden im Rahmen dieser Arbeit die Formine **mDia1** aus Maus und **ForA** bzw. **dDia3** aus *Dictyostelium discoideum* Amöben genauer untersucht.

Eine genaue Analyse des Maus Formins **mDia1** führte zur Entdeckung von zwei Phospholipid-Binderegionen, die *in vitro* direkt Phosphatidylinositol-4,5-diphosphat (PIP₂) und Phosphatidylserin (PS) binden. Verantwortlich für diese Interaktionen sind Cluster basischer Aminosäuren in der N-terminalen basischen Region (BR) und am C-Terminus. Es ist besonders interessant, dass sich diese beiden Regionen funktionell unterscheiden. Der N-Terminus ist für die Verankerung von mDia1 an der Membran verantwortlich, während der C-Terminus ein regulatorisches Signal darstellt und die Elongation hemmt, solange PIP₂ gebunden ist. Diese für Formine absolut neuartigen Aktivitäten ermöglichen nun eine große Zahl experimenteller Versuchsansätze, die zu unserem Verständnis der Formin-spezifischen Signalkaskaden beitragen werden.

Darüber hinaus wurden die *D. discoideum* Formine ForA und dDia3 mit molekulargenetischen, zellbiologischen und biochemischen Techniken untersucht. **dDia3** ähnelt in seiner nukleierenden Aktivität und seiner Akkumulation in Filopodienspitzen dem bereits veröffentlichten dDia2, allerdings zeigt es keine selektive Interaktion mit den Profilin Isoformen und enthält im N-terminalen Bereich eine Proteinkinase C Domäne (C1), die vermutlich mit Lipiden interagieren kann. **ForA** enthält im N-Terminus ebenfalls eine konservierte Region der Proteinkinase C (C2 Domäne), die, wie in der vorliegenden Arbeit gezeigt werden konnte, an verschiedene Phospholipide, einschließlich PIP₂, bindet. Im Unterschied zu mDia1 verändert allerdings die Deletion der Lipid-Bindedomäne von ForA nicht die Lokalisierung unter der Plasmamembran, was zusätzliche Signale für die Lokalisierung im Cortex vermuten lässt. Zur genaueren in vivo Analyse wurde durch Gendisruption eine ForA-Nullmutante generiert. Neben vermehrter Blasenbildung, die wahrscheinlich durch eine Störung im Aktin-Cortex hervorgerufen wird, zeigten die Null-Mutanten auch einen starken Defekt in der Zellmigration. Die Motilität der Einzelzellen war herabgesetzt und während des multizellulären Stadiums kam es zu einem eindeutigen und durch ektopische Expression reversiblen Phototaxis Defekt. Die Daten lassen vermuten, dass das Formin ForA für die Generierung von Aktinfilamenten im Cortex und somit für die Stabilität des Cortex auch bei koordinierter Zellbewegung von *D. discoideum* Amöben wichtig ist.

1 Introduction

1.1 The actin cytoskeleton

There are three major components of the cytoskeleton in eukaryotes: (1) microfilaments, (2) microtubules and (3) intermediate filament. Actin that constitutes the microfilament system is a ubiquitous, highly conserved, major protein found in metazoan cell types and was initially purified from muscle as acto-myosin complex (Halliburton, 1887; Schleicher and Jockusch, 2008; Zallar and Szabo, 1989). Actin exists in two forms: (1) monomeric globular or G-actin and (2) filamentous or F-actin polymers. The latter is a component of at least 15 diverse dynamic structures including lamellipodia, filopodia, endosomes and cell cortex in eukaryotic cells (Chhabra and Higgs, 2007). Actin filaments in these structures are built from common G-actin reserves with the help of several actin-binding proteins that play a pivotal role not only in construction (actin polymerization) but also destruction (actin depolymerization) of such actin-based networks.

The actin cytoskeleton in non-muscle cells is extremely dynamic otherwise cellular processes such as cell migration, endocytosis, wound closure, organelle transport and development would not be possible (Pollard and Borisy, 2003). Not surprisingly, the deletion of the single actin gene in *Saccharomyces cerevisiae* is lethal (Shortle et al., 1982). However, in many organisms actin is encoded by more than one gene. In *Homo sapiens* there are at least six actin isoforms and the *Dictyostelium discoideum* genome contains 42 'actin' genes, among them even 17 distinct genes that code for 17 identical actin proteins (Joseph et al., 2008).

The 42 kDa globular actin can be stored in its original form easily for weeks. However, an addition of millimolar concentrations of salts such as KCl or MgCl₂ and ATP will spontaneously stimulate the formation of highly viscous filamentous actin. There are three major phases in the actin polymerization process:

Nucleation or lag phase: The formation of actin dimers and trimers is extremely unfavourable and it requires time until an increased number of trimers allows significant elongation of these 'actin nuclei'. This is the rate-limiting step in actin polymerization which can be accelerated in vitro by an addition of pre-formed actin filaments or, also in vivo, by a class of actin-binding proteins that are capable of stabilizing dimers and trimers thus shifting the reaction towards elongation.

Elongation phase: Actin filaments elongate rapidly and continue to do so until polymerization reaches equilibrium at which the G-actin is nearly depleted. Under routine in vitro conditions elongation proceeds at a speed of $0.027 \mu\text{m}/\text{sec}$ which is roughly an addition of 10 subunits per second (Breitsprecher et al., 2008).

Steady state: At the steady state net actin polymerization is zero and the extent of G-actin added to the filaments depends upon the concentration of free G-actin in solution. This constant concentration of G-actin subunits that remains in equilibrium with the actin polymer is termed as ‘critical concentration or C_c ’. Several actin-binding proteins can influence the rate of polymerization; proteins that decrease the C_c will favor depolymerization, whereas proteins that increase the C_c will eventually favor polymerization. The role of various actin-binding proteins governing the rate of actin assembly and disassembly is discussed in section 1.2.

Actin filaments display polarity as they possess two distinguishable ends. The plus end (+) and the minus (-) end of the actin filament contains ATP-bound or ADP-bound actin subunits, respectively. Looking at the orientation of myosin on an actin filament the two ends can easily be identified. The attached myosin heads resemble arrows pointing toward the (-) end whereas the barbed ends of arrow orient toward the (+) end of the actin filament (Figure 1). Actin filaments grow at least 10 times faster at barbed or (+) ends as compared to the pointed or (-) end (Wegner and Isenberg, 1983). Therefore, the C_c of barbed ends is about $0.1 \mu\text{M}$ in contrast to $>0.6 \mu\text{M}$ G-actin at the pointed ends (Pollard and Cooper, 1986).

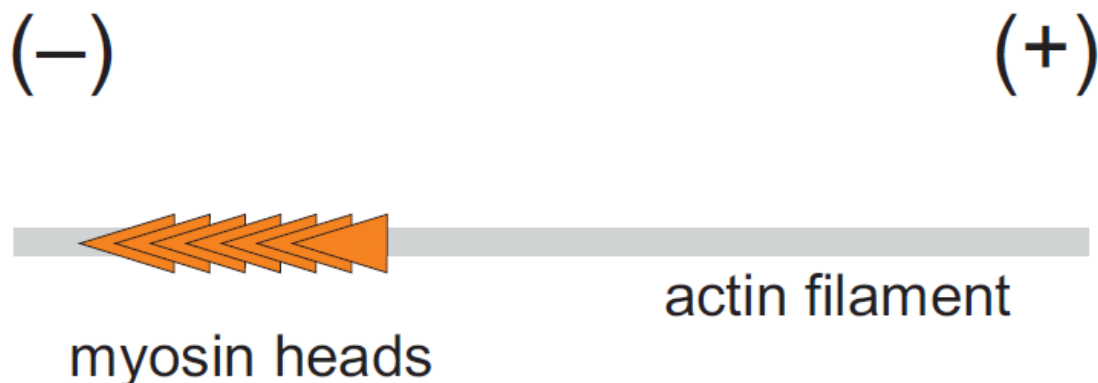


Figure 1: Actin filaments are polar.

F-actin possesses distinguishable ends, i.e. the slow growing minus or pointed end (decorated by myosin heads) and the fast growing plus or barbed end.

‘Actin treadmilling’ controls the actin turnover which in turn is important to keep the filament length constant while actin subunits are incorporated at the barbed end and dissociated from the pointed end (Lappalainen and Drubin, 1997; Neuhaus et al., 1983). Essentially, actin subunits can exist as either the ATP bound *T form* or the ADP bound *D form* (Hama et al., 1969; Kasai, 1969; Kasai and Hama, 1969; Nakaoka and Kasai, 1969). As stated above, variable concentrations of these two monomeric actin forms could potentially influence the actin polymerization process. ATP in G-actin is hydrolysed to ADP but not immediately when the monomeric actin is added to the filament end. The addition of actin subunits is faster than the hydrolysis per se therefore, a small cap of ATP-actin could remain at the barbed ends (Carlier et al., 1984; De La Cruz et al., 2000).

1.2 Actin-binding proteins

As previously stated, several actin-binding proteins control the kinetics of actin assembly and disassembly. There are at least 5 important classes of actin-binding proteins:

(1) *G-actin sequestering proteins*: Proteins such as profilin and thymosin β 4 are found in all eukaryotic cells tested so far. Profilins are small actin-binding proteins with a molecular mass of approximately 15 kDa, are rather abundant cytoplasmic proteins, and can be denatured and renatured during their purification. Many eukaryotes if not all harbor more than one profilin gene, for example there are three profilin isoforms in *D. discoideum*, again at least the same number in *Acanthamoeba* and surprisingly only two in human. Yeast contains only one profilin (Arasada et al., 2007; Kovar et al., 2003).

Profilins function as a nucleotide exchange factor since they catalyze the exchange of ADP-ATP (Jockusch et al., 2007; Mockrin and Korn, 1980). Besides, they also accelerate the filament turnover in the presence of cofilin (a depolymerizing factor, see below), prevent the hydrolysis of ATP that is bound to G-actin, and promote actin assembly by delivering ATP-bound actin subunits to the site of polymerization (Didry et al., 1998; Kovar, 2006). Some cell types utilize thymosin β 4, one of the smallest actin-binding proteins with a molecular mass of about 5 kDa, to maintain the G-actin pool in cells (Nachmias, 1993).

(2) *Capping proteins*: Capping proteins bind actin filament ends and subsequently prevent the exchange of actin subunits. Typical capping proteins at the barbed end are CapZ or Cap32/34 (Cooper et al., 1984; Isenberg et al., 1980; Schleicher et al., 1984) and at the pointed end -

tropomodulin (Fowler et al., 1993). There are a few actin-binding proteins that can compete with capping proteins for the filament ends, especially at barbed ends (Applewhite et al., 2007; Cooper and Sept, 2008; Schirenbeck et al., 2006). Also phospholipids can inhibit the capping activity (Haus et al., 1991; Heiss and Cooper, 1991).

(3) *Actin filament severing proteins*: Actin depolymerization factor (ADF)/cofilin and gelsolin play a pivotal role in shortening average actin filament lengths by severing F-actin. ADF/cofilin is a major protein that takes care of the depolymerization of actin filaments, while gelsolin accelerates the transition of an actin gel to a less viscous solution justifying its name (Janmey et al., 1985; Lappalainen and Drubin, 1997). Also this class of actin-binding proteins is structurally and functionally conserved throughout evolution (Yin et al., 1990).

(4) *Actin cross-linking and bundling proteins*: The strength of a filamentous network is regulated by several accessory proteins such as α -actinin (Noegel et al., 1987), filamin (Popowicz et al., 2006), vasodilator stimulated phosphoprotein (VASP) (Schirenbeck et al., 2005; Schirenbeck et al., 2006), cortexillin (Faix et al., 1996), fascin (Edwards and Bryan, 1995; Otto et al., 1979), hisactophilin (Schleicher et al., 1995), talin and vinculin (Tempel et al., 1995). These proteins are known to reorganize the 3-dimensional architecture of the F-actin network by either cross-linking or bundling.

(5) *Actin nucleators*: Actin nucleators belong to the most important classes of actin-binding proteins because they help to bypass the rate-limiting step of polymerization (Chesarone and Goode, 2009). There are three major types of actin nucleators:

- > the binding of WASp homology (WH2) domains of Neuronal-Wiscott Aldrich Syndrome protein (Stradal et al., 2004) to actin monomers and the subsequent interaction between the acidic (A) domain of N-WASp and the actin-related protein (Arp) subunit of the Arp2/3 complex may mimic an actin trimer,

- > *formins* nucleate actin by stabilizing spontaneously formed dimers, the leaky capping activity of formins allows the addition of actin subunits while the nucleator remains associated with the barbed end, and

- > *Spire, Cobl, Lmod*: All these proteins harbor one to four G-actin binding WH2 domains and structurally align monomeric actin to favor nucleation. Such architecture suggests that Spire (Quinlan et al., 2005), Cobl (Ahuja et al., 2007) and Lmod (Chereau et al., 2008) share a similar nucleation mechanism. However, there may be some minor differences between

actin nuclei generated by these proteins, for instance the orientation in which the nucleus is stabilized could be unique.

In addition, actin assembly/disassembly can also be manipulated both in vitro and in vivo by several drugs and toxins such as phalloidin (Lengsfeld et al., 1974), latrunculin (Coue et al., 1987), cytochalasin (Cooper, 1987), jasplakinolide (Bubb et al., 1994), dolicolide (Bai et al., 2002), hectochlorin (Marquez et al., 2002), mycalolide (Saito et al., 1994) and RTX toxin (Fullner and Mekalanos, 2000).

1.3 Formins

Formins are large and multi-domain actin- and microtubule-binding proteins that are characterized by the presence of highly conserved 'Formin Homology' or FH domains (Goode and Eck, 2007). The mouse *limb deformity* (*ld*) gene was the first member of formin family proteins. During a genetic screen aiming at identification of mouse *ld* alleles in the respective locus led to an accidental discovery of the three interesting *ld* alleles, *ld*^{TgHd}, *ld*^{TgBri} (arose by transgenic insertion) and *ld*^{In2} (arose by translocation or inversion). Subsequently *Fmn1* (Formin1) and related mRNA transcripts were identified. Mouse with truncated protein products displayed zeugopod fusion in both the forelimb (radius/ulna) and hindlimb (tibia/fibula), and syndactyly of the digits and metacarpal bones (Maas et al., 1991).

Over 10 years later the concept changed as a report claimed that limb defects arose because of changes in the adjacent gene gremlin (Zuniga et al., 2004). Nevertheless, the name formins remained unchanged as their functions mainly involved formation of cellular actin based structures. However, the complete regulatory cascade of limb formation is still a mystery and there is a renaissance of formin as a major regulator in this developmental stage. In a very recent report the authors generated Formin1 knockout mice and the results showed clearly that Formin1 disruption conferred oligodactylism (Zhou et al., 2009). The exact molecular basis of the aberrant phenotype is not known, but it might be a result of formin-dependent cytoskeletal activities in distinct limb cell populations.

Formins are essential for several cellular processes including cytokinesis, cell migration, intracellular trafficking and tumor cell invasion (Faix and Grosse, 2006). Tumor cell invasion against tissue borders that result in metastasis relies on tumor cells' ability to dissolve the basement membrane and to migrate subsequently into the 3-dimensional collagen network.

Proteolytic digestion of the extracellular matrix by matrix metalloproteinases will facilitate such tumor cell invasions. Interestingly, actin-rich ‘invadopodia’, reported to be assembled by formins in addition to the Arp2/3 complex and N-WASp, are important for matrix proteolysis (Lizarraga et al., 2009). Furthermore, the matrix proteolytic activities are thought to be restricted to invadopodia.

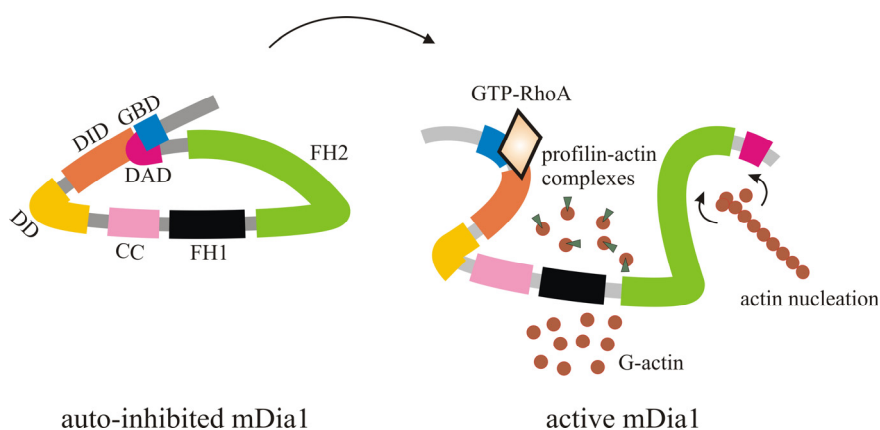


Figure 2: Schematic representation of mDia1 regulation.

The disruption of the DID/DAD intra-molecular interaction by GTP bound RhoGTPase results in the activation of mDia1. Active mDia1 nucleates the formation of actin filaments that are elongated in the presence of profilin/actin complexes. FH-formin homology, CC-coiled coil, DD-dimerization domain, DID-Diaphanous-inhibitory domain, GBD-GTPase-binding domain and DAD-Diaphanous-autoinhibitory domain.

Formins play diverse roles in distinct cell types, probably this explains how important these proteins are and why eukaryotes express more than one formin isoform. For instance, in mammals 15 distinct genes coding for formin proteins have been reported, yeast contains 5, *Drosophila* and *C. elegans* contain 6 each, and the expression of 10 formin genes was detected in the social amoeba *D. discoideum*. *Arabidopsis thaliana* accounts for the maximum number of formin proteins in a given single organism to date as it harbors 21 formin genes (Higgs and Peterson, 2005).

The domain structure is characteristic for nearly all formin isoforms. The proline-rich formin homology domain 1 (FH1) recruits profilin-actin complexes for filament elongation which is accomplished by the adjacent FH2 domain (Kovar et al., 2006). Members of the family of Diaphanous-related formins (DRF) fold on themselves and are thus intrinsically inactive by virtue of additional regulatory sequences located in the N- and C-terminal regions of these proteins (Alberts, 2002). As shown in Figure 2 the binding of activated small Rho family

GTPases such as RhoA to the GTPase-binding domain (GBD) releases this intra-molecular inhibition by disrupting the interaction between the C-terminal Diaphanous-auto-regulatory domain (DAD) and the N-terminal Diaphanous-inhibitory domain (DID) (Lammers et al., 2008; Lammers et al., 2005; Nezami et al., 2006). The dimerization domain (DD) is sufficient to dimerize the N-terminal region leaving the role of a coiled-coil (CC) region obscure, while a short linker between the FH1 and FH2 facilitates the dimerization of the C-terminus (Goode and Eck, 2007; Shimada et al., 2004; Xu et al., 2004).

1.4 *Dictyostelium discoideum* as a model system

The amoeba *D. discoideum* is a powerful model system which was first reported over seventy years ago. Forest soil and decayed leaves are habitats for this simple eukaryote that feeds on bacteria (Raper, 1935). Depletion of the nutrients triggers a developmental program that leads to multicellular aggregates which later differentiate into two major cell types, the prestalk and prespore cells. Prestalk and prespore cells will undergo further development to form a mature fruiting body that is composed of a mass of spore cells on top of dead cells that constitute a thin and long stalk. The oval shaped, extremely stable spores will germinate once favourable conditions are restored (Figure 3). The entire life cycle of *D. discoideum* can be mimicked within 24 hours under laboratory conditions (Chisholm and Firtel, 2004)

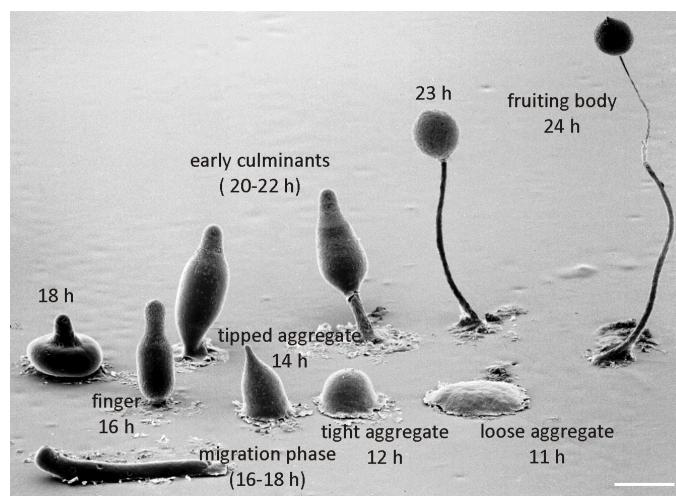


Figure 3: *D. discoideum* life cycle.

Various developmental stages of *D. discoideum* are depicted. The slug migration phase (16-18 h) is sometimes bypassed in native conditions, however, all indicated stages are observed under laboratory conditions. The scale bar represents 500 μm . Courtesy of Lawrence Blanton and Mark Grimson.

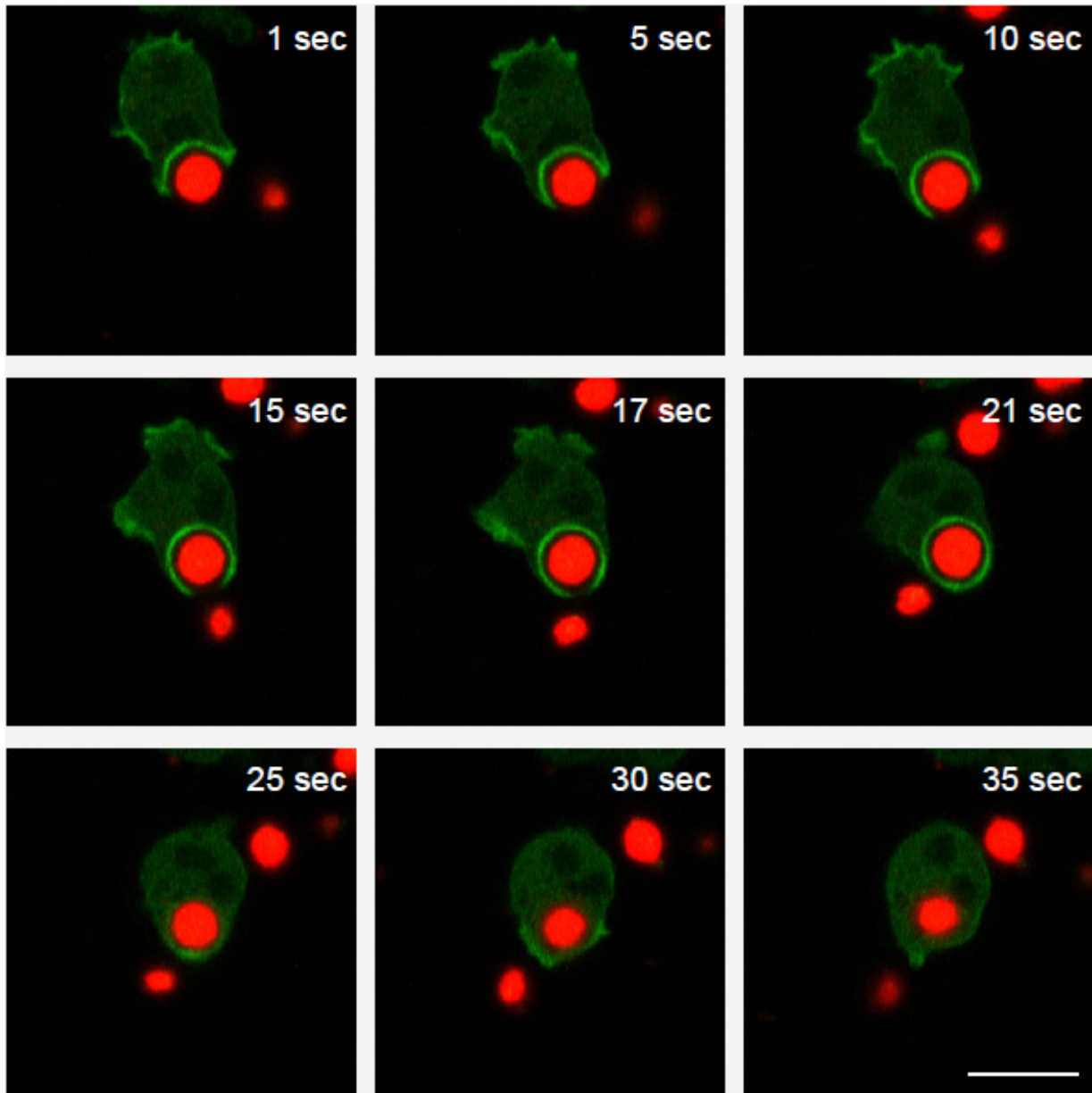


Figure 4: *D. discoideum* is a phagocyte.

The images show phagocytosis of TRITC labelled yeast particles by a *D. discoideum* cell. GFP-labelled RapGTPase activating protein is enriched in the phagosome during the early stages of the uptake (Nagendran Ramalingam, unpublished results). The scale bar represents 10 μm .

D. discoideum cells share activities with human neutrophils (Devreotes and Zigmond, 1988), including cell motility, chemotaxis and phagocytosis (Figure 4). The availability of the completely sequenced genome, the established methods in molecular genetics, cell biology and biochemistry render *D. discoideum* a prime organism to study the activities of single molecules in their cellular environment.

1.5 Goals of the thesis

Two major questions had to be answered in the present work:

1. Are formins regulated by an auto-inhibition independent mechanism?

Formins are large multi-domain proteins that nucleate and elongate linear actin filaments. Members of the family of Diaphanous-related formins (DRF) fold on themselves and are thus auto-inhibited. Several key actin-binding proteins are regulated by more than one mechanism. One of the major goals of the thesis is to discover the auto-inhibition independent mechanism controlling the localization and activity of the mouse DRF mDia1 if any. Since mDia1 is a plasma membrane-associated DRF the possible role of phospholipids in its regulation is to be explored using a combination of in vitro and in vivo techniques.

2. What are the functions of the *D. discoideum* formins ForA and dDia3 in vitro and in vivo?

Among the 10 formin proteins in *D. discoideum*, ForA and dDia3 are unique as they harbor the two protein kinase conserved domains C2 and C1, respectively. These domains are rare and not part of the classical formin topologies. The aim of this section of the thesis was not only to characterize the loss-of function and gain-of function of these formins in detail but also to study the importance of C2 and C1 domains. In addition, the subcellular distribution of these two formins needed to be investigated because the redundancy of formins can be addressed only after characterizing formin isoforms individually.

2 Materials and Methods

2.1 Materials

Cell culture plates, 24 wells, flasks	Nunc
Cell culture dishes \varnothing 100 mm \times 20 mm	Greiner bio-one
Cell culture dishes, \varnothing 3.5 mm with glass bottom	MatTek Corporation
Dialysis membranes Type 8, 20, 27, 25A	Biomol
Microconcentrators Centricon	Amicon
Nitrocellulose membrane Protran BA85	Schleicher & Schüll
Parafilm	American National Cal
PCR tubes 0.5 ml, Petri dishes, \varnothing 92 mm \times 16 mm,	
Pipettes, 10 and 25 ml, 15 ml and 50 ml tubes ('Falcon'),	
1.5 ml centrifuge tubes	Sarstedt
Pipette tips	Braun Melsungen
Plasmid DNA Purification Maxi Kit	Macherey Nagel
QIAprep Spin Miniprep and Gel Extraction kits	Qiagen
Sterile filter, 0.22 μ m Millex GV	Millipore
Ultracentrifuge tubes 1.5 ml	Beckman
Mini-extruder	Avanti polar lipids

2.1.1 Computer programs

Adobe photoshop 8.0, Adobe acrobat 8.0 and	
Acrobat Distiller 8.0	Adobe Systems
askSam 4.0	Seaside Software
AxioVS40 V4.3.101, LSM image browser	Carl Zeiss Vision GmbH
CorelDraw 12	Corel Corporation
DIAS 3.4.1	Solltech Inc.
imageJ 1.34n	Wayne Rasband
Microsoft Office 2003	Microsoft Corporation
Openlab 2.2.5	Improvisation Ltd
Origin 7 SRI	OriginLab Corporation

2.1.2 Instruments

Centrifuges: Optima LE-80K, TL Ultracentrifuges, GS-6KR Centrifuge, J2-21M/E Centrifuge, J6-HC Centrifuge	Beckman
Table top centrifuge 5415	Eppendorf
Rotors: JA-14, JA-20, Ti 45	Beckman
Inverted microscopes (Axiovert 25, 40 CFL, 200 M)	Zeiss
Stereo microscope (Leica MZ FLIII)	Leica
Confocal microscope (LSM 510 meta)	Zeiss
BioDocAnalyze	Biometra
Electroporator GENEPulser-Xcell	BioRad
Fluorescence-Spectrometer	PerkinElmer-LS55
Shaking incubator with temperature control	Memmert
PCR-Thermocycler (Uno and Tpersonal)	Biometra
Photometer Ultrospec 2100 pro	Amersham
Protein transfer Trans-Blot SD	BioRad
Ultrasonicator 820/H Elma	
UV-transilluminator IL-200-M	Bachofer

2.1.3 Reagents

All chemicals used had the degree of purity "p.a."

Adenosine-5'-triphosphate- Na_2 -salt	Serva
Acrylamide (30% Acrylamide with 0.8% Bisacrylamide)	Roth
Agar-Agar, Type RG	Euler/BD
Agarose (SeaKem LE)	BMA
Ammonium persulfate (APS)	Roth
Bacto-Peptone/-Tryptone	Oxoid
BCIP (5-Bromo-4-chloro-3-indolyl phosphate)	Gerbu
Bodipy-TMR-PI(4,5) P_2	Echelon
Bovine Serum Albumin Fraction V	PAA
Coomassie Brilliant Blue R 250, G 250	Roth, Sigma

Complete EDTA-free protease inhibitor cocktail tablets	Roche
Disodiumpyrophosphate	Sigma
DMSO (Dimethylsulfoxide)	Serva
Diphenylhexatriene (DPH)	Invitrogen
DTT (1,4-Dithio-D, L-threitol)	Gerbu
EDTA (ethylenediaminetetraacetic acid)	Biomol
EGTA (ethylene glycol bis[2-aminoethyl ether]- -N, N, N', N'-tetraacetic acid)	Sigma
Ethidium bromide	Sigma
Glutathion-Sepharose	Sigma
HEPES (4-[2-hydroxyethyl]-1-piperazineethanesulfonic acid)	Roth
IPTG (Isopropyl- β -D-thiogalactopyranoside)	Gerbu
n-octyl polyoxyethylene	Bachem
NP-40 (octyl phenoxy polyethoxyethanol)	Fluka
Nucleotides	PQ labs
1-Palmitoyl-2-{6-[(7-nitro-2-1, 3-benzoxadiazol-4-yl) amino] hexanoyl}-sn-glycero-3-phosphoserine (NBD-PS)	
1-Palmitoyl-2-oleoyl-sn-glycero-3-phosphatidylcholine (POPC)	
1-Palmitoyl-2-oleoyl-sn-glycero-3-phosphatidylethanol-amine (POPE)	
1-Palmitoyl-2-oleoyl-sn-glycero-3-phosphatidylserine (POPS)	
L- α -phosphatidylinositol-4,5-bisphosphate (PIP ₂)	Avanti polar lipids
L- α -phosphatidylinositol-4,5-bisphosphate (PIP ₂)	Sigma
2-Propanol	Roth
Protein A-Sepharose CL-4B	General Electric Healthcare
Protease peptone	Oxoid
SDS (Sodium dodecylsulfate)	Serva
Silicon dioxide	Sigma
TEMED (N, N, N', N'-Tetramethylethylenediamine)	Pierce
Triton X-100	Roth
Yeast extract	Oxoid

2.1.4 Media

All media used were prepared with deionised water, which had been filtered over an ion exchanger (Millipore) and were sterilized either by autoclaving or by passing through a microfilter.

AX (#AXM0102) pH 6.7, HL5-C (#HLC0102) pH 7.5 and LB-broth (#LBX0102) were purchased from FORMEDIUM.

SM agar (pH 6.5)

9 g agar, 10 g peptone, 50 mM glucose, 1 g yeast extract, 4 mM MgSO₄, 16 mM KH₂PO₄ and 5.7 mM K₂HPO₄. Made up to 1 l with H₂O.

2.1.5 Bacterial strains and *D. discoideum* cell lines

E. coli strains:

DH5 α	Invitrogen
BL21 RIL	Stratagene
BL21 ArcticExpress RIL	Stratagene
BL21 ArcticExpress RP	Stratagene

D. discoideum cell lines:

AX2-214 (laboratory wild type)	
ForA null	present study**
ForA null + GFP-ForA	present study
ForA null + GFP-ForA Δ C2	present study
ForA null + GFP-ForA-N-terminus	present study
ForA null + GFP-ForA-C-terminus	present study*
ForA null + GFP-ForA Δ DAD	present study
ForA null + GFP-ForA Δ C2 Δ DAD	present study
AX2 + GFP-ForA	present study
AX2 + GFP- Δ DAD	present study
dDia3 null	present study**
dDia3 null + GFP-dDia3	present study
dDia3 null + GFP-dDia3 Δ DAD	present study
AX2 + GFP-dDia3	present study

AX2 + GFP-dDia3 Δ DAD	present study
ForA/dDia3 double null	present study
Myosin II null	(Manstein et al., 1989)
Myosin II null + GFP-ForA Δ DAD	present study
Myosin II/ForA double null	present study
DGAP1/GAPA double null	(Faix et al., 2001)
DGAP1/GAPA double null + GFP-ForA Δ DAD	present study*

* only transient transformants

** isolated by Dr. Jan Faix

2.1.6 Parental and recombinant plasmids

pDGFPXaMCS-Neo	(Dumontier et al., 2000)
pDEXRH	(Faix et al., 1992)
pGEX 4T-1, pGEX 5X-1 and pGEX 6P-1	General Electric Healthcare
pDGFPXaMCS-Neo	(Dumontier et al., 2000)
pLPBLP	(Faix et al., 2004)
pDGFPXaMCS Δ Sac-Neo	present study
YFP-ACA	(Kriebel et al., 2008)
ForA knock out construct	obtained from Dr. Jan Faix
pDGFPXaMCS-Neo-ForA	present study
pDGFPXaMCS-Neo-ForA Δ C2	present study
pDGFPXaMCS-Neo-ForA N-terminus	present study
pDGFPXaMCS-Neo-ForA C-terminus	present study
pDGFPXaMCS-Neo-ForA Δ DAD	present study
pDGFPXaMCS-Neo-ForA Δ C2 Δ DAD	present study
pDGFPXaMCS-Neo-ForAC2	present study
pGEX 5X-1-ForAFH2DAD	present study
pGEX 5X-1-ForADAD	present study
pGEX 5X-1-ForA N-terminus	present study
pGEX 5X-1-ForA Δ C2N-terminus	present study
pGEX 5X-1-ForAC2	present study

pGEX 6P-1-ForA	present study
pGEX 6P-1-ForAFH2DAD	present study
pGEX 6P-1-ForAFH1FH2DAD	present study
pGEX 6P-1-ForADAD	present study
pGEX 6P-1-ForA N-terminus	present study
pGEX 6P-1-ForA Δ C2N-terminus	present study
pGEX 6P-1-ForAC2	present study
pGAD-ForAFH1	present study
pGAD-ForAGBD	present study
pGBK-profilin I	(Schirenbeck et al., 2005)
pGBK-profilin II	(Schirenbeck et al., 2005)
pGBK-profilin III	(Schirenbeck et al., 2005)
pGEX 4T-1-mDia1FL	obtained from Dr. Alfred Wittinghofer
pGEX 4T-1-mDia1FL-6x His	present study
pGEX 4T-1-mDia1FH2DAD	present study
pGEX 4T-1-mDia1N570	present study
pGEX 4T-1-mDia1 Δ BRN570	present study
pGEX 4T-1-mDia1 Δ 47-54N570	present study
pGEX 4T-1-mDia1 Δ 12-46N570	present study
pGEX 6P-1-mDia1FL	present study
pGEX 6P-1-mDia1FL-6x His	present study
pGEX 6P-1-mDia1N500	present study
pGEX 6P-1-mDia1N570	present study
pGEX 6P-1-mDia1 Δ BRN570	present study
pGEX 6P-1-mDia1 Δ 47-54N570	present study
pGEX 6P-1-mDia1 Δ 12-46N570	present study
pGEX 6P-1-mDia1 54	present study
pGEX 6P-1-mDia1 46	present study
pGEX 6P-1-mDia1 12-21	obtained from Dr. Jan Faix
pGEX 6P-1-mDia1FH2DAD	present study

pGEX 6P-1-mDia1FH1FH2DAD	obtained from Dennis Breitsprecher
pGEX 6P-1-mDia1FH1FH2	present study
pGEX 6P-1-mDia1FH1FH2DAD-Mut1	present study
pGEX 6P-1-mDia1FH1FH2DAD-Mut2	present study
pGEX 6P-1-mDia1FH1FH2DAD-Mut3	present study
pGEX 6P-1-mDia1DAD	present study
pGEX 6P-1-mDia2FH1FH2DAD	present study
pGEX 6P-1-mDia3FH1FH2DAD	present study
pEGFP-mDia1FL	obtained from Dr. Jan Faix
pEGFP-mDia1ΔDAD	obtained from Dr. Jan Faix
pEGFP-mDia1ΔBRΔDAD	present study
pEGFP-mDia1BR	present study
pEGFP-mDia1GST-BR	present study
pEGFP-mDia1BRGBD	present study
dDia3 knock out construct	obtained from Dr. Jan Faix
pDGFPXaMCS-Neo-dDia3	present study
pDGFPXaMCS-Neo-dDia3ΔDAD	present study
pGEX 5X-1-dDia3FH2DAD	present study
pGEX 6P-1-dDia3FH2DAD	present study
pGEX 6P-1-dDia3FH1FH2DAD	present study
pGEX 6P-1-dDia3 N-terminus (1-950)	present study
pGEX 6P-1-dDia3 N-terminus (571-1000)	present study
pMAL C2-dDia3 N-terminus (571-1000)	present study
pGAD-dDia3FH1	present study
pGAD-dDia3GBD	present study

2.2 Methods

2.2.1 Molecular biology

Standard molecular biological methods were used to generate various expression constructs. Genomic DNA from *D. discoideum* was isolated using the Qiagen High Pure PCR Template Preparation Kit following the protocol for mammalian cell culture. Total RNA from different developmental time points was purified from *D. discoideum* or various mouse tissues with the Qiagen RNeasy Mini Kit. Subsequently cDNA was synthesized using Superscript II reverse transcriptase. Polymerase chain reactions (PCRs) were performed with either home made Taq-Polymerase in PCR buffer (10 mM Tris pH 8.8, 50 mM KCl, 2 mM MgCl₂, 0.1 mg/ml BSA, 2% DMSO) or Phusion-Hot start high-fidelity DNA polymerase from FINNZYMES according to the manufacturer's protocol. Plasmid DNA was obtained following the modified alkaline lysis protocol with silica (Lakshmi et al., 1999) or using the Macherey Nagel Ax500 Plasmid DNA Purification Maxi Kit. Chemically competent *E. coli* cells were prepared with the CaCl₂ method (Dagert and Ehrlich, 1979).

2.2.2 Biochemistry

2.2.2.1 SDS-Polyacrylamide Gel Electrophoresis and western blotting

Protein mixtures were separated by standard discontinuous SDS-PAGE (Laemmli, 1970). Western blots were done using the semi dry system according to a modified Towbin protocol (Towbin et al., 1979) with transfer buffer (25 mM Tris pH 8.5, 190 mM glycine, 20 % methanol, 0.02 % SDS). The nitrocellulose membranes were blocked with non fat milk in NCP buffer (10 mM Tris pH 7.3, 150 mM NaCl, 0.05 % Tween20) and developed using the alkaline phosphatase/BCIP method in conjunction with appropriate antibodies.

2.2.2.2 GST-tagged protein expression and purification

Constructs in pGEX vectors, expressing the proteins with an N-terminal GST tag, were transformed into DH5 α , BL21 RIL, BL21 ArcticExpress RIL or BL21 ArcticExpress RP. Cultures were inoculated and grown overnight at 37°C, subsequently cultures with 10% inoculum were grown at 30°C to an OD₆₀₀ of 0.4-0.8. Expression was induced with 0.5 mM IPTG and cells were grown overnight at 16 or 10°C. Cells were resuspended in PBS + 2 mM

DTT, 1 mM EDTA, 5 mM benzamidine, 100 μ M PMSF and one protease inhibitor cocktail tablet/50 ml lysis buffer) and opened by sonication in the presence of 0.5 mg/ml lysozyme. Lysates were centrifuged (35,000 g for 45-60 min at 4°C) and the supernatants were bound to Glutathione-Sepharose 4B for 3-4 h. The matrix was washed with 10-20 column volumes of lysis buffer and the bound proteins were eluted with lysis buffer containing 30 mM reduced glutathione. The presence of protein in different fractions was tested by Bradford's method (Bradford, 1976) and analyzed on SDS-PAGE. The appropriate fractions were pooled and dialysed against PBS.

2.2.2.3 Cleavage of the GST tag

PreScission protease was used to cleave the GST tag from pGEX-6P-1 based polypeptides. Following elution of the GST fusion protein from Glutathione Sepharose, the eluate was dialysed extensively against PBS containing 1 mM EDTA and 1 mM DTT in order to remove reduced glutathione and protease inhibitors from the sample. Roughly, 10 μ g of the protease cleave 1 mg of GST fusion protein. Cleavage was carried out at 4°C overnight on a rotatory shaker. Once digestion was complete, the sample was passed through a washed and equilibrated Glutathione Sepharose to remove free GST and the PreScission Protease from the protein of interest.

If pGEX-4T vectors were used for expression of fusion protein, the GST tag was cleaved off by thrombin. The eluates were dialysed against PBS, subsequently up to 1 mg of fusion protein was digested with 1 unit of thrombin. Cleaved GST was removed by passing the sample through a washed and equilibrated Glutathione Sepharose. The protein of interest was then further purified by a p-Aminobenzamidine Agarose to remove residual thrombin.

2.2.2.4 Preparation of multilamellar and unilamellar lipid vesicles

Lipid vesicles were made and concentrations calculated as described (Prehoda et al., 2000) with minor modifications. Briefly, for multilamellar vesicles, PC, PS and PIP₂ were dissolved separately in chloroform/methanol/water (20:9:1) and dried under nitrogen. The lipids were then resuspended in 20 mM HEPES pH 7.3 and 150 mM NaCl followed by sonication until the solution became clear. At indicated ratios the lipids were mixed and sonicated again just prior to usage. To obtain unilamellar vesicles, liposomes were extruded through a polycarbonate filter (100-nm pore size) using a mini-extruder (Avanti Polar Lipids).

2.2.2.5 Lipid spin-down assays

Spin-down assays were performed by mixing ~3 μM protein and ~50 μM phospholipid vesicles at indicated ratio in 20 mM HEPES pH 7.3, 150 mM NaCl, 2 mM EGTA (total assay volume 50 μl), incubated at 25°C for 60 min, and centrifuged at 10,000 g for 30 min at room temperature. The pellets were washed once with 100 μl of the reaction buffer. Subsequently, the volumes of the pellets and supernatant fractions were normalized and analyzed by SDS-PAGE and Coomassie Blue staining (Eichinger and Schleicher, 1992).

2.2.2.6 Fluorescence spectroscopy

All fluorescence measurements were performed in quartz cuvettes with 3 mm path length. Fluorescence spectra and diphenylhexatriene (DPH) anisotropy were measured with a PerkinElmer-LS55 spectrometer with both emission and excitation band passes set at 10 nm. Spectra were corrected for the contribution of light scattering in the presence of vesicles. NBD-PS fluorescence was excited at 470 nm and the emission spectra was recorded from 490 nm to 560 nm with band passes set at 5 nm and 10 nm, respectively. Bodipy-TMR-PI(4,5) P_2 fluorescence was excited at 547 nm and the emission spectra were recorded from 555 to 600 nm in the presence of different concentrations of proteins. The percentage of quenching was calculated using the following equation:

$$\% \text{ quenching} = (1 - F/F_0) \times 100$$

Where F is the fluorescence intensity in the presence of protein or liposomes, and F_0 is the fluorescence intensity in the absence of protein or liposomes.

Fluorescence anisotropy of DPH was measured by including DPH into liposomes at $X = 0.002$. Fluorescence anisotropy for DPH was measured with excitation at 360 nm and emission at 450 nm, using 10nm bandwidths.

The lipid concentration used was 40 μM for DPH anisotropy, NBD-PS, and bodipy-TMR-PI(4,5) P_2 fluorescence measurements.

2.2.2.7 Preparation of actin from rabbit skeletal muscle

Actin was prepared either from rabbit skeletal muscle or from chicken breast muscle according to the methods described by Spudich and Watt (Spudich and Watt, 1971). The back and upper thigh muscles of a freshly bled rabbit or breast muscle of chicken were sliced into pieces, minced and, to remove myosin, extracted with high-salt extraction buffer for 10 min with

agitation. The mixture was centrifuged (4,000 g, 10 min) and re-extracted. The sediment was resuspended in water and the pH adjusted to a value between 8.2 and 8.5 with a 1 M Na₂CO₃ solution. Following centrifugation (4,000 g, 10 min), the supernatant was discarded and the process was repeated until swelling of the sediment was observed. The sediment was then washed with cold acetone, dried overnight. Finally the acetone powder was stored at -20°C for subsequent actin preparations.

10 g muscle acetone powder were extracted with 200 ml of G-buffer at 0°C for 30 min, filtered through nylon nets and re-extracted at 0°C for 10 min. The filtrate was centrifuged (30,000 g, 30 min, 4°C) and the actin in the supernatant allowed to polymerize for 2 h at room temperature or overnight at 4°C after addition of KCl (50 mM), MgCl₂ (2 mM) and ATP (1 mM). For removal of tropomyosin, solid KCl was then slowly added till a final concentration of 0.8 M was reached. The actin filaments were then sedimented by centrifugation (150,000 g for 3 h, at 4°C). For depolymerization, the F-actin pellet was dialysed against several changes of G-buffer, spun again at 150,000 g for 3 h, and about 65% from the top supernatant further purified using a Sephacryl S300 gel filtration column (2.5x45 cm Pharmacia). From its optical density at 290 nm, the G-actin concentration could be calculated easily (1mg/ml pure actin: 0.65 OD₂₉₀) (Wegner, 1976). The G-actin prepared could be stored on ice up to 3 weeks for most applications.

Extraction buffer: 0.5 M KCl and 0.1 M K₂HPO₄

G-buffer (pH 8.0): 2 mM Tris/HCl, 0.2 mM CaCl₂, 0.2 mM ATP, 0.02% NaN₃ and 0.5 mM DTT

2.2.2.8 Pyrene-actin labelling

Actin was labelled with N-(1) pyrenyliodoacetamide (pyrene) following the protocol of Kouyama and Mihashi (Kouyama and Mihashi, 1981). After the ultracentrifugation step in the course of the actin preparation, 2/3 of the supernatant were carefully collected and dialysed against buffer P. Actin polymerization was initiated by the addition of KCl (150 mM) and MgCl₂ (2 mM), and 3-5 fold molar excess of pyrene (in DMSO) was added immediately to the vigorously stirred actin solution. From this step onwards, all activities were carried out in the dark since pyrene is light sensitive. The solution was rotated end-over-end in a 50 ml tube at room temperature overnight after which the actin filaments were sedimented (150,000 g, 3 h,

4°C). The F-actin pellet was homogenized in G-buffer and dialysed against G-buffer to allow depolymerization. After a second centrifugation step (150,000 g, 3 h, 4°C), the pyrene-labelled G-actin was purified by gel filtration as described above and later stored at -70°C. Buffer P (pH 7.6) 1 mM NaHCO₃, 0.1 mM CaCl₂ and 0.2 mM ATP.

2.2.2.9 In vitro actin polymerization assays

Pyrenyliodoacetamide-labelled actin monomers (pyrene actin) provide a fluorescent readout of actin filament polymerization because a 30-fold increase in fluorescence occurs on incorporation of a labelled actin subunit into the polymer. Only low levels (5–10%) of pyrene labelled actin are required for a strong signal. For actin assembly, a final concentration of 2 or 3 μM actin were routinely used. The reaction (800 μl) was started by addition of actin and the assays were performed in a buffer containing 10 mM imidazole, 2 mM MgCl₂, 0.2 mM CaCl₂, 1 mM NaATP, and 50 mM KCl (pH 7.2).

For assays involving lipid vesicles, formin was initially preincubated for 30 seconds with lipids at desired concentrations, buffers were added and eventually the reaction was started by adding the actin mix (unlabelled and pyrene actin). The preincubation step was also carried out for auto-inhibition experiments involving the N- and C-terminal formin fragments.

2.2.2.10 TIRF assays

Time-lapse evanescent wave fluorescence microscopy was performed as described (Breitsprecher et al., 2008). Briefly, the assembly of 1 μM ATP-actin and 0.3 μM Alexa-Fluor-488-labelled ATP-actin in TIRF buffer (10 mM imidazole (pH 7.4), 50 mM KCl, 1 mM MgCl₂, 1 mM EGTA, 0.2 mM ATP, 50 mM DTT, 15 mM glucose, 20 μg/ml catalase, 100 μg/ml glucose oxidase and 0.5% methylcellulose) on cover slips coated with 10 nM N-ethylmaleimide (NEM) myosin II and formins (in the presence or absence of multilamellar liposomes). Images from an Olympus IX-81 inverted microscope were captured every 10 or 15 s with exposures of 200 or 500 ms with a Hamamatsu ER C8484 CCD camera (Hamamatsu Corp., Bridgewater, NJ).

2.2.3 Cell biology methods

2.2.3.1 Mouse cell culture and transfection

NIH 3T3 fibroblasts were maintained in DMEM with 10% FBS and 2 mM glutamine. Cells were transfected with 2 µg plasmid DNA using LipofectAMINE 2000 (Invitrogen). Microscopy was performed essentially as described (Schirenbeck et al., 2005). Briefly, 10 hours after transfection live cells expressing GFP-fusion proteins were imaged in phosphate buffer using a LSM 510 Meta (Zeiss, Germany) at 30°C.

2.2.3.2 *D. discoideum* cell culture

D. discoideum AX2 (referred to as wild type) and derived mutants were grown in HL5-C or AX medium under standard conditions essentially as described (Arasada et al., 2006). Cells were allowed to grow up to maximal cell densities of 5×10^6 cells/ml to avoid the stationary phase. Spores for long term storage were obtained from *K. aerogenes* lawns on SM agar plates and stored in Soerensen buffer (14.6 mM KH_2PO_4 , 2 mM NaHPO_4 , pH 6.0) at -70°C.

2.2.3.3 Transformation of *D. discoideum* cells

D. discoideum cells were transformed with the appropriate plasmids by electroporation essentially as described (Faix et al., 2004). Briefly, 10^7 growth-phase cells were washed extensively with ice cold electroporation buffer and electroporated with ~35 µg of DNA in a 4 mm electroporation cuvette using a Gene Pulser Xcell (Biorad) and the Standard settings (two pulses at 5 s interval, 1 ms, at 1 kV and 10 µF). After electroporation, the cells were transferred to a petri dish and after 15 min under constant motion (50 rpm) at 20°C, 2 mM CaCl_2 and 2 mM MgCl_2 were added for another 15 min. Finally, 12 ml HL5-C medium was added, and the cells were allowed to recover for 24 h before adding the appropriate antibiotic to select for transformants. Single clones were obtained after 10-15 days following spreader dilution on *K. aerogenes* SM plates.

2.2.3.4 Phototaxis assay

During development *D. discoideum* forms a multicellular aggregate, the so called slug, which can move towards light. Phototactic behavior of wild type and mutants was tested as described previously with minor modifications (Khaire et al., 2007). Briefly, cells from the edges of

colonies growing on *K. aerogenes* lawns were transferred to water agar plates to form slugs. The plates were transferred into a dark box with a 2 mm wide opening for the entry of light. Plates were incubated at 21°C for at least 48 h. To visualize the slugs and their tracks, cells were transferred onto a nitrocellulose membrane and were stained with 0.1% amidoblack in 25% 2-propanol and 10% acidic acid for 10 min and destained in water.

2.2.4 Yeast-two hybrid assay

2.2.4.1 Yeast strains, maintenance and routine culturing

AH109 supplied with the Match Maker 3 system (BD Biosciences) was used for mating experiments. The yeast strain is stored in YPD medium with 25% glycerol at -70°C. To prepare new glycerol stock cultures of yeast an isolated colony from the agar plate was scraped with a sterile inoculation loop and resuspended in 20-50 ml of YPD medium (or the appropriate minimal medium) and incubated on a shaker at 30°C and 200 rpm overnight. Usually it takes longer for cells to grow in selection media.

2.2.4.2 Yeast plasmids

Two shuttle plasmid vectors for *E. coli* and yeast were supplied along with the kit. pGBKT7 harbors the DNA-binding region of the Gal4 transcription factor and a kanamycin resistant marker for selection in *E. coli*. The pGADT7 vectors harbor the activation domain of the Gal4 transcription factor and an ampicillin resistance marker.

2.2.4.3 Yeast transformation

To test the interaction between two proteins, the bait and the target vectors carrying the appropriate genes were transformed into the yeast strain AH109 yeast strain using the LiAc/PEG method. Briefly, the yeast strains were inoculated into 5 ml of liquid medium (2x YPAD) and incubated on a shaker at 30°C and 200 rpm. 2 ml of an overnight YPAD culture (1 and 2 x 10⁸/ml) were harvested in a sterile 1.5 ml microcentrifuge tube by centrifuging for 30 s. To the cell pellet the following components of the transformation mixture were added in the order listed.

<u>Component</u>	<u>Volume (µl)</u>
PEG 3500 50% w/v	240 µl
LiAc 1.0 M	36 µl
Boiled SS-Carrier DNA (2 mg/ml)	50 µl
Plasmid DNA (0.1 to 1 µg) plus	
water	34 µl
Total volume	360 µl

The tubes were incubated in a water bath at 42°C for 10 min. The transformation mix is then removed by centrifugation for 30 s; the cell pellet was resuspended in 1.0 ml of sterile water and plated onto the appropriate selection plates.

2.2.4.4 YPAD medium (YPD plus adenine)

(Yeast Extract - Peptone - Dextrose plus Adenine medium)

6.0 g	yeast extract (Difco)
12.0 g	peptone (Difco)
12.0 g	glucose
60 mg	adenine hemisulphate
600 ml	distilled water

For agar medium 10 g of bacto-agar was added and sterilised by autoclaving at 121°C for 15 min.

2.2.4.5 Synthetic complete drop out (SC drop-out medium)

4.0 g	yeast nitrogen base (without amino acids)
12.0 g	glucose
0.50 g	synthetic complete drop-out mix
600 ml	distilled water
10.0 g	bacto agar (add for solid medium)

The ingredients (except agar) were mixed in water and the pH was adjusted to 5.6 with 10 N NaOH (this step is important for efficient transformation). The media were sterilised by autoclaving at 121°C for 15 min.

Synthetic complete drop-out medium mix (SC drop-out)

2.0 g	Adenine hemisulfate
2.0 g	Arginine HCl
2.0 g	Histidine HCl
2.0 g	Isoleucine
2.0 g	Leucine
2.0 g	Lysine HCl
2.0 g	Methionine
3.0 g	Phenylalanine
6.0 g	Homoserine
3.0 g	Tryptophan
2.0 g	Tyrosine
1.2 g	Uracil
9.0 g	Valine

Omit the appropriate component(s), indicated in bold, to prepare SC-Ade, SC-His, SC-Leu, SC-Trp, SC- Trp/Leu, and SC-Trp/Leu/His. Combine the ingredients in a clean 250 ml plastic bottle. Add three or four clean glass marbles and shake vigorously to mix. This quantity will be sufficient for approximately 100 (600 ml) batches of SC drop-out medium.

3 Results

3.1 Characterization of the mDia1-phospholipid interaction

3.1.1 mDia1 is a Diaphanous-related formin (DRF) from *Mus musculus*

The mouse DRF superfamily contains three mDia isoforms of which the ubiquitously expressed mDia1 is considered to be one of the most potent actin nucleators among 15 formins in mammals. The well studied mDia1 protein consists of 1255 amino acids with a molecular mass of 139.37 kDa is encoded by 27 exons in chromosome number 18. The widely spread research on formins resulted in multiple names for formin proteins; mDia1 too has several names including D18Wsu154e, Dia1, Drf1, KIAA4062, mKIAA4062, p140 mDia. A part of the confusion in the formin nomenclature must be due to their poorly understood in vitro and in vivo functions. However, now mDia1 is basically a cytoskeletal protein with distinct functions.

3.1.2 Domain structure of mDia1

From the protein sequence it is obvious that like other formins, mDia1 is a multi-domain protein with well conserved domains including the characteristic Formin Homology (FH) domains (Figure 5). The proline-rich FH1 domain modulates the signals via the G-actin sequestering protein profilin and SH3 domain containing proteins. It is the core FH2 domain that confers actin nucleation activity to formins. Binding of GTP bound Rho to the GTPase-binding domain (GBD) triggers the activation of formin by disrupting the Diaphanous-autoregulatory domain (DAD)/Diaphanous-inhibitory Domain (DID) intra-molecular interaction. The dimerization domain (DD) is sufficient to dimerize the N-terminal region leaving the role of a coiled-coil (CC) region obscure, while a short linker between the FH1 and FH2 facilitates the dimerization of the C-terminus.

3.1.3 BR is the N-terminal phospholipid-binding region in mDia1

The first 60 residues of mDia1 referred to as the basic region (BR) harbor three, clearly separated polybasic clusters encompassed by aa 12-21, aa 35-42 and aa 47-54 (Figure 6A). A similar basic region is also present in mDia2 and DAAM proteins (Figure 6B). To test whether the basic region of mDia1 can interact with negatively charged phospholipids, the complete N-terminus of mDia1 (N570 aa) was expressed as a GST-fusion protein and tested for its ability

(A) mDia1 domain structure



(B) Protein sequence

```

1     MEPSGGGLGP GRGTRDKKKG RSPDELPATG GDGGKHKKFL ERFTSMRIKK
51    EKEKPNSAHR NSSASYGDDP TAQSLQDISD EQVLVLFEQM LVDMNLNEEK
101   QQPLREKDIV IKREMVSOYL HTSKAGMNQK ESSRSAMMYI QELRSGLRDM
151   HLLSCLES LR VSLN NN PVSW VQTFGAEG LA SLLDILKRLH DEKEETSGNY
201   DSRNQHEI IR CLKAFMNNKF GIKTMLETEE GILLLV RAMD PAVPNMMIDA
251   AKLLSALCIL PQPEDMNERV LEAMTERAEM DEVERFQPLL DGLKSGT SIA
301   LKVGCLQLIN ALITPAEELD FRVHIRSELM RLGLHQVLQE LREIENEDMK
351   VQLCVFDEQG DEDFFDLKGR LDDIRMEMDD FGEV FQIILN TVKDSKAEPH
401   FLSILQHLLL VRNDYEARPQ YYKLIEECVS QIVLHKNGTD PDFKCRHLQI
451   DIERLVDQMI DTKKVEKSEA KATELEKKLD SELTARHELQ VEMKKMENDF
501   EQKLQDLQGE KDALDSEKQQ ITAQKQDLEA EVSKLTGEVA KLSKELEDAK
551   NEMASLSAVV VAPSVSSAA VPPAPPLPGD SGTVIPPPPP PPPLPGGVVP
601   PSPPLPPGTC IPPPPPLPGG ACIPPPQLP GSAAIPPPPP LPGVASIPPP
651   PPLPGATAIP PPPPLPGATA IPPPPPLPGG TGIPPPPPPL PGVGVPPPP
701   PLPGGPGLPP PPPPFGAPG IPPPPPGMGV PFFFFGFV PAAPVLPFGL
751   TPKKVYKPEV QLRRPNWSKF VAEDLSQDCF WTKVKEDRFE NNELFAKLT L
801   AFSAQTKTSK AKKDOEGGEE KKS VQKKVK ELKVLDSKTA QNLSIFLGSF
851   RMPYQEIKNV ILEVNEAVLT ESMIQNLIQ MPEPEQLKML SELKEEYDDL
901   AESEQFGVVM GTVPRLRPRL NAILFKLQFS EQVENIKPEI VSVTAACEEL
951   RKSENFSSLL ELTLLVGNYM NAGSRNAGAF GFNISFLCKL RDTKSADQKM
1001  TLLHFLAELC ENDHPEVLKF PDELAHVEKA SRVSAENLQK SLDQMKKQIA
1051  DVERDVQNFP AATDEKDKFV EKMTSFVKDA QEQYNKLRMM HSNMETLYKE
1101  LGDYFVFDPK KLSVEEFFMD LHNFRNMFLQ AVKENQKRRE TEEKMRRAKL
1151  AKEKAEKERL EKQOKREQLI DMNAEGDETG VMSLLEALQ SGAAFRRKRG
1201  PRQVNRKAGC AVTSL LASEL TKDDAMAPGP VKVPPKSEGV PTILEEAKEL
1251  VGRAS

```

Figure 5: Domain structure of mDia1.

(A) A schematic representation of the mDia1 domain architecture (GBD: GTPase-binding domain [72-130 aa], DID: Diaphanous-inhibitory domain [131-377 aa], DD: dimerization domain [378-452 aa], CC: coiled-coil region [453-570 aa], FH1: formin homology 1 [571-735 aa], FH2 [736-1179 aa], DAD: Diaphanous-autoregulatory domain [1180-1200 aa]) and the newly identified N-terminal basic region BR [1-60 aa]. (B) Amino acid sequence of mDia1. The functional domains are indicated by the same colour code as in A.

to cosediment with mixed multilamellar lipid vesicles containing phosphatidylcholine (PC), phosphatidylserine (PS) and phosphatidylinositol-4,5-bisphosphate (PIP₂) at the respective ratios of 48:48:4. After low-speed sedimentation, proteins from pellets and supernatants were analyzed by SDS-PAGE. The results revealed the BR-phospholipid interaction.

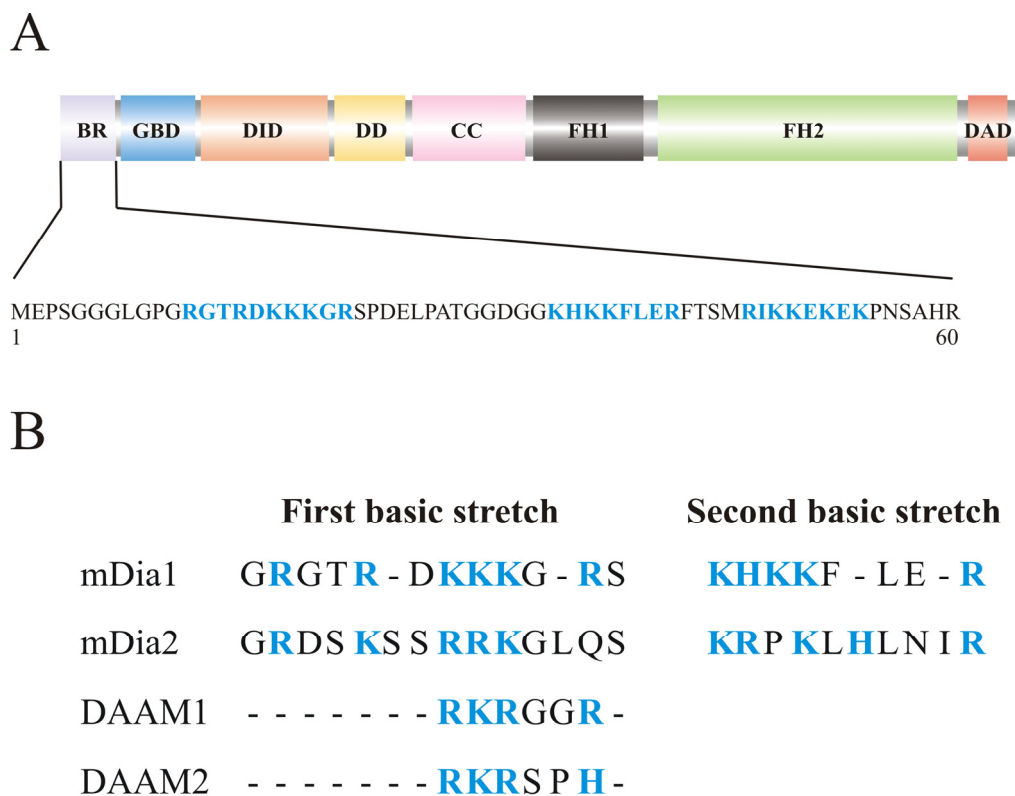


Figure 6: The N-terminal basic region of mDia1, mDia2 and DAAM proteins. The amino acid sequence of mDia1-BR is depicted in (A). The poly-basic clusters are highlighted in blue. (B) Multiple alignments of N-terminal basic regions of various DRFs.

3.1.4 BR alone is sufficient for phospholipid interaction

In order to identify the minimal lipid-binding region several truncation and deletion constructs based on N570 were generated and the respective purified protein fragments tested in spin-down assays. The obtained results confirmed not only the BR-phospholipid interaction but also ruled out any contribution of other regions in the N-terminus. Also the third poly-basic cluster was found to be dispensable for the interaction, which indicated that the first 46 aa (N46) encompassing the first two poly-basic clusters are sufficient and essential for lipid-binding (Figure 7).

GST-mDia1 constructs						phospholipid-binding
BR	GBD	DID	DD	CC	N570	yes
	GBD	DID	DD	CC	Δ BRN570	no
BR	GBD	DID	DD	CC	Δ 47-54N570	yes
R	GBD	DID	DD	CC	Δ 12-46N570	no
BR					N46	yes

Figure 7: BR is essential for interaction with phospholipids.

The spin-down assay results obtained from various truncation and deletion constructs are summarized. Only BR binds to lipids, other regions in the N-terminus did not interact with multilamellar vesicles containing 48:48:4 – PC/PS/PIP₂.

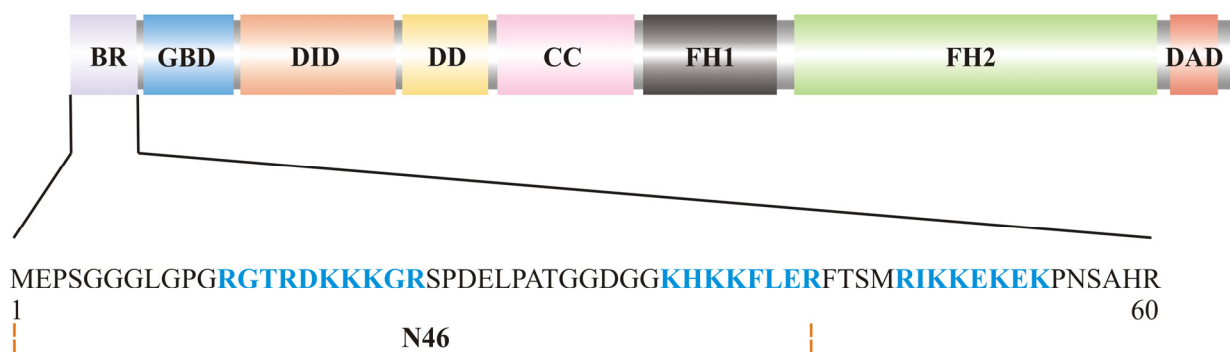
3.1.5 The first two poly-basic clusters are important for lipid-binding

To further map the lipid-binding region(s) within the N46 construct, sedimentation assays were repeated in the presence of synthetic peptides A and B derived from the BR. The first two positively charged stretches (12-21 aa and 35-42 aa) were required and compete with mixed multilamellar lipid vesicles containing PIP₂ and PS (Figure 8). However, the lipid-binding ability of the second basic stretch was at least 5 fold higher than that of the first poly-basic cluster (Figure 8B).

3.1.6 The N-terminal BR interacts specifically with PS

The lipid specificity exhibited by mDia1 N-terminal region was then identified by spin-down assays with varying lipid compositions. The results revealed that the mDia1N46 interacted with mixed lipid vesicles containing both PS and PIP₂. Interestingly, the interaction was also found with liposomes lacking PIP₂ but containing PS, the only negatively charged lipid present in the vesicle bilayer. Cosedimentation assays revealed a noticeable dose-dependent binding of the formin mDia1 BR to PS but not to PIP₂. However, phosphatidylcholine (PC) showed no interaction with the N-terminal formin domain, demonstrating the requirement of negative charges (Figure 9).

A



B

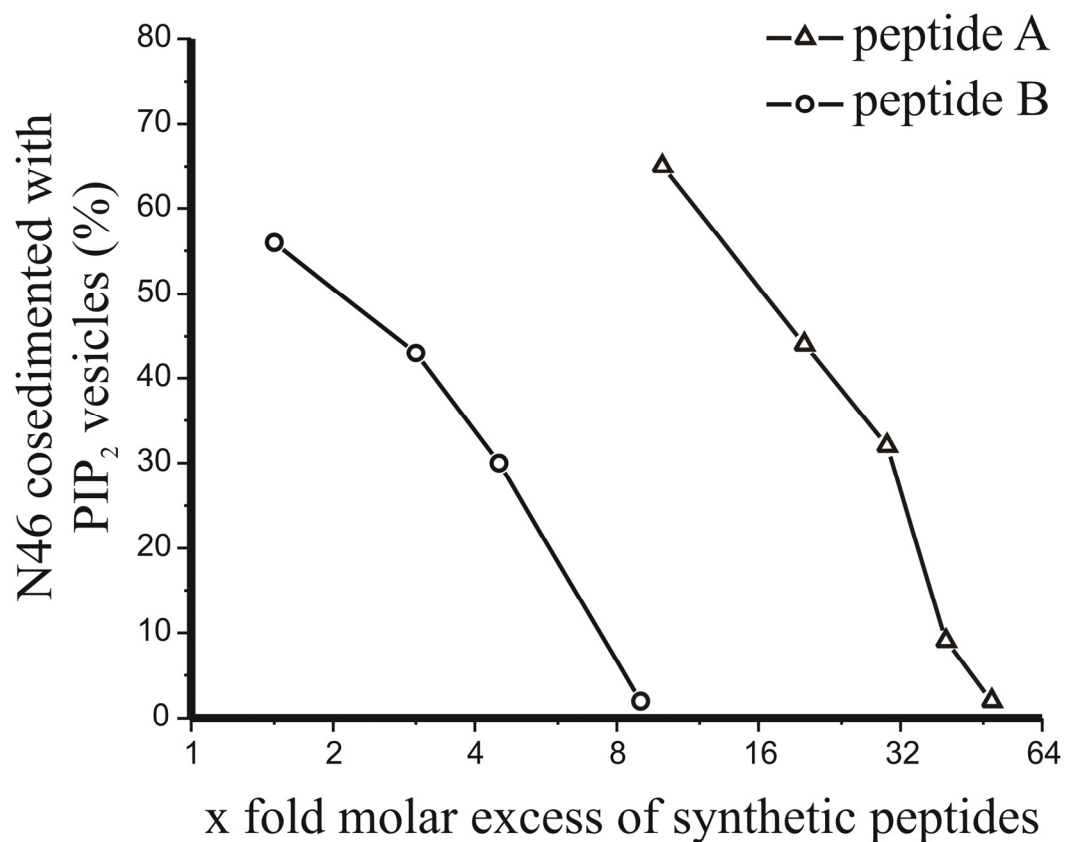


Figure 8: The first two poly-basic clusters are important for interaction with phospholipids. (A) The schematic diagram highlighting the corresponding synthetic peptides. (B). The protein/lipid interaction of N46 requires both basic stretches because each of the synthetic peptides can completely block binding to PIP₂.

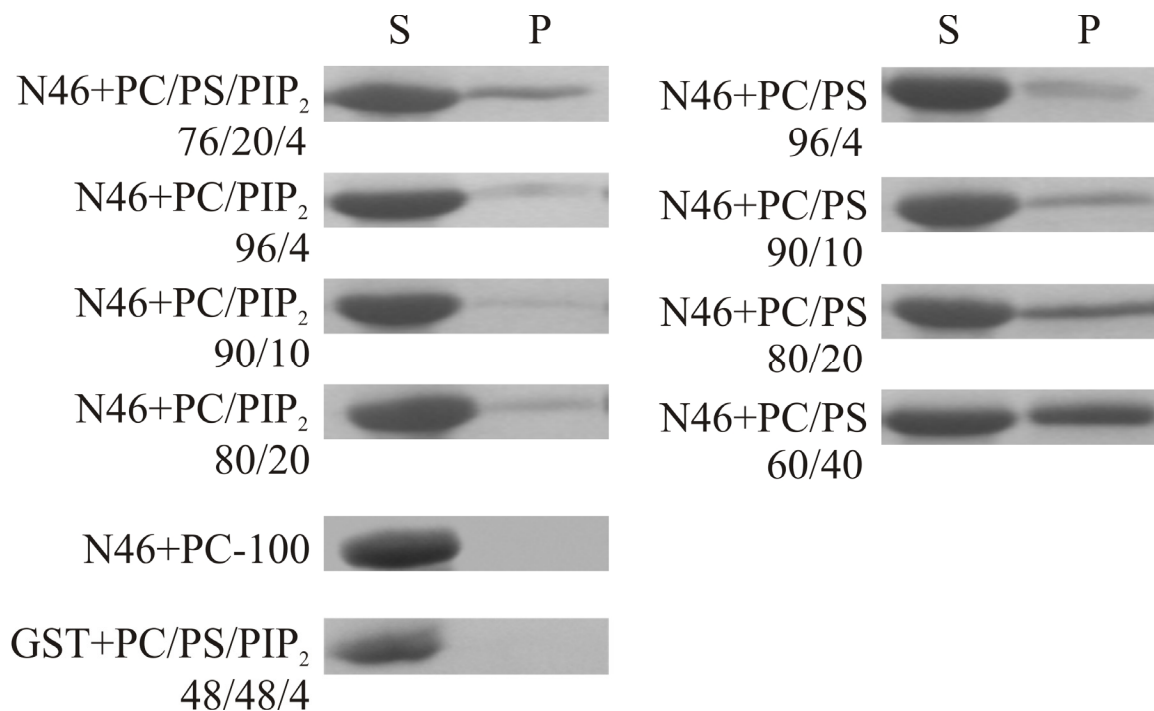


Figure 9: BR specifically interacts with multilamellar vesicles containing PS.

Cosedimentation assays (S: supernatant, P: pellet) revealed that GST-tagged mDia1N46 interacts with mixed lipid vesicles both in the presence (76:20:4 PC/PS/PIP₂) and absence of PIP₂ (96:4, 90:10, 80:20 and 60:40 PC/PS), but not with PC alone. Increased concentrations of PIP₂ (96:4, 90:10, 80:20 PC/PIP₂) did not influence the extent of protein-lipid interaction in the absence of PS. The GST control did not bind lipid vesicles containing PC, PS and PIP₂.

3.1.7 mDia1 N-terminus clusters PS and PIP₂

The mDia1N46-phospholipid interaction was further tested by an additional technique that tells not only the interaction but also if the mDia1 N-terminus clusters lipids. This was done in collaboration with Drs. Hongxia Zhao and Pekka Lappalainen at the Institute for Biotechnology, University of Helsinki (Finland). The GST tags of the protein fragments mDia1N570, mDia1NΔ60N570 and mDia1N46 were cleaved off (see Materials and Methods) and tested for quenching of the fluorescently labelled lipids which would tell if there is a protein-lipid interaction and subsequently the lipid clustering. Essentially, all of the three constructs quenched lipids in a dose-dependent manner but the N-terminal protein fragment missing the BR exhibited only minimum quenching and clustering. Under these conditions the mDia1 N-termini constructs quenched also PIP₂ with a higher magnitude compared to that of the PS (Figure 10). Taken together, the results indicated that the BR-PIP₂ interaction was stronger than that of the BR-PS per se.

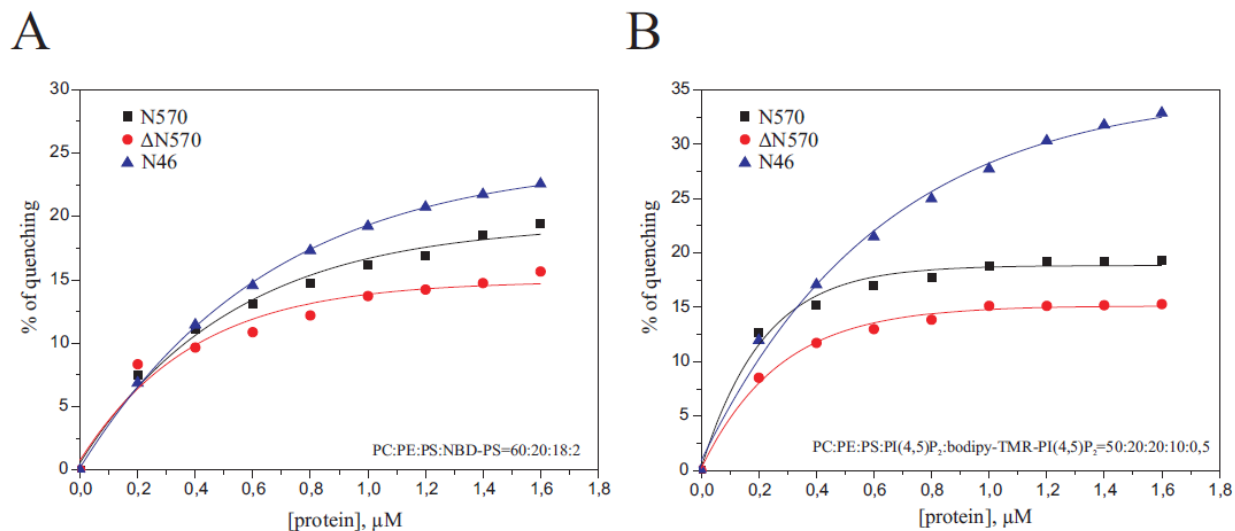


Figure 10: Quenching of lipid fluorescence upon interaction with the basic region of mDia1. Constructs containing or lacking the BR quench the signals of both fluorescently labelled lipids PS (A) and PIP₂ (B). The clustering of PIP₂ by BR only (N46) was most efficient. A protein fragment lacking the BR (Δ BRN570) showed in both cases the least lipid interaction (courtesy of Dr. Hongxia Zhao).

3.1.8 mDia1 N-terminus inserts into the plasma membrane

In the frame of the collaboration with the laboratory of Dr. Lappalainen (Helsinki) we also tested the insertion of BR into the membrane and a resulting membrane deformation. The same three constructs used for the lipid clustering assay were tested for their abilities to insert into the membrane using 'Steady State Fluorescence Diphenylhexatriene Anisotropy'.

Indicated protein constructs under respective concentrations were incubated with the artificially reconstituted plasma membrane comprising PC, phosphatidylethanolamine (PE), PS and PIP₂ in the form of unilamellar liposomes. mDia1N570 was found to be inserted into the membrane containing PIP₂, while the N-terminal construct lacking BR mDia1 Δ 60N570 showed a marked reduction in its ability to insert into the membrane.

Surprisingly, BR alone i.e mDia1N46 did not insert into the membrane (Figure 11). It is also to be emphasized that apart from membrane insertion, the mDia1 N-terminus did not induce noticeable membrane deformations (not shown).

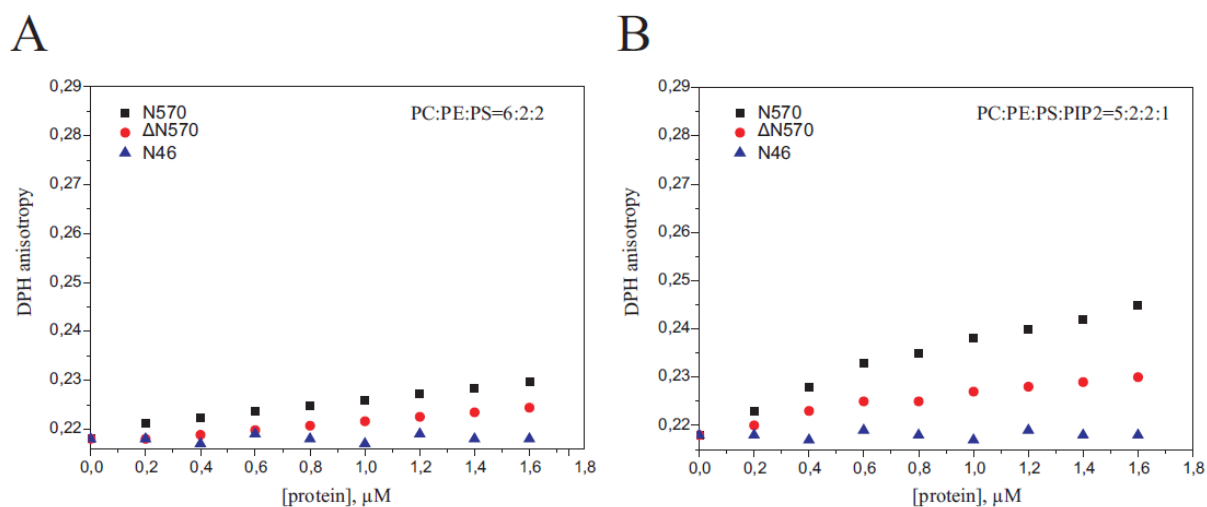


Figure 11: The mDia1 N-terminus inserts into the membrane.

Changes of diphenylhexatriene (DHP) anisotropy implied that both N570 and Δ BRN570 inserted into the plasma membrane independent of the presence of PIP₂. BR only (N46) is apparently too short and did not show significant changes of anisotropy. However, both PIP₂ and the presence of BR in N570 (left panel) boost insertion into the membrane. (Courtesy of Dr. Hongxia Zhao)

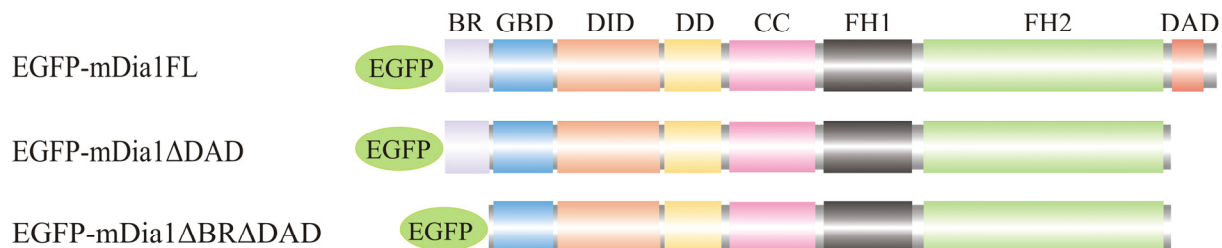
3.1.9 BR is essential for plasma membrane targeting of mDia1

Previously it was shown that the complete N-terminus of mDia1 up to the CC domain was localized to the plasma membrane and that the inactivation of GBD by a point mutation abolished membrane attachment only partially (Seth et al., 2006). This triggered the claim for a membrane binding activity beyond the GBD. In order to figure out if the missing domain resides in the BR, different mDia1 constructs have also been analyzed *in vivo*.

Wild type mDia1 and truncated mDia1 were expressed as enhanced green fluorescent protein (EGFP) fusions in mouse NIH 3T3 fibroblasts (Figure 12A). As expected, the auto-inhibited full-length mDia1 (EGFP-mDia1FL) was distributed uniformly throughout the cell (Figure 12B).

However, in addition and consistent with the *in vitro* data, the BR-lipid interaction was found to be crucial for mDia1 localization since expression of a constitutively active construct lacking both BR and the DAD (EGFP-mDia1 Δ BR Δ DAD) lost its pronounced association with the plasma membrane. However, in less than 5% of all cells expressing EGFP-mDia1 Δ BR Δ DAD, the protein still accumulated at the plasma membrane (Figure 13).

A



B

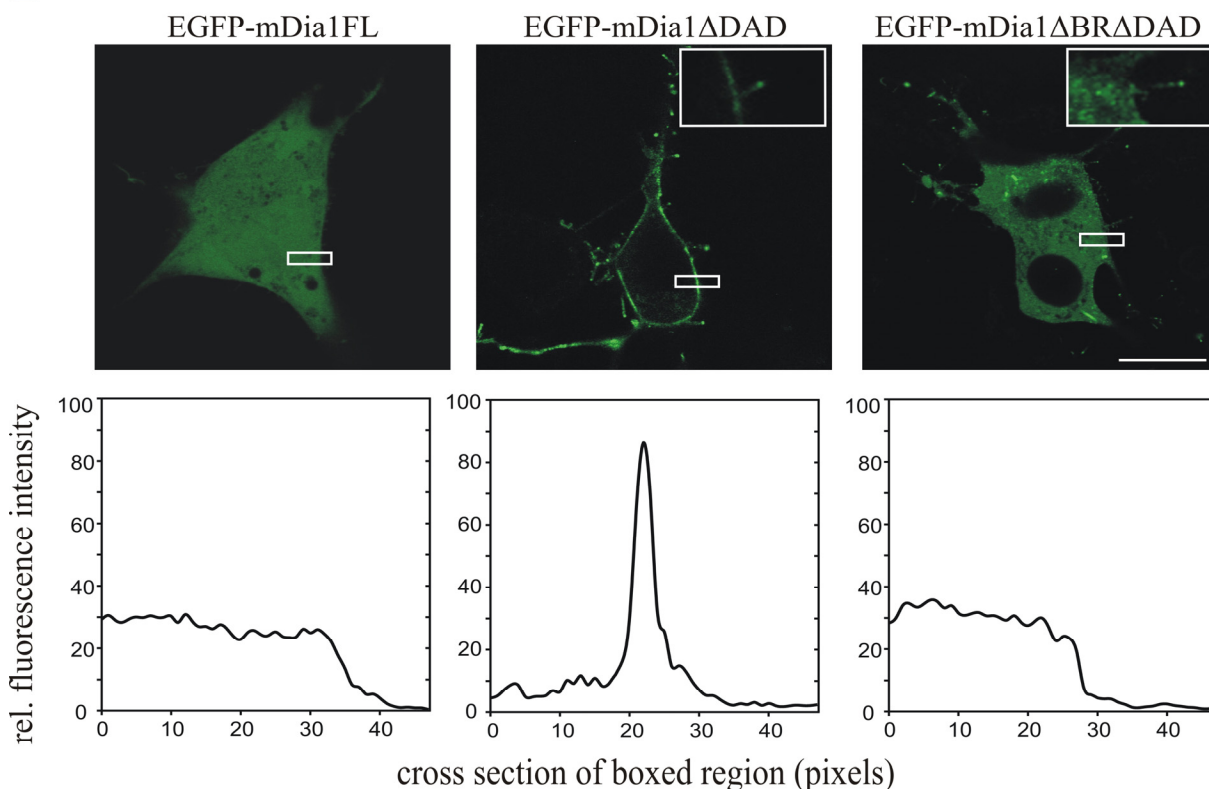


Figure 12: The basic region is essential for recruitment of mDia1 to the plasma membrane.

(A) Schematic representation of the constructs used for the transfections. Indicated constructs were expressed in NIH 3T3 fibroblasts and the live cells were imaged using a LSM510 Zeiss confocal microscope. (B) Representative cells of each mutant are shown; emerging filopodia are enlarged in insets. The scale bar represents 20 μ m. Depicted below are the corresponding plots showing the fluorescence intensity profiles across the plasma membrane (white boxes).

Consequently, expression of a constitutively active construct that still contained the BR but lacked the DAD (EGFP-mDia1 Δ DAD) was recruited to the membrane. Both EGFP-mDia1 Δ DAD and EGFP-mDia1 Δ BR Δ DAD constructs also decorated the filopodial tips (Figure 12B).

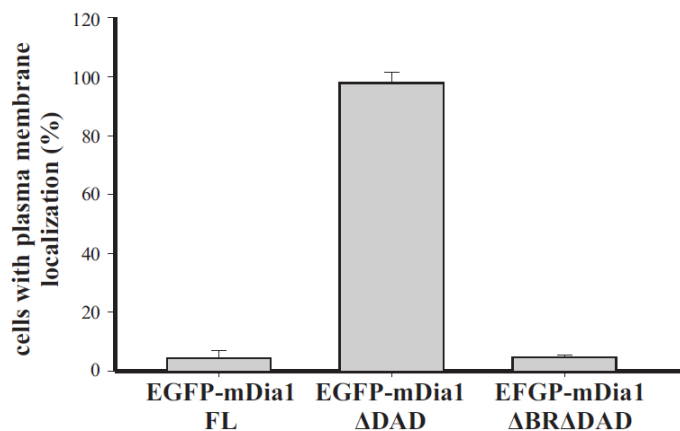


Figure 13: Percentage of cells with plasma membrane localization for each mutant is plotted as a bar chart.

The error bars indicate mean standard deviation of four independent transfections. Overall EGFP-mDia1FL (n = 68), EGFP-mDia1 Δ DAD (n = 88) and EGFP-mDia1 Δ BR Δ DAD (n = 125) cells were counted.

To rule out a putative misfolding of EGFP-mDia1 Δ DAD, assays were done with the constitutively active fragments mDia1 Δ DAD and mDia1 Δ BR Δ DAD as GST fusions. The actin assembly kinetics of both constructs was comparable, so the distinct cellular distributions were not a result of differences in biochemical activity (Figure 14).

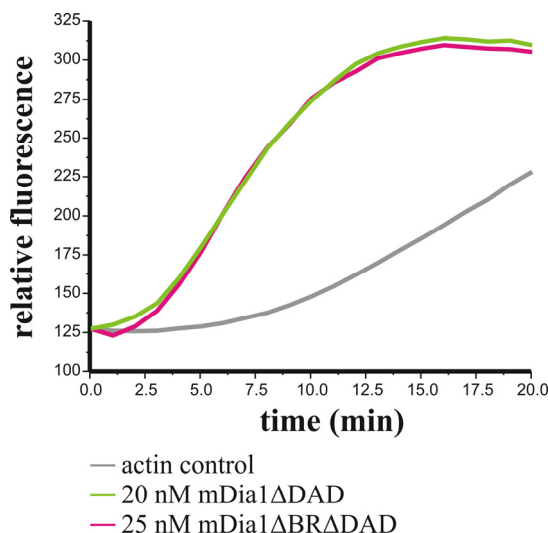


Figure 14: mDia1 Δ DAD and Δ BR Δ DAD constructs are equally active in vitro.

2 μ M actin was polymerized in the presence of recombinant mDia1 constructs mDia1 Δ DAD or mDia1 Δ BR Δ DAD. The actin assembly mediated by mDia1 Δ BR Δ DAD is identical to that of the mDia1 Δ DAD at the respective nanomolar concentrations.

3.1.10 PIP₂-BR interaction does not influence the activity of mDial1

The domain architecture of mDial1 is reminiscent of N-WASp whose auto-inhibition is completely relieved by both Cdc42 and PIP₂ and, therefore, in vitro actin polymerization assays were carried out to decipher the role of PIP₂ in mDial1. The tool for this assay was the artificial inhibition of FH1FH2DAD by a four fold molar excess of N570. The two distinct proteins bind to each other in the same fashion as it is the case in auto-inhibited full-length formin. This intermolecular DID/DAD interaction was partially abolished by an addition of nearly a thousand fold molar excess of constitutively active RhoAV14.

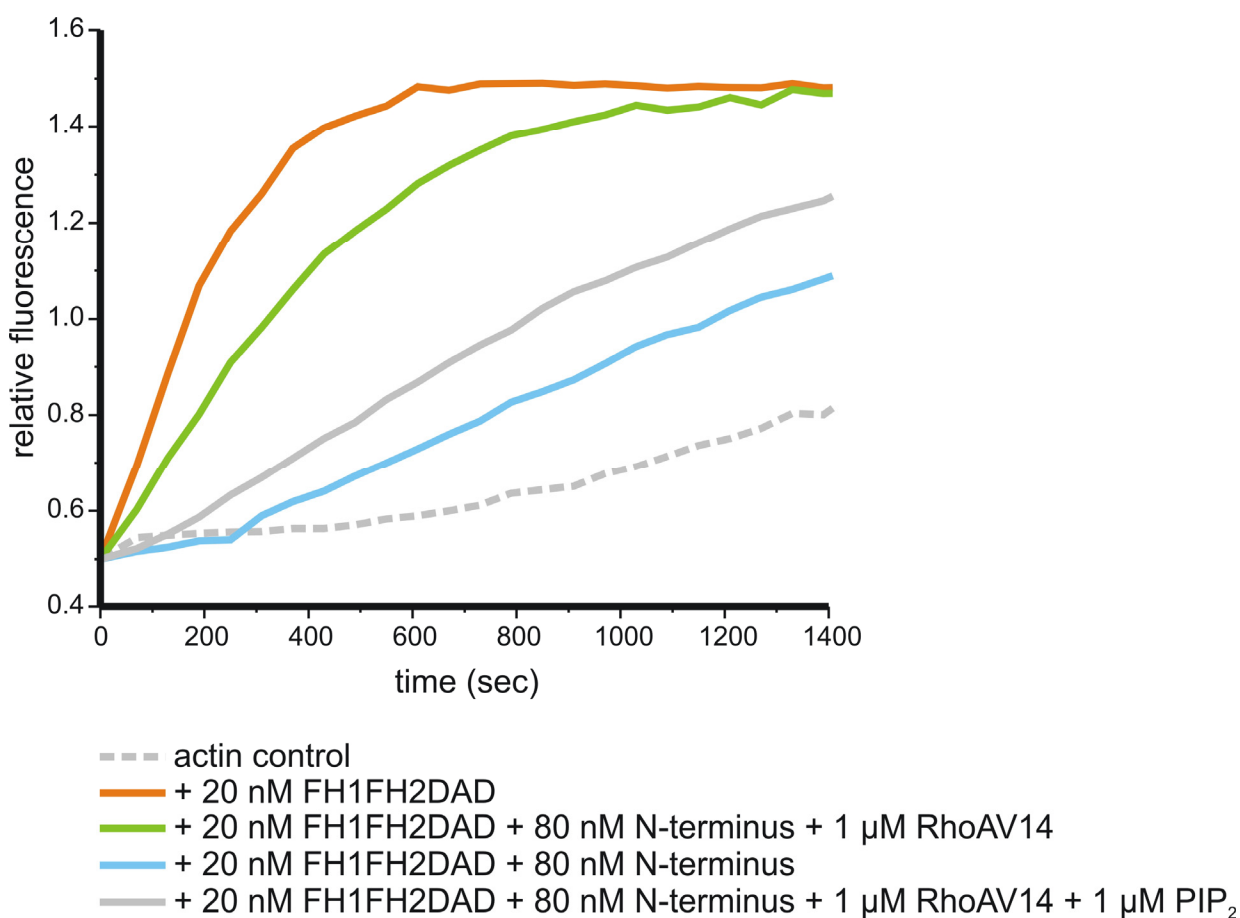


Figure 15: PIP₂ inhibits RhoA induced mDial1 activity.

2 μM actin was polymerized in the presence of mDial1FH1FH2DAD (orange). Addition of the N-terminus of mDial1 resulted in auto-inhibition (blue). Auto-inhibition was relieved by adding constitutively active RhoA GTPase (green) and this activation was inhibited by PIP₂ (grey). Actin control is indicated by a dotted grey line.

Assuming that PIP₂ will synergistically activate formin activity along with RhoAV14, the multilamellar liposomes (48:48:4, PC/PS/PIP₂) were added to the cocktail of protein mixtures containing FH1FH2DAD, N-terminus and RhoAV14.

Surprisingly, an inhibition in the formin activity was evident and not due to the BR-PIP₂ interaction as the control actin assembly in the presence of FH1FH2DAD was significantly affected (Figure 15). The results suggest very clearly that

(1) the BR-PIP₂ interaction did not influence the formin activity synergistically with RhoA, and

(2) the presence of a second phospholipid-binding region in mDia1, possibly at the C-terminus which is important for the negative regulation of formin activity.

3.1.11 PIP₂ negatively regulates the activity of mDia1

To get further insight into the effects of PIP₂ on formin-mediated actin assembly in vitro **T**otal **I**nternal **R**eflection **F**luorescence (TIRF) microscopy was employed to evaluate the impact of PIP₂ on formin-mediated actin assembly at the single filament level. mDia1-associated actin filaments were previously shown to grow indistinguishable from the actin control in the absence of profilin (Kovar et al., 2006).

Although profilin enhances mDia1-mediated actin assembly about 5-fold, allowing discrimination between formin-mediated and spontaneous actin assembly, profilin could not be used in the experimental set up because PIP₂ has also been shown to be a potential inhibitor of the profilin-actin interaction (Lassing and Lindberg, 1985). Therefore, glass slides were coated with GST-formin constructs and low amounts of **N**-**e**thyl**m**aleimide (NEM)-myosin II. After addition of actin monomers in the absence of profilin the appearance of actin filaments was analyzed in a 100 μm² area.

In many cases, emerging actin filaments were immediately captured by NEM-myosin and immobilized formin. The formin-enhanced addition of actin monomers at the barbed end elongated the filament but there was no free movement possible if the pointed was glued to a NEM-myosin (see also Figure 16).

Consequently, three characteristic features could be observed under these conditions:

(1) the appearance of “buckling” filaments due to the insertional assembly of monomers at the barbed ends while the filaments were also attached to the substrate by NEM-myosin II,

- (2) the capture of spontaneously growing and passively attached actin filaments by formins, also resulting in filament buckling, and
- (3) the fluorescence of filaments is bright at the immobilized growing barbed ends while it fades away towards the pointed end due to bleaching.

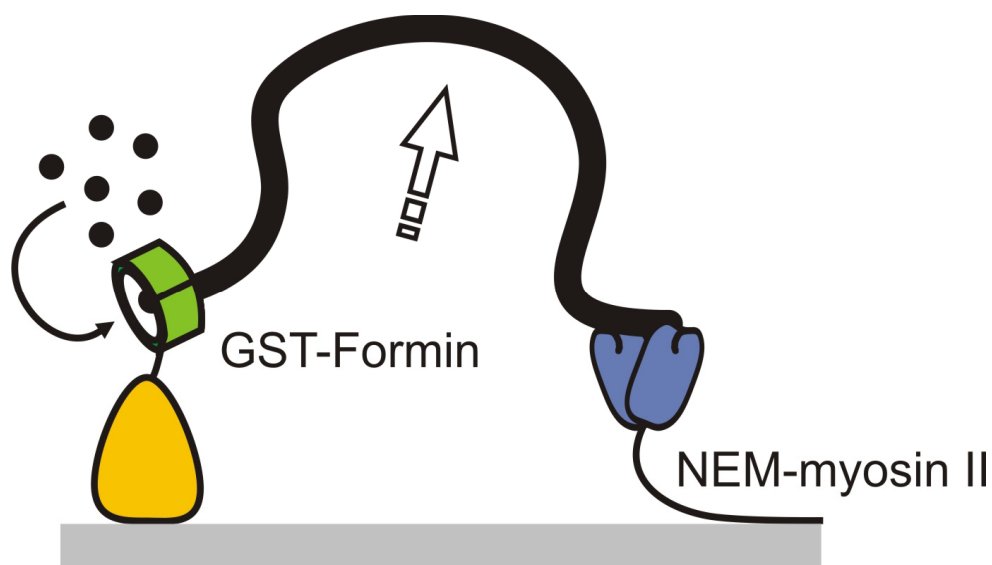


Figure 16: Scheme of insertional assembly of monomers to a filament bound to GST-mDia1 and NEM-myosin II.

The regulation of full-length mDia1 activity was tested in the presence of RhoA GTPase and phospholipids, thus for the first the time the regulation of full-length mDia1 has been elucidated.

Predictably, auto-inhibited full-length mDia1 (mDia1-FL) alone exhibited only a basal activity accounting for less than 5 active formins of the total filament assembly. An addition of constitutively active RhoAV14 enhanced mDia1-mediated actin assembly up to a maximum of 100 active formins; incubation of PIP₂ containing vesicles to GTPase-activated mDia1 drastically impaired its activity (Figure 17).

A detailed examination of mDia1FH1FH2DAD (697-1255 aa) revealed that about 350 of all growing filaments were assembled by a formin, whereas its activity was inhibited by the addition of PIP₂ containing vesicles. A mixture of PS and PC in the absence of PIP₂ failed to inhibit actin polymerization demonstrating specificity of inhibition by the phospholipid (Figure 18).

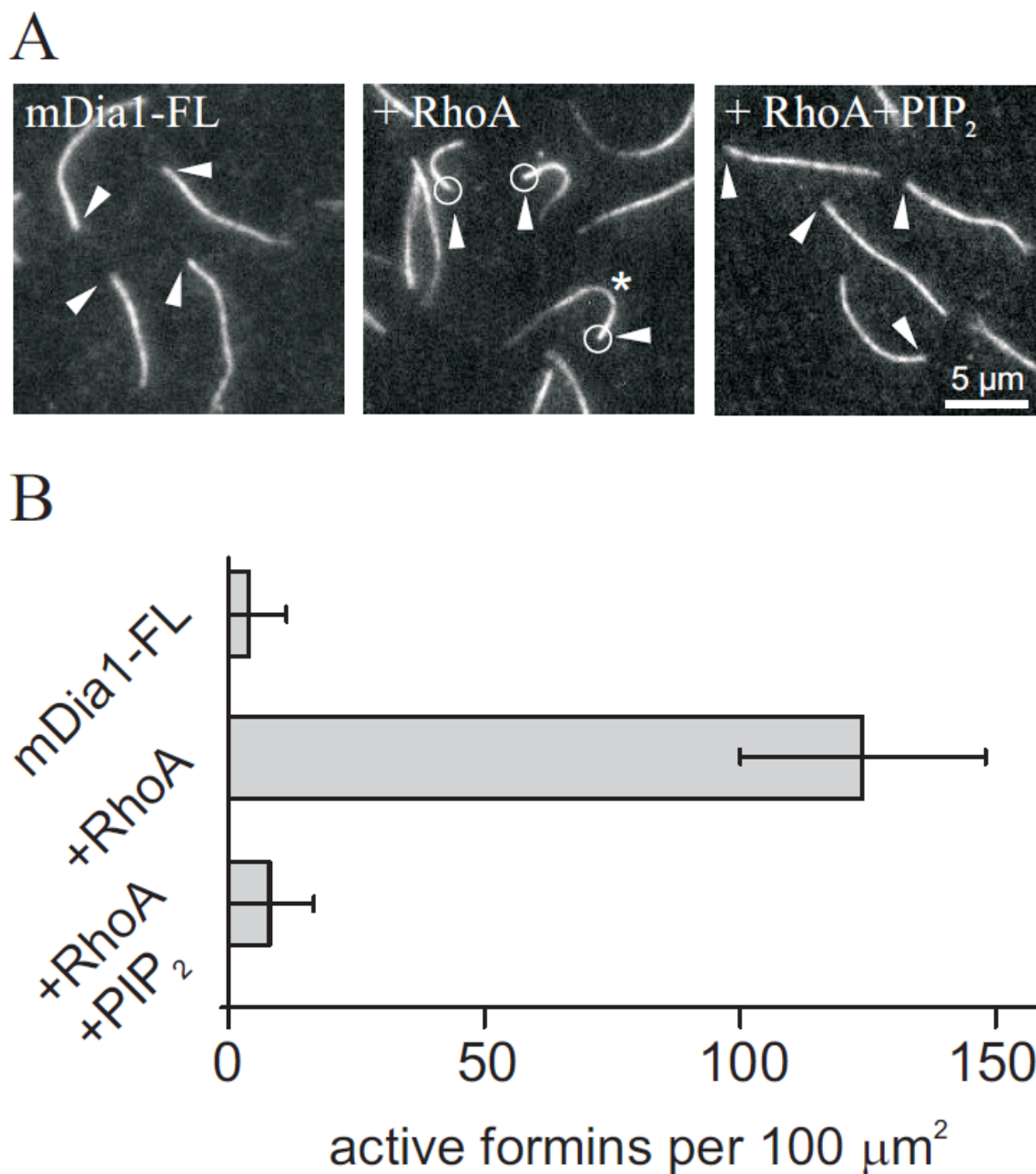


Figure 17: TIRF-microscopy of actin filaments assembled by full-length mDia1. (A) Micrographs of the assembly of 1 μM ATP-actin and 0.3 μM Alexa-Fluor-488-labelled actin in TIRF buffer on cover slips coated with 10 nM NEM-myosin II and 400 nM of mDia1-FL. Addition of 5 μM GTP-bound RhoAV14 resulted in activation of mDia1. Addition of 1 μM PIP₂ (48:48:4, PC/PS/PIP₂) inhibited formin-mediated actin assembly. Arrows indicate growing filament barbed ends, circles mark barbed ends captured by a RhoA-activated mDia1. The asterisk highlights a representative formin-induced buckling filament. (B) Quantification of active mDia1-FL molecules. For each experiment an area of 100 x 100 μm^2 was analyzed, error bars indicate standard deviations.

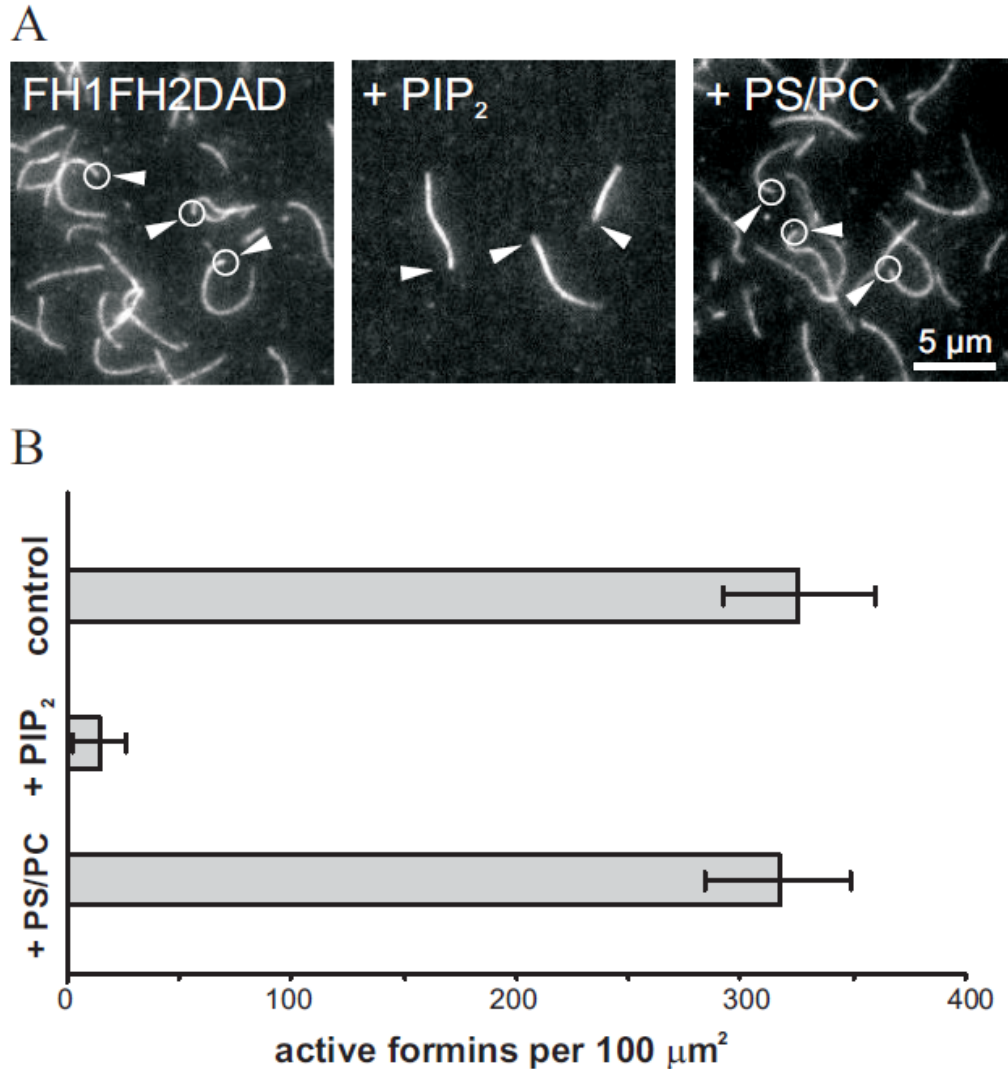


Figure 18: TIRF-microscopy of actin filaments assembled by mDia1FH1FH2DAD. (A) Micrographs of the assembly of 1 μM ATP-actin and 0.3 μM 488 actin in TIRF buffer on cover slips coated with 400 nM FH1FH2DAD. 1 μM PIP₂ (48:48:4, PS/PC/PIP₂) inhibits FH1FH2DAD-mediated actin assembly. The addition of vesicles lacking PIP₂ (only 50:50, PS/PC) had no effect on formin activity, indicating a specific inhibition by PIP₂. Symbols as in Figure 13. (B) Quantification of active FH1FH2DAD. Error bars indicate standard deviation.

The regulation of formins by PIP₂ occurs also in other formins and in different species. PIP₂ inhibits the activities of at least four DRFs: mDia1, mDia2, mDia3 (Figure 19) and *D. discoideum* ForA (not shown) by an auto-inhibition independent mechanism. Since neither filament nucleation nor the capture of spontaneously growing filaments was observed in the presence of PIP₂, it is assumed that this acidic lipid as part of multilamellar liposomes entirely blocks the interaction of the formins with actin.

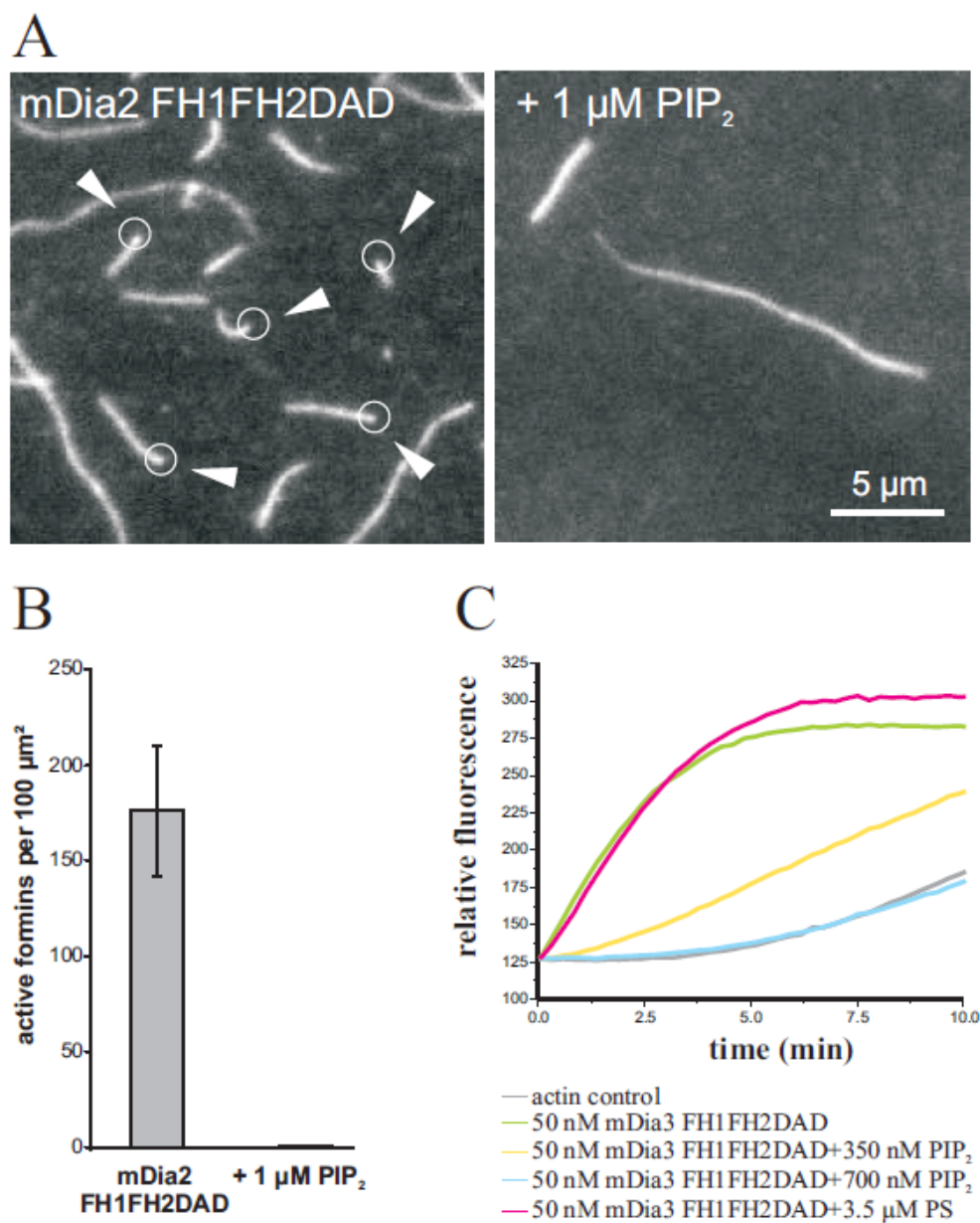


Figure 19: PIP₂ inhibits the activities of mDia2 and mDia3 as well.

(A) Micrographs of the assembly of 1 μM ATP-actin and 0.3 μM 488-actin in TIRF buffer on cover slips coated with 10 nM NEM-myosin II and 400 nM of mDia2FH1FH2DAD. Addition of 1 μM PIP₂ inhibits the activity of mDia2. Arrows indicate growing filament barbed ends and circles mark barbed ends captured and/or buckled by mDia2. (B) Quantification of active mDia2 FH1FH2DAD. Error bars indicate standard deviation. (C) 2 μM actin was polymerized in the presence of indicated concentration of mDia3 FH1FH2DAD and as much as 700 nM PIP₂ inhibits its activity. Multilamellar vesicles lacking PIP₂ exhibit no effect.

All in vitro TIRF based experiments were done together with Dennis Breitsprecher and Dr. Jan Faix, Department of Biophysical Chemistry, Hannover Medical School, Hannover.

3.1.12 Potential phospholipid-binding sites at the C-termini of formins

Sequence analysis of the C-terminal regions encompassing the DAD of various formin proteins across the species ranging from yeast and social amoebae to mammals (Figure 20) revealed the presence of a highly conserved poly-basic cluster. Poly-basic clusters of amino acids, in general are thought to be potential targets for protein-lipid interaction.

mDia1 (O08808)	1196	R R K R	1199	
hDia1 (O60610)	1213	R R K R	1216	
mDia2 (AAH85191)	1257	R R K R	1260	
hDia2 (NP_001035982)	1078	R R K R	1081	
mDia3 (O070566)	1069	R R K R	1072	
hDia3 (AAI17415)	1079	R R K R	1082	
INF2 (ABI20145)	1264	K R R K K R	1269	mammalian formins
DAAM1 (AAR05118)	1053	K R N R K R	1058	
DAAM2 (AAR05119)	1091	K R N R K R	1096	
FHOD1 (BAC27106)	1161	R K R S R	1165	
FHOD2 (BAC98303)	1391	R K R S R	1395	
dDia1 (CAH23234)	1005	R R R L K	1009	
dDia3 (CAH23233)	1529	K G R R R	1532	
dDia4 (CAH25332)	925	K K K K	928	<i>D.discoideum</i> formins
ForA (Q54WH2)	1200	R R R R	1203	
ForJ (Q54ER5)	2333	K K H K K	2337	
Bni1 (CAA63225)	1548	K L R K	1551	
Bnr1 (P40450)	1332	R R R K	1335	
Cdc12 (Q10059)	1722	R G R R R	1726	yeast formins
For3 (O94532)	1427	R R K G H	1431	
Fus1 (Q10719)	1347	N K K R	1350	

Figure 20: The poly-basic cluster in the DAD is conserved in most formins.

The multiple alignments of various formin proteins (GenBank accession number IDs are shown in parenthesis) from mammals (red), *D. discoideum* (blue) and yeast (green) show the conserved basic residues (flanked by amino acid positions), possibly modulating the PIP₂-mediated negative regulation.

3.1.13 DAD relieves the PIP₂-mediated inhibition of mDia1 activity

The intra-molecular interaction of DID and DAD was previously shown to be crucial for auto-inhibition of formins in vitro and in vivo. The inhibitory activity by PIP₂ employs an entirely different mechanism. This was unequivocally shown by addition of an excess of the mDia1DAD (aa 1180-1255) containing the poly-basic RRKR motif to the mDia1FH1FH2DAD

fragment and incubation with PIP₂. In a strictly dose-dependent manner the inhibition by PIP₂ could be outcompeted at increasing concentrations of the DAD (Figure 21).

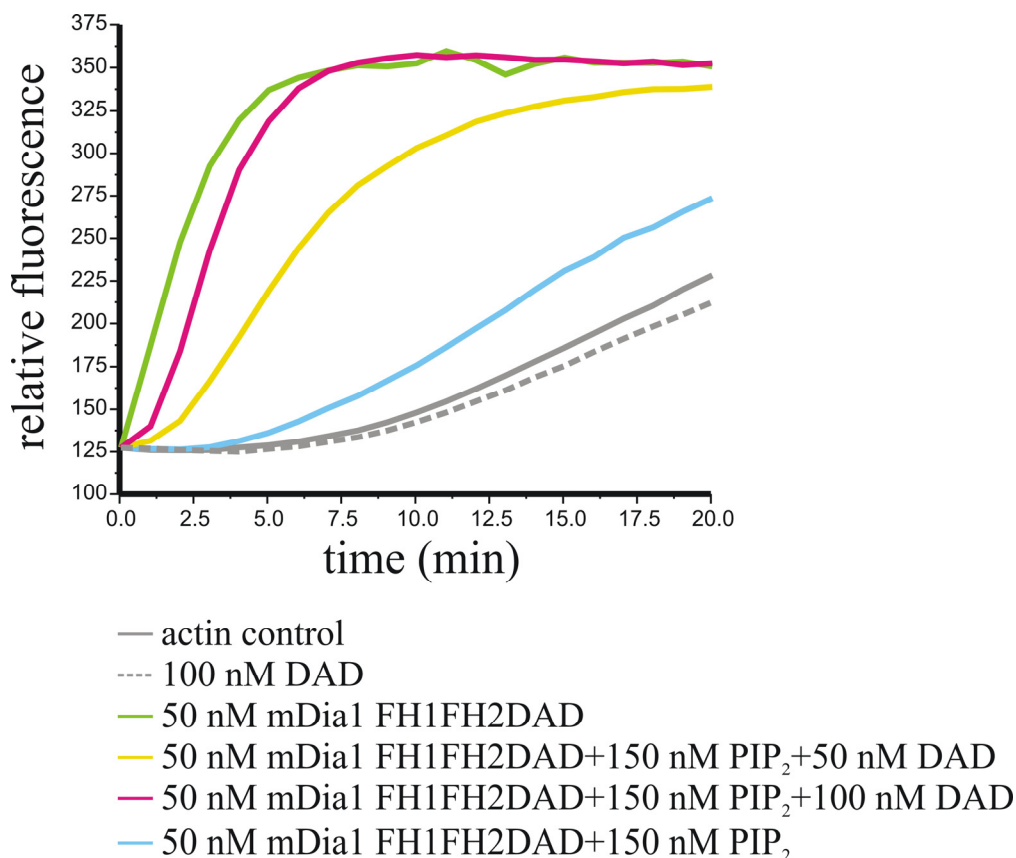


Figure 21: mDia1DAD relieves PIP₂-mediated inhibition of FH1FH2DAD activity.

The green line represents actin assembly mediated by FH1FH2DAD. While PIP₂ inhibited the assembly (blue line), the addition of increasing amounts of mDia1DAD relieved the inhibition by PIP₂ in a dose-dependent manner (yellow and magenta). However, mDia1DAD alone did not influence the actin assembly (dotted grey lines). Grey line represents the actin control.

3.1.14 mDia1FH1FH2DAD is inhibited also by unilamellar PIP₂ vesicles

The common procedure to 'solubilize' distinct lipids or lipid mixtures leads in most cases to multilamellar vesicles and triggers frequently the criticism that this type of vesicles does not reflect in vivo conditions. Therefore, further experiments were carried out with unilamellar liposomes that have been produced by the mini-extruder (see Materials and Methods). Titrations with different ratios (96:4, 90:10, 80:20 and 70:30; PC/PIP₂) of the liposome mixtures showed that also unilamellar lipid vesicles inhibited formin-induced actin assembly in a dose-dependent fashion with increasing concentrations of PIP₂ (Figure 22).

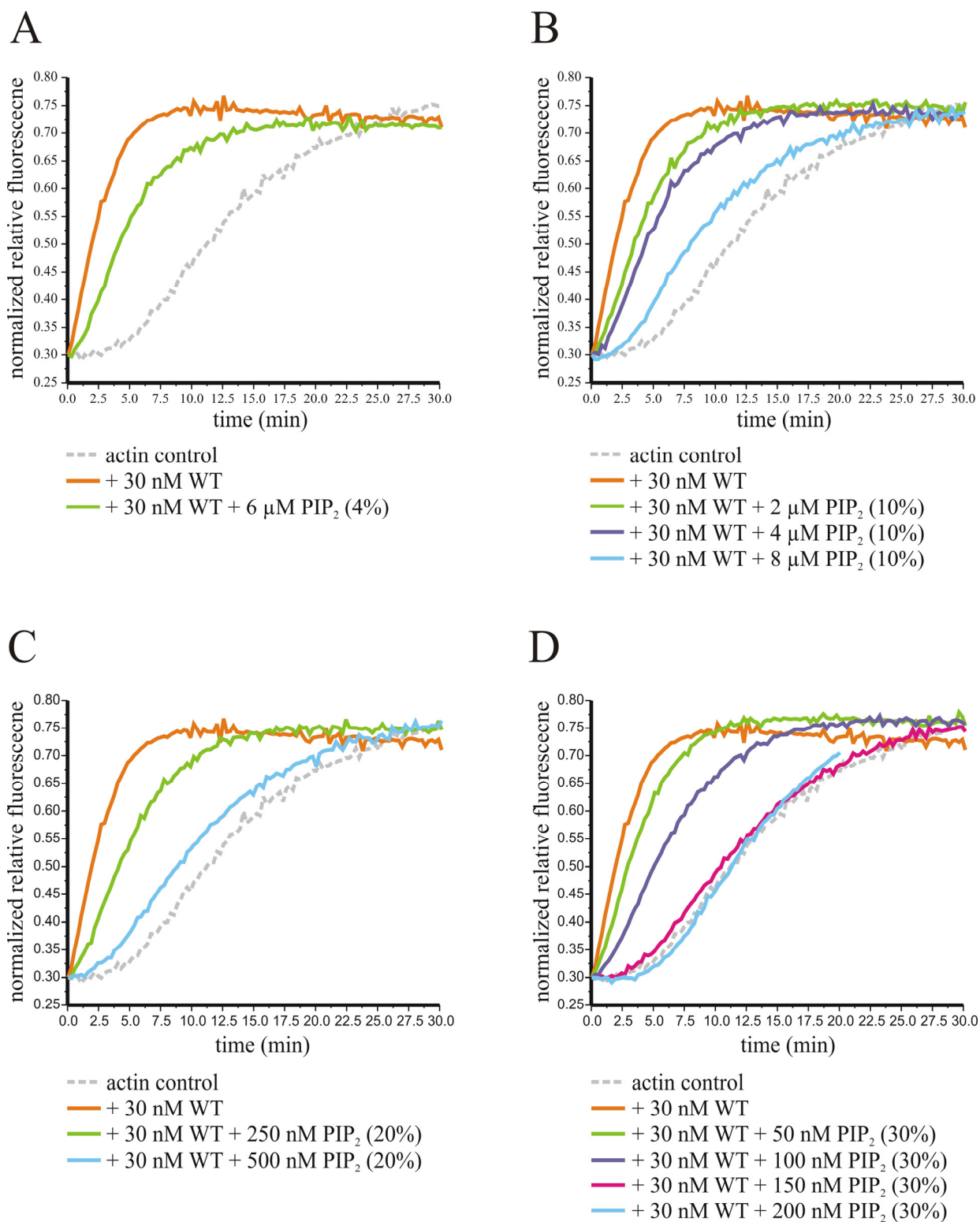


Figure 22: Unilamellar PIP₂ vesicles also inhibited mDia1-mediated actin assembly.

Lipid vesicles with PC/PIP₂ ratios of 96:4, 90:10, 80:20 and 70:30 and their impact on formin-induced actin polymerization are shown in (A), (B), (C) and (D), respectively. 3 μM actin was used throughout.

3.1.15 The C-terminal region of mDia1 harbors at least two PIP₂-binding sites

An alanine screening identified the conserved poly-basic cluster that contributes to PIP₂-binding and, consequently, changes of actin polymerization kinetics by mDia1 (Figure 23). The recombinant mDia1-Mut1 fragment carrying a quadruple alanine substitution (1196-RRKR-1199 > 1196-AAAA-1199) exhibited increased actin assembly in the presence of PIP₂ in comparison to the wild type construct mDia1FH1FH2DAD (Figure 24A and B). This confirms that DAD is not only crucial for auto-inhibition of full-length formin but also for the negative regulation of an active mDia1 by PIP₂.

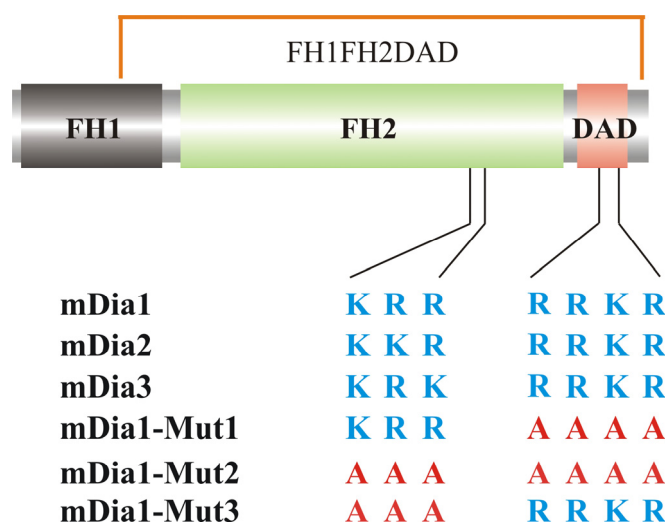


Figure 23: The C-terminus of mDia1 contains two potential PIP₂-binding regions (blue). mDia1 constructs carrying respective Ala point mutations are marked in red.

Notably, the quadruple Ala mutation construct did not entirely restore actin polymerization in the presence of PIP₂. Further screening revealed the presence of yet another PIP₂-binding site within the FH2 domain. An additional triple alanine substitution of the highly conserved basic residues (1137-KRR-1139 > 1137-AAA-1139) in the FH2 domain (mDia1-Mut2) rendered the mutated construct significantly PIP₂-insensitive (Figure 24C). mDia1-Mut3 carrying only the triple alanine substitutions also behaved like the Mut1 variant (Figure 24D). These data demonstrate that both PIP₂-binding sites are important for negative regulation of mDia1. The lipid sensitivity of the protein constructs were summarized as WT>Mut1=Mut3>Mut2 (Figure 25) but it is also to be noted that the 7x alanine substitutions did not completely prevent the inhibition by PIP₂.

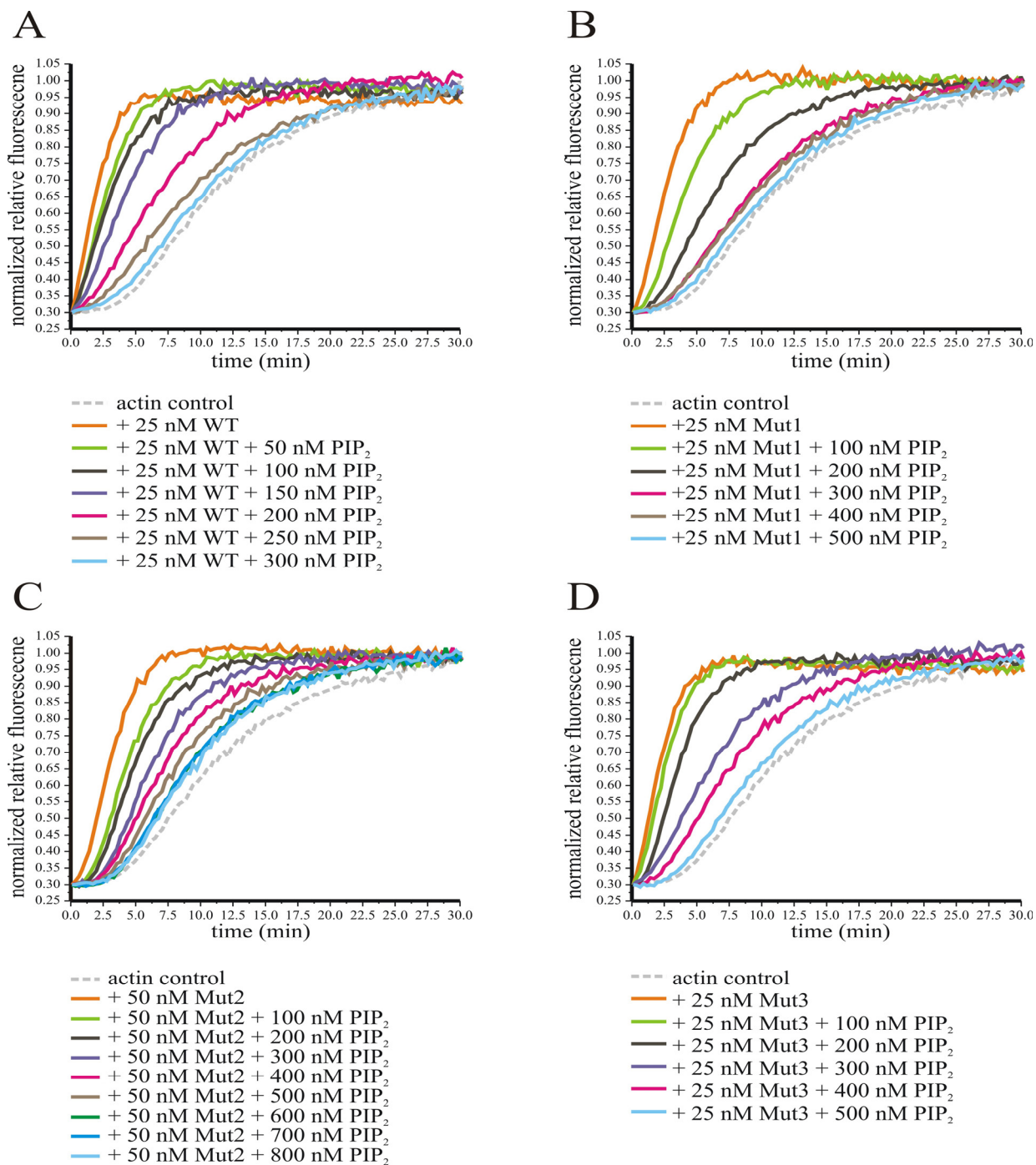


Figure 24: Differential sensitivity of the mDia1FH1FH2DAD variants to PIP₂.

(A) Actin assembly mediated by mDia1-WT is affected by unilamellar PIP₂ (70:30, PC/PIP₂), but filaments assembled by mDia1-Mut1 and mDia1-Mut3 (B and D) are inhibited only at high concentrations of the lipid. mDia1-Mut2 promoted actin polymerization that remained least affected by PIP₂. 3 μ M actin was used throughout.

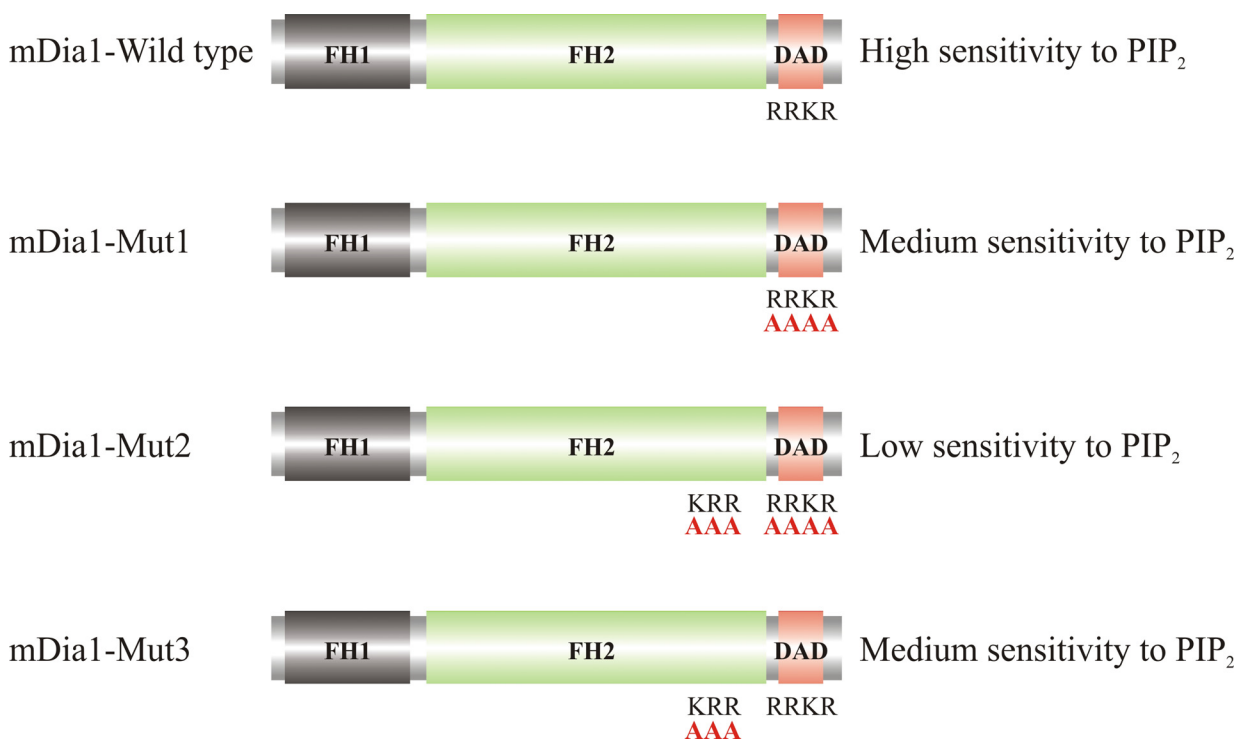


Figure 25: Summary of the PIP₂-mDia1FH1FH2DAD interaction.

A schematic representation of sensitivity of various recombinant protein fragments including mDia1FH1FH2DAD wild type and variants to PIP₂ is depicted.

3.1.16 mDia1FH1FH2DAD clusters PIP₂ and inserts into the plasma membrane

Pyrene assays suggested that the C-terminus of mDia1 spanning the FH1FH2DAD region might cluster unilamellar PIP₂ vesicles. Upon uptake of fluorescent lipids into a membrane the intensity of the signal is reduced and thus the quenching of fluorescence is a measure for clustering and lipid insertion. Wild type and point mutated constructs used in pyrene assays were tested for their abilities to cluster PIP₂. Indeed, wild type mDia1FH1FH2DAD quenched fluorescent PIP₂ in a dose-dependent manner more effectively than fluorescent PS (Figure 22A and B). In consistent with the pyrene assays the PIP₂ clustering activities of mDia1 FH1FH2DAD wild type and variants are in the descending order of wild type-Mut1=Mut3-Mut2 (Figure 26A and B).

The mDia1 C-terminal region spanning the FH1FH2DAD was also found to insert into the artificially reconstituted membrane like the BR. Surprisingly, there were no differences observed in the extent of membrane insertion with wild type and various mutation constructs.

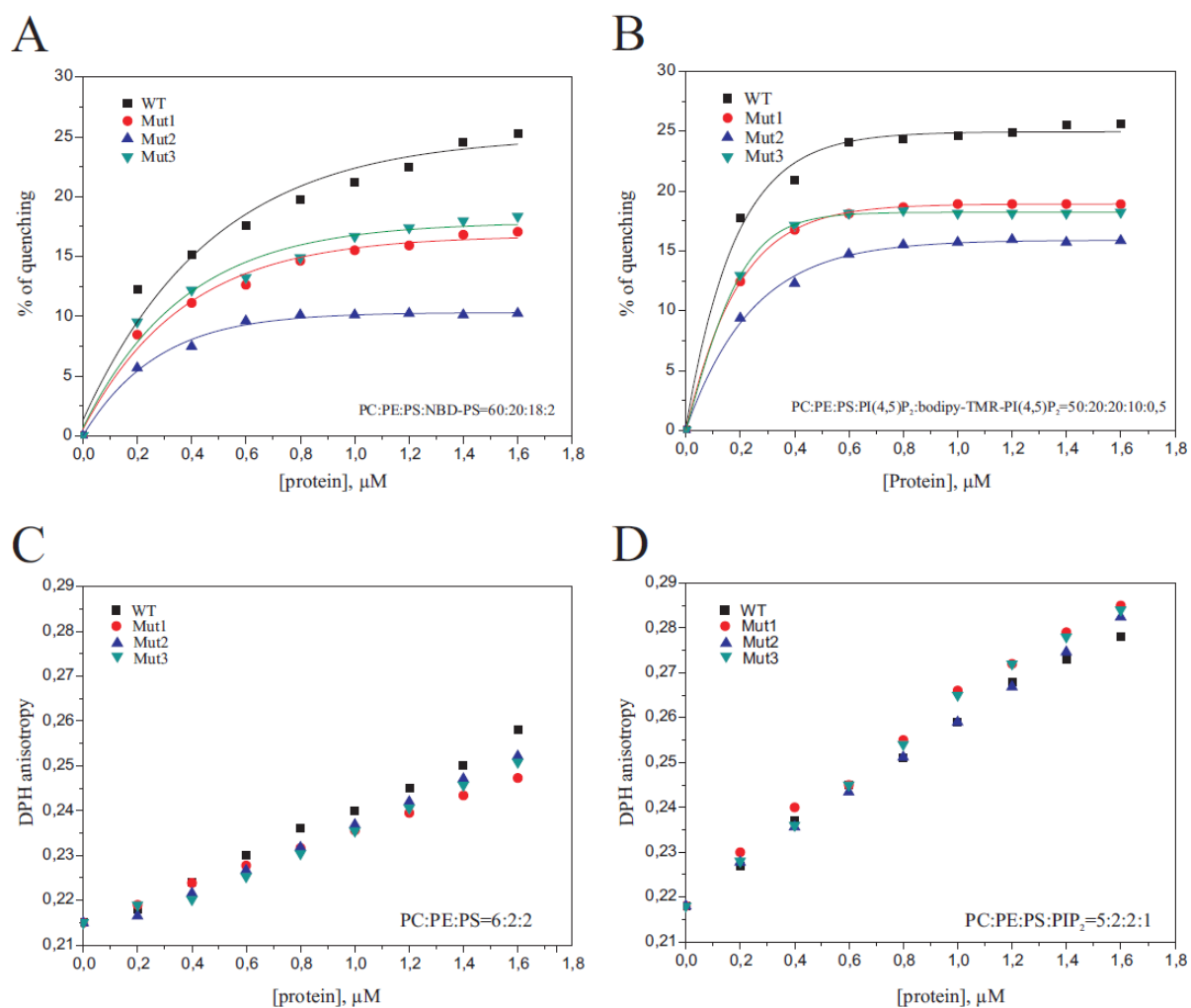


Figure 26: Clustering and membrane insertion of PIP₂ induced by the mDia1FH1FH2DAD. Wild type mDia1FH1FH2DAD effectively clusters PIP₂ (A) and PS (B). Both Mut1 and Mut3 were less efficient than wild type, while Mut2 was the weakest. The same constructs were tested for membrane insertion. All constructs exhibited a more or less similar behavior, but better membrane insertion was seen with unilamellar vesicles containing PIP₂ (C, D).

The PIP₂ clustering activity of mDia1FH1FH2DAD seems to be independent of the membrane insertion phenomenon. In agreement with the pyrene assay data the magnitude of plasma membrane insertion was several folds higher in the presence of PIP₂ than its absence suggesting the phospholipids specificity (Figure 26C and D).

3.2 Characterization of ForA

3.2.1 Formins from *D. discoideum*

The complete sequencing of the *D. discoideum* genome revealed the presence of 10 formin genes and their respective protein products are named as ForA through ForJ. The *D. discoideum* life cycle is finely tuned by a developmental program that is completed within 24 hours under laboratory conditions. Real-Time PCR shed light on the expression pattern of different formin genes during distinct stages of the life cycle. ForC, D, I and J turned out to be developmentally regulated genes while the rest of the formin genes seem to be active throughout development (Rivero et al., 2005). Since several scientific groups (including our own lab) initiated formin research before the genome project was finished, the nomenclature is still confusing. The formins ForD (DDB0205290), ForE (DDB0190413), ForF (DDB0188569) and ForH (DDB0186588) are also known as dDia4, dDia3, dDia1 and dDia2 respectively.

3.2.2 *D. discoideum* contains conventional DRFs and more specialized formins

Analyses of N-terminal regions of the 10 different formin proteins suggested that at least 6 (dDia1, dDia2, dDia3, dDia3, ForA and ForB) belong to the DRF family as they possessed clearly a GBD (Figure 27). The other four are devoid of the characteristic GBD and are, therefore, grouped as non-DRFs. In addition to the classical formin domains that have been identified in mammalian cells, several formins in the social amoeba *D. discoideum* contain additional domains. Most notably, dDia3 and ForA harbor protein kinase conserved region 1 (C1) and 2 (C2), respectively.

Amongst the 10 formin isoforms, only two formins ForC and dDia2 have been characterized in more detail (Kitayama and Uyeda, 2003; Schirenbeck et al., 2005). ForC, a DRF which lacked both the structural and functional FH1 domain has been implicated in the regulation of multicellular development, while dDia2 (an ortholog of mammalian mDia2) happened to be essential for the formation and maintenance of filopodia.



Figure 27: Putative GBD of *D. discoideum* DRFs.

dDia1, dDia2, dDia3, dDia4, ForA and ForB are part of the DRF family as they harbor distinct GBD at their N-termini which are aligned with mDia1. Amino acid residues in the GBD of mDia1 shaded in yellow are important for Rho interaction (Lammers et al., 2005), identical residues in *D. discoideum* formins are also shaded in yellow. The arrow head points out the essential amino acid for Rho binding. Please note that the crucial methionine residues are leucines or isoleucines in dDia2, dDia3, dDia4, ForA and ForB (grey shades). The rest of the conserved residues are in green shades. The gap between the two amino acid clusters represents less conserved regions (approximately 20-30 aa).

3.2.3 ForA is a DRF and contains a C2 domain

ForA is encoded by 6 exons in the *forA* gene (3657 bp) on chromosome 3, the protein consists of 1218 amino acids with a calculated molecular mass of 135 kDa protein (Figure 29B). Both the mRNA (Figure 28A) as well as the protein (Figure 28B) are present throughout the *D. discoideum* development.

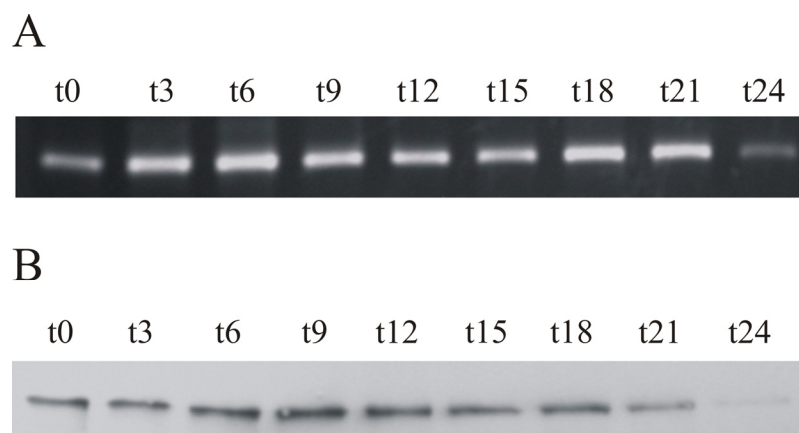


Figure 28: ForA expression profile.

(A) RT-PCR and (B) western blot analyses from different stages of development indicate that ForA is expressed throughout the *D. discoideum* life cycle.

3.2.2 Domain architecture of ForA

(A) Multi-domain structure



(B) Protein sequence

```

1   MADKLYQIKL DIKKGKNIVG SDGSVCSPYL RVTWGGKKQQ KTKVITKSAE
51  PEWNFSCLEL IKKEKNPQKP GLEFELIEHK QFSEKEISST TYQLPESLIL
101 GEACNYSVPM SIATSKGDQK CEILIAITAI NFGKDKQDEE KKRHDEIQKK
151 FAQLVEQLAT DSKAREGMMK LPYEARAQLV EQHRDKLANE KHPDEYVLL
201 IKEITRKNIQ LAGGLQKSHS ASNASLGSLP PVTPRVDDGL SVAELKNISV
251 ALRSRGLDWI HQFHKLQGATT RLVELLSLYV NKKSHTEESL QKQLECLNCI
301 KNLMNNAVGI GYIFGIKDSF KTIVLCLGSE YEKVNELAIG LLNTICFLPK
351 INGHKLLIEL LNYFKEEKKE SRRFISIVKS LKSKAGVIET KETLKTCSIY
401 LSFINIIVNT PAEIDLRLAL RQEFYWLGIK EILVKLSNYT YDESPELDTQ
451 ITVFEEEEKS DNKEMSERFQ EFKGLNLDNV DDVLKTLMDR IRPKGLVDCM
501 REISKDLLLL PIDDDVGIRN WVLASRIIQI ISLRDKNIGI DEDILPLENL
551 LLMCEQEAKE VPLKSQIESL KKDAQDLAKK ITTQDIELKE KVEI IKKNEE
601 LTTKQLEEVI NIAKKKDEEI NQKALVEQL KLTQGTAKPD SAAASTSVAP
651 PPPPPMTGG  GAPP PPPPPP  PMTGGGGPPP  PPPPPMTGG  GPPPPPPPPP
701 MTGGGPPPPP  PPPGGGPPP  PPPPGAKAGG  PPPPPPPFGK  GPPPPPPGGFG
751 MKKAAAPPRK  EVPVPALKMK  GLQVSLNDK  KIQGTIFSKE  NLDTSKDINL
801 DYKDIEGVFA  AKVIEKKEST  APKKTGPVSI  IDPKTSQNLS  IFLSQFKGKS
851 YDDICGAISK  GDETVFQPNH  IDALIGFLPS  EDDINNINEF  LREEKDITKL
901 GPPEQFSMKI  HSVPQVKARL  QAMKFKYAYE  SKKSDLKVDI  DNFKQGTQEI
951 KGSEKIPKLL  EVILILGNFI  NGGTARGNAY  GFKLNTITKL  ADTKSTDNKL
1001 SLVNYLTRVV  IKDFPHLNSF  AQDLGHVEAA  GRVSLSQVQA  EVATLRKEFV
1051 QVQKSIETLN  SGTGEEAVDP  FKVKYEEFCT  QTAEDIDLIT  SSSQDIETDY
1101 KDLLAMFGED  SKSEPSEFFG  MFTKFMDOYD  KATKENEQLS  IQAEKIAKRE
1151 AAKKLKEEED  AKKQLAEER  KQKGETVEVK  ESVVDDLLDT  IASGDAFKNR
1201 RRRARKTDQD  STIEPIDL

```

Figure 29: Domain structure and protein sequence of ForA.

(A) ForA is a multi-domain formin with highly conserved FH domains. In addition to a GBD and DAD, this DRF harbors a protein kinase C conserved region 2 (C2) in its N-terminus. (B) Amino acid sequence of ForA. Formin domains are highlighted by colour codes; C2 domain [12-87 aa], GBD [139-348 aa], FH3 [366-600 aa], FH1 [634-746 aa], FH2 [750-1137 aa] and DAD [1138-1218 aa]. Note: Because of the lack of structural data the regions DID, DD, CC are grouped as the FH3.

```

ForA  KNIVGSD-GS  VCSPYLRVTW  GGKK-Q---Q  KTKVITKSAE  PEWNFSCLE  IKKEKNPQK
PKC $\alpha$   KNLIPMDPNG  LSDPYVKLKL  IPDPKNESKQ  KTKTIRSTLN  POWNESFTFK  LKPSDKDRR
PKC $\beta$   KNLVPMDPNG  LSDPYVKLKL  IPDPKSESQ  KTKTIKCSLN  PEWNETFRFQ  LKESDKDRR
PKC $\gamma$   RNLPPKDKKG  TSDPYVKVSL  GGDKKQ--KK  KTKVVKKTLL  PVWNETFTFE  VPPPESSL

```

Figure 30: The C2 domain of ForA.

The protein kinase C conserved region 2 (C2 domain) is aligned with the respective regions of conventional protein kinases. Identical residues are shaded in grey.

As in other formins, the GBD-FH3/DAD intra-molecular interaction is expected to guarantee the auto-inhibited state until a small RacGTPase triggers activation upon binding to the GBD. However, ForA contains upstream of the conserved GBD a C2 domain at the N-terminus (Figure 29A and 30). C2 domains have been found in various proteins and are thought to be important for modulating lipid signals within proteins (Lemmon, 2008).

3.2.3 ForA interaction with actin

One of the pivotal functions of formins is to nucleate actin polymerization. A recombinant FH2DAD (749-1218 aa) as GST fusion was tested for its activity. Even nano molar concentrations of the C-terminal fragment induced a burst in actin polymerization in a dose-dependent manner (Figure 31A). Furthermore, the barbed ends of the filaments are protected by ForAFH2DAD and this resulted in the reduced filament depolymerization rate. The data indicated that ForA indeed protected barbed end dissociation after diluting the filaments below the critical concentration (Figure 31B).

Full-length DRFs are due to the intra-molecular DID/DAD interaction in vitro always inactive. This inhibition can also be demonstrated in vitro by incubating the N-terminal formin regions containing the FH3 domain with the FH2DAD as separate polypeptides. A complete inhibition of the FH2DAD mediated actin assembly was observed in the presence of N-terminal regions of formin either with or without the C2 domain. However, the DID/DAD interaction was found to be regulated at least in part by the C2 domain (Figure 31C).

A majority of studies on formin regulation is based on mDia1, because the crystal structure of its N-terminus revealed further defined regions such as the DID, coiled-coil region and the dimerization domain. There are no structural data available for ForA. Therefore, the regions between the GBD and the FH1 are still designated as FH3 similar to other DRFs such as mDia2, DAAM, FHOD, i.e any FH3 domain encompasses the DID.

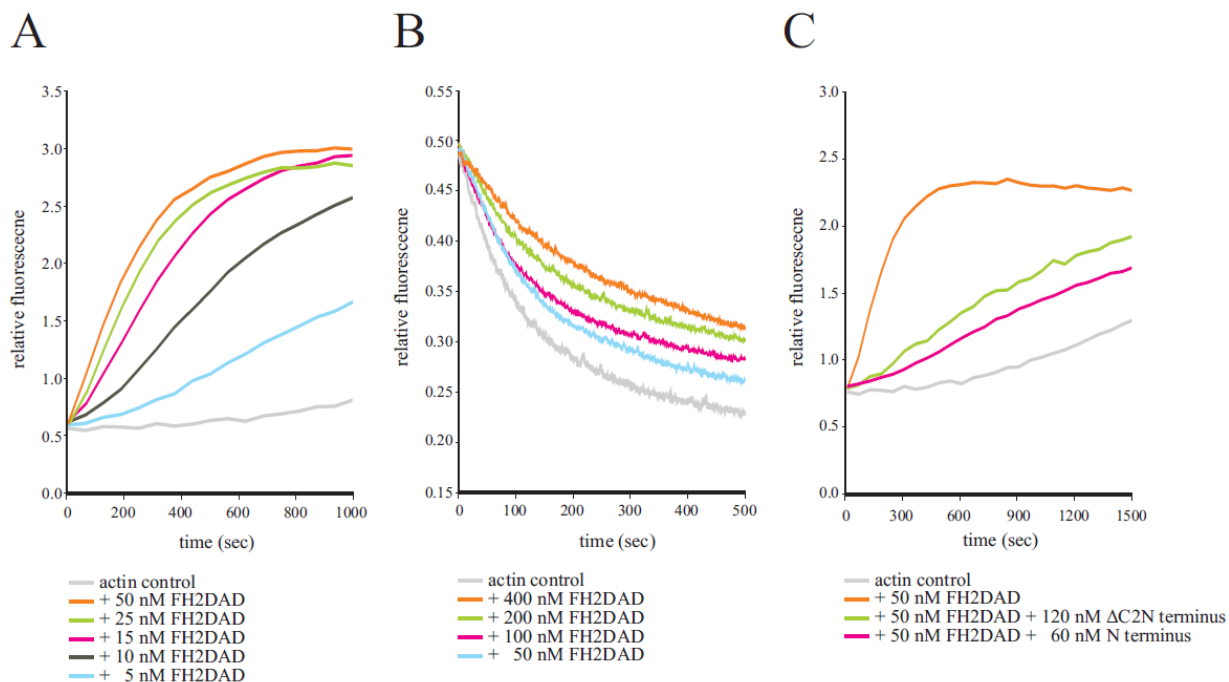


Figure 31: Recombinant ForA interacts with actin.

The FH2 domain of ForA behaves like the homologous domains in other DRFs: it accelerated nucleation and assembly of actin filaments in a dose-dependent manner (A), significantly inhibited the depolymerization of the F-actin (B), and the intra-molecular DID/DAD interaction is functional as the nucleation activity can also be inhibited in the presence of two individual constructs (C).

3.2.4 ForA interacts with profilin I

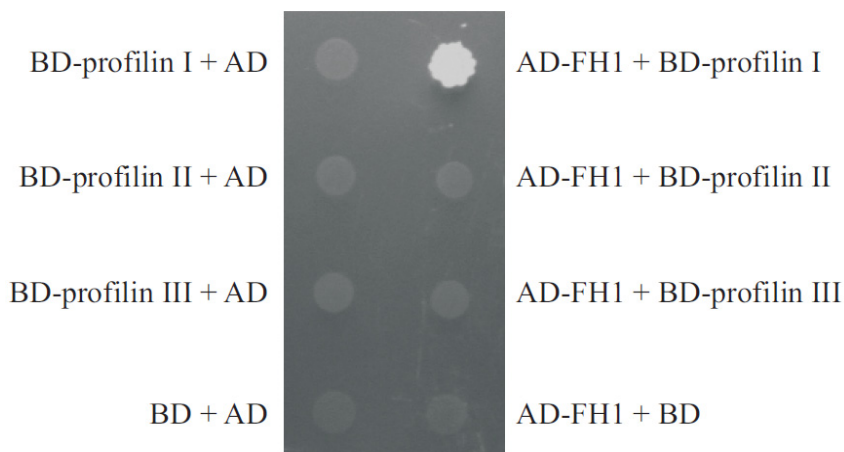


Figure 32: ForA specifically interacts with profilin I.

The yeast cells were transformed with the activation domain vector containing proline-rich FH1 domain and plated onto medium lacking leucine, tryptophan, histidine and adenine. The result indicated that ForA interacts specifically with the profilin I isoform.

In general, efficient filament elongation by formins depends on profilin which creates as G-actin sequestering protein a local G-actin pool at the fast growing end. Three profilin isoforms have been reported in *D. discoideum* (Arasada et al., 2007). The FH1 domain of ForA physically interacted in yeast two hybrid assays unequivocally only with profilin I (Figure 32). But, in vitro TIRF measurements suggested that both profilin I and II equally accelerated filament elongation mediated by GST-ForAFH1FH2DAD (not shown). Considering that profilin III is much less abundant in *D. discoideum* cells it is unlikely that this profilin isoform plays a major role in the ForA-mediated filament elongation machinery.

3.2.5 Generation of a ForA null mutant

The ForA null mutant was isolated by inserting a blasticidin S resistance cassette into the *forA* gene thus disrupting its expression. The *forA* gene targeting vector was constructed by cloning the genomic PCR products BamHI/PstI at the 5' end and BamHI/PstI or Sall/HindIII at the 3' ends into the corresponding sites of pLPBLP. The target vector was then digested with BamHI/Sall and used to disrupt the *forA* gene in wild type cells. Null mutants were initially screened by PCR using two sets of primers as shown in the scheme (Figure 32A) and the disruption was confirmed by western blots using a polyclonal antiserum generated against the N-terminal region spanning ForA GBD-FH3 (Figure 32B).

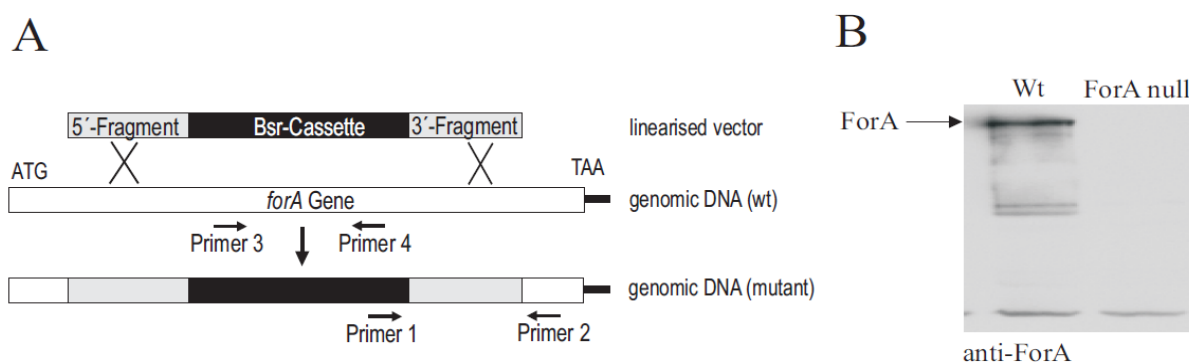


Figure 33: Gene disruption strategy.

(A) The schematic diagram represents the strategy for knocking out *forA* in wild type strain, in the dDia3 null and the myosin II heavy chain null strains. The homologous recombination event was initially tested by PCR with indicated primer pairs. (B) Western blot analysis with anti-ForA polyclonal antiserum generated against the N-terminal region encompassing GBD-FH3 confirmed that ForA is not expressed in the null mutant. Wild type (Wt) cells served as a positive control for ForA expression.

3.2.6 ForA null mutant development is largely unaffected

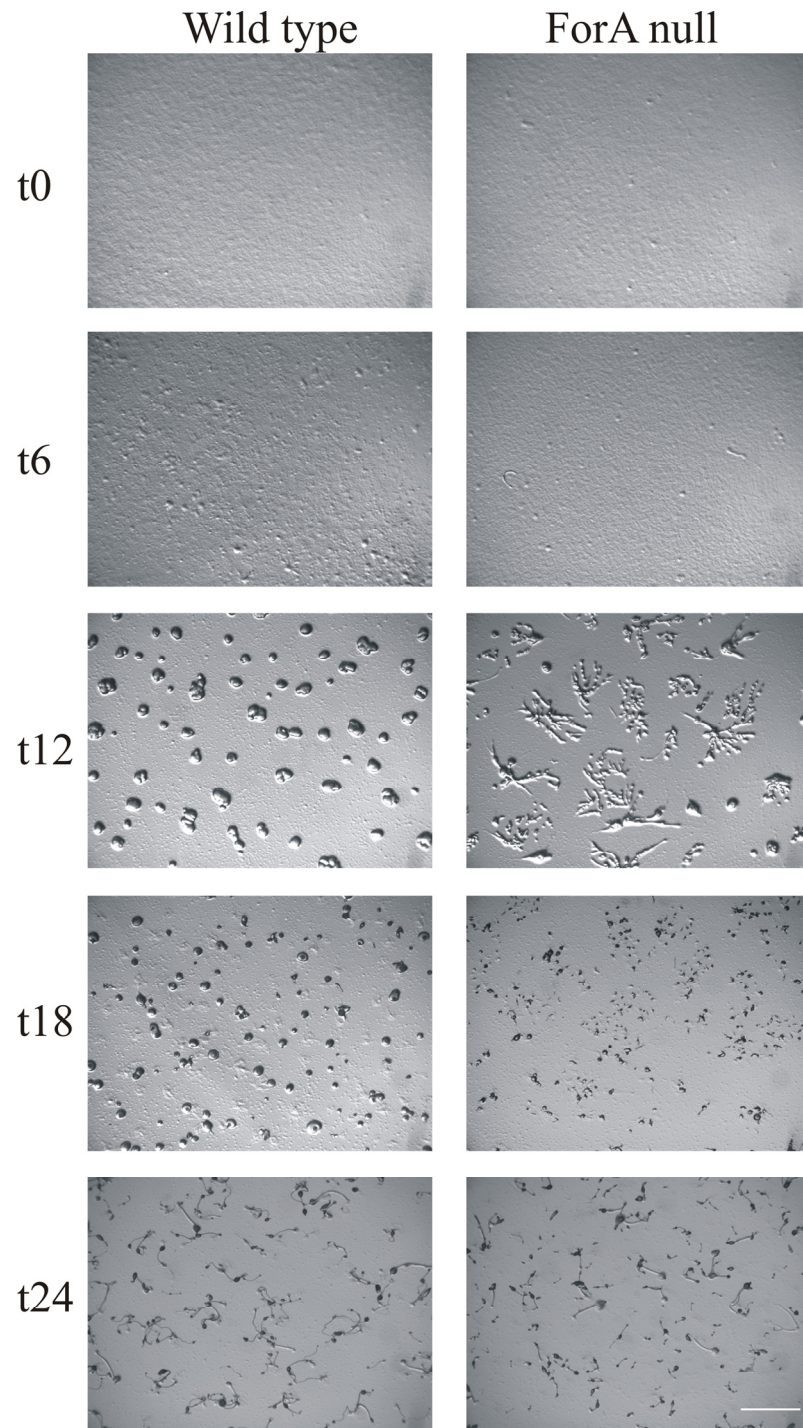


Figure 34: Development of ForA null mutant cells. Wild type and ForA null mutant cells were seeded onto phosphate agar plates to induce development. The developmental stages of both cell lines were imaged at different time points. ForA null mutant cells showed a slight delay in development. The scale bar represents 3 mm.

The ForA null mutant underwent the complete developmental program, i.e when the null mutant cells were starved in phosphate buffer, they formed aggregates, developed into multicellular structures such as slugs, and eventually culminated into fruiting bodies (Figure 34). However, broken streams were observed frequently during early aggregation which resulted in small fruiting bodies (Figure 35).

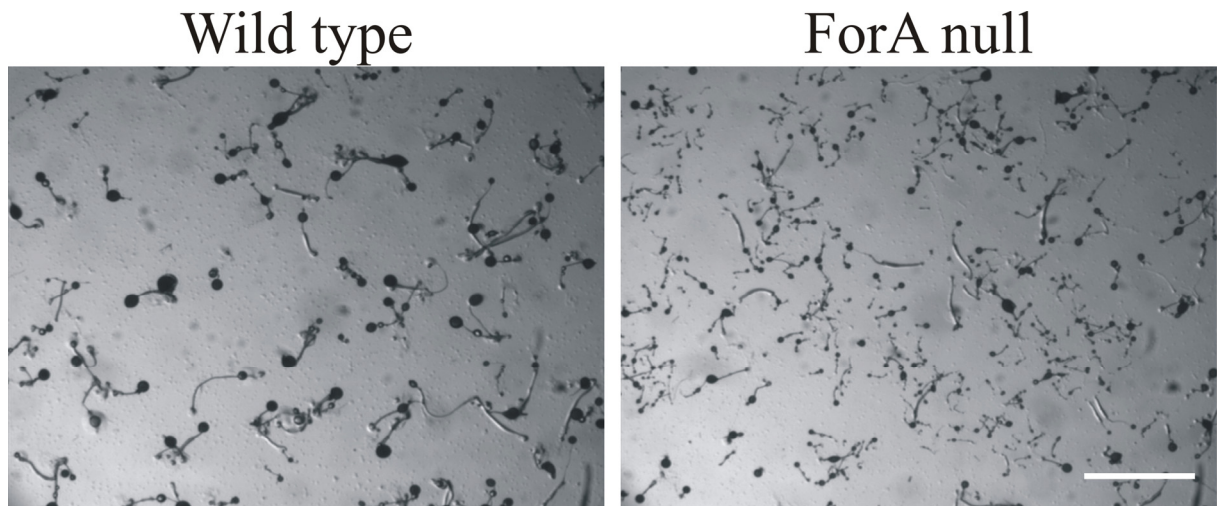


Figure 35: Null mutant spores are smaller.

The size of the ForA null mutant spore heads was often found to be smaller. Nevertheless the spores germinate into unicellular amoeba. The scale bar represents 3 μ m.

In addition to these subtle defects, up to 3 hours delay in the development was also noticed repeatedly. However, this delay may be considered to be normal as many *D. discoideum* knock out mutants lacking the cytoskeletal or non cytoskeleton proteins have been shown to display such behaviors.

3.2.7 ForA is essential for directed cell migration of slugs during phototaxis.

The multicellular slug migration in response to light was severely affected in ForA null mutant. Even after seven days of incubation of the null mutant slugs in a phototaxis chamber, the coordinated cell movement towards the light source did not improve. So, the results indicated that directed cell migration of ForA null mutant slugs are completely inhibited and not just that the migration is slower. The defect in phototactic behaviour of ForA null mutant could be partially rescued by the ectopic expression of GFP-ForA driven by actin 15 promoter which

implied the defect is ForA specific. Since the phenotype is at least in part rescued the possibility that overexpressed GFP-ForA behaving like a dominant negative form can be ruled out. The partial rescue of the phenotype however, could also be a consequence of ForA overexpression and/or misfolded GFP fusion protein. Furthermore, the angle at which the slugs of ForA null expressing GFP-ForA migrate does not seem to be directed towards the light source.

Interestingly, the expression of GFP-ForA Δ C2 completely rescued the phototaxis defect exhibited by ForA null mutants. This observation further validates the previous biochemical data that the C2 domain could be important for auto-inhibition of ForA. In other words, the GFP-ForA Δ C2 is likely to be more active than GFP-ForA. Less surprisingly, the overexpression of ForA fused to GFP did not show any noticeable difference in the slug migration pattern compared to that of the wild type (Figure 36).

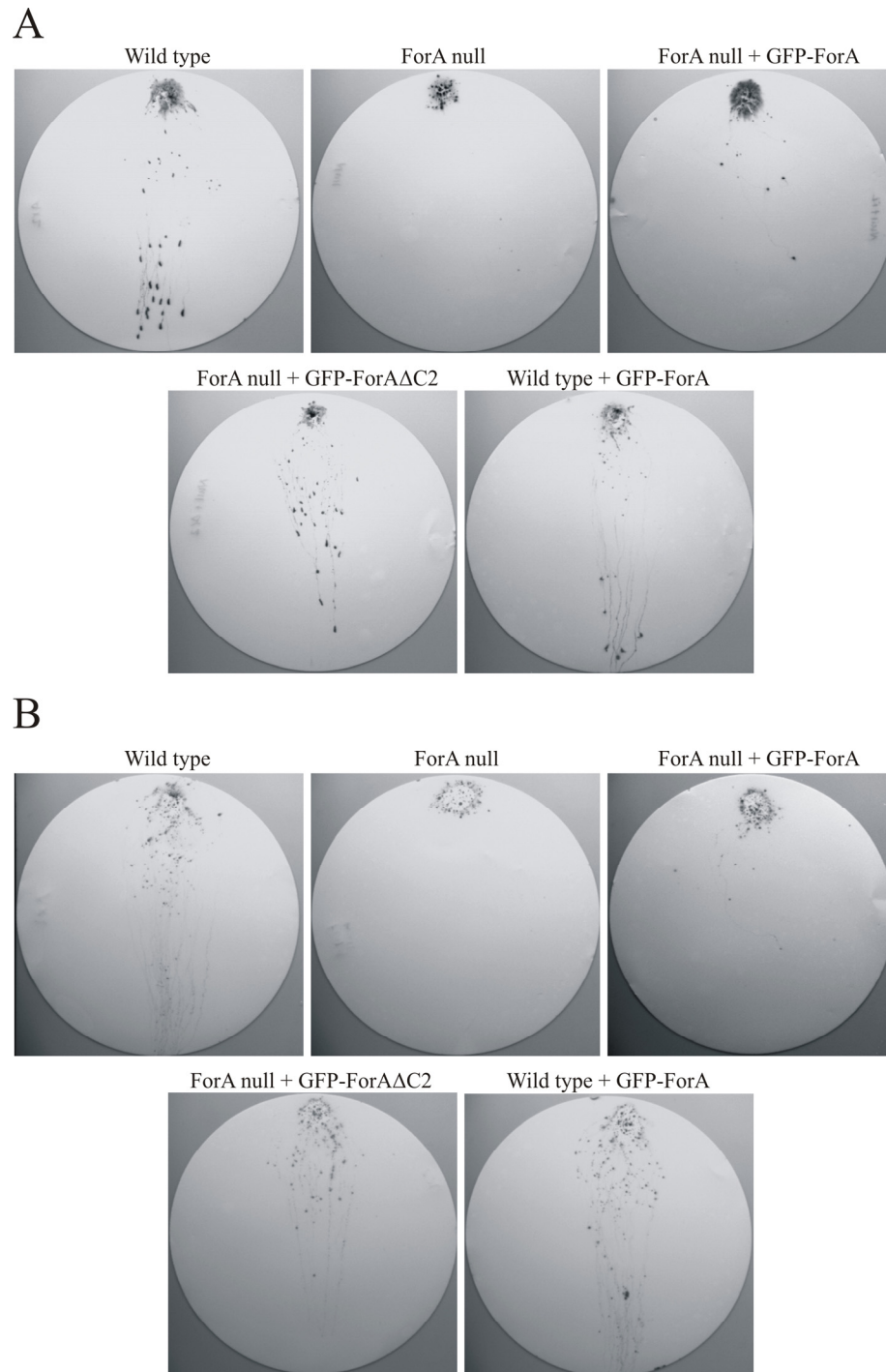


Figure 36: ForA slugs are phototaxis defective.

(A) The migration pattern of the wild type and ForA mutant slugs towards light was studied by transferring after two days of incubation the slug tracks onto a nitrocellulose membrane and staining the tracks with amidoblack. The null mutant shows severe inhibition of directed multicellular movement and the ectopic expression of GFP-ForA constructs rescued the phenotype to different extents. (B) Slug migration after seven days.

3.2.8 ForA null mutant cells show reduced random motility

Random motility of single cells during growth phase showed a significant reduction in cell motility. This happened in axenic medium as well as after transferring the cells to non-nutrient buffer (Figure 37). Though the random cell motility was affected in ForA null mutant cells, polarized cell migrated towards a capillary filled with the chemoattractant cAMP. This observation is not surprising because the ForA null cells formed streams and aggregates during development as well. It requires more detailed quantitative analyses to determine minor differences in the chemotactic index of wild type vs. mutant cells.

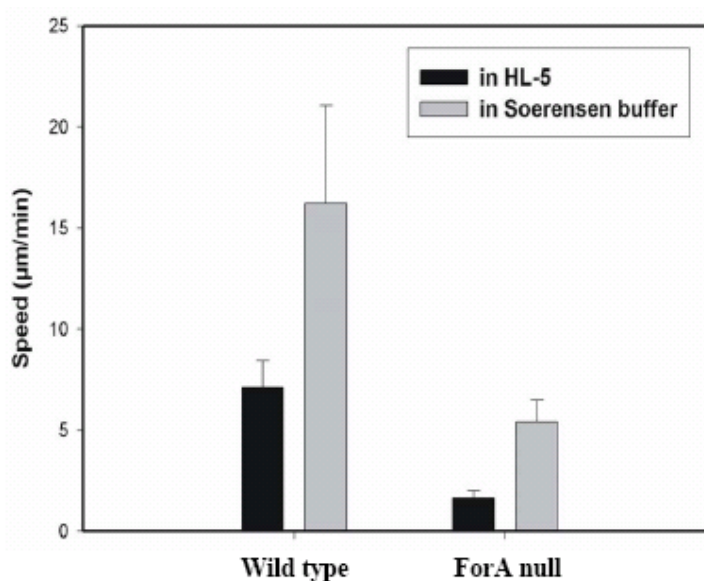


Figure 37: Random motility of ForA null mutant cells.

To measure random motility, the vegetative cells were plated at low cell density onto glass bottom dishes in HL-5 growth medium and allowed to adhere. In each case four movies were recorded (20x magnification, 100 frames at 10 seconds interval). The medium was then decanted and immediately replaced by phosphate buffer which causes always an increase of cell motility. Again four movies were recorded and the data were evaluated using the DIAS software. In each case around 25 cells have been analyzed, error bars indicate standard deviation.

3.2.9 ForA null mutant cells are prone to membrane blebbing

Previously reported microarray data suggested that ForA gene expression was thought to be controlled by osmotic stress (Na et al., 2007). In fact, ForA null mutant cells displayed non-apoptotic membrane blebbing usually within minutes after transfer into phosphate buffer as shown in (Figure 38).

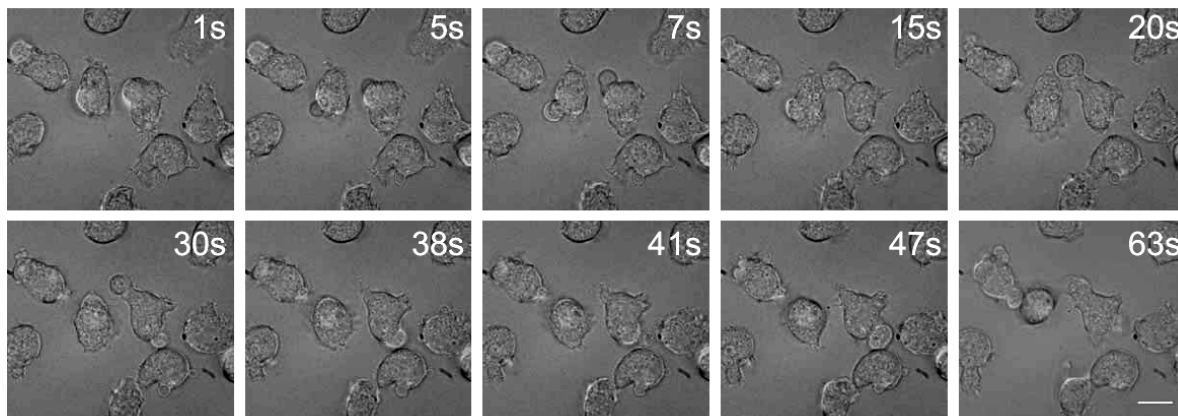


Figure 38: Blebbing ForA null mutant cells.

ForA null mutant cells were seeded onto the glass bottom dish and subsequently cells were washed extensively to remove the residual medium. Cells were then imaged for 2 minutes, every second to record non-apoptotic membrane blebs. ForA null mutant cells did not bleb in culture medium. The scale bar represents 10 μm .

YFP-adenylate cyclase A (ACA) was used as a plasma membrane marker in ForA null mutant and the distribution of the label confirmed that the blebbing was indeed associated with the plasma membrane (Figure 39). Surprisingly, the ectopic expression of both constitutively active ΔDAD and the full-length ForA (not shown) as GFP fusions in ForA null mutant background completely failed to rescue the blebbing phenotype (Figure 40B). This suggested that either lack or overexpression of ForA, i.e. an imbalance of ForA concentration leads to membrane blebbing.

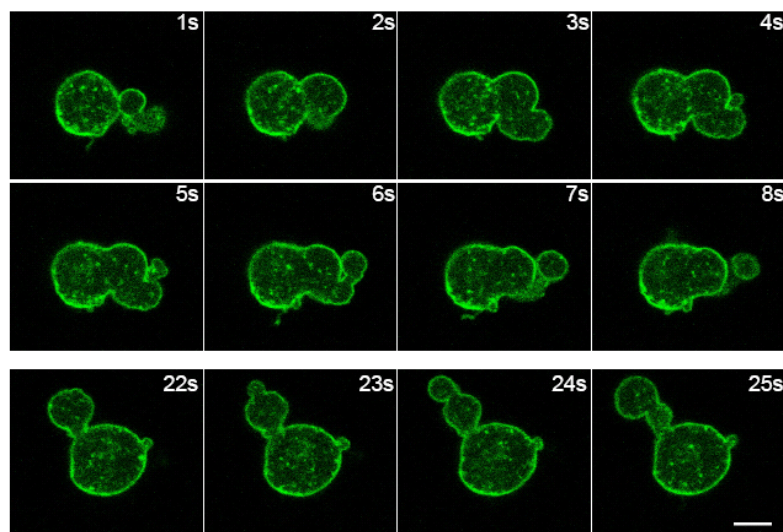


Figure 39: YFP-ACA expression in ForA null cell.

The expression of ACA, a plasma membrane marker tagged to YFP confirms the plasma membrane blebbing. The scale bar represents 10 μm .

Therefore, GFP-ForA and GFP-ForA Δ DAD constructs were expressed in the wild type background. As expected, cells overexpressing either construct (GFP-ForA data not shown) displayed severe plasma membrane blebbing (Figure 40A).

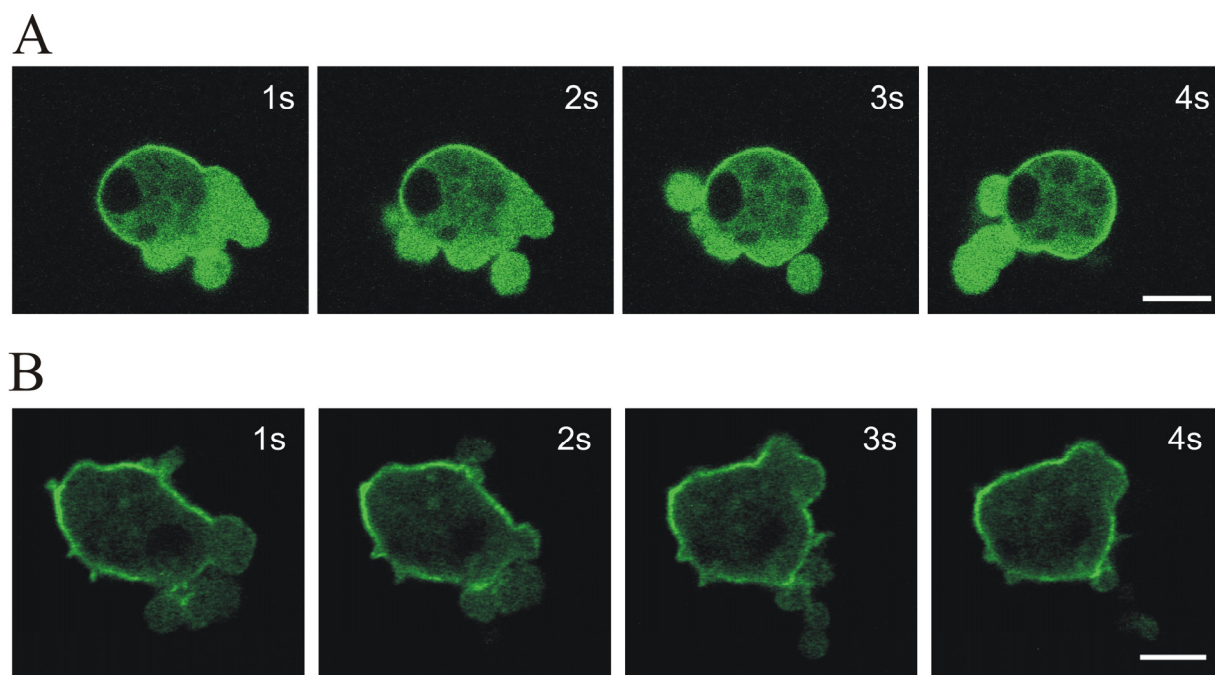


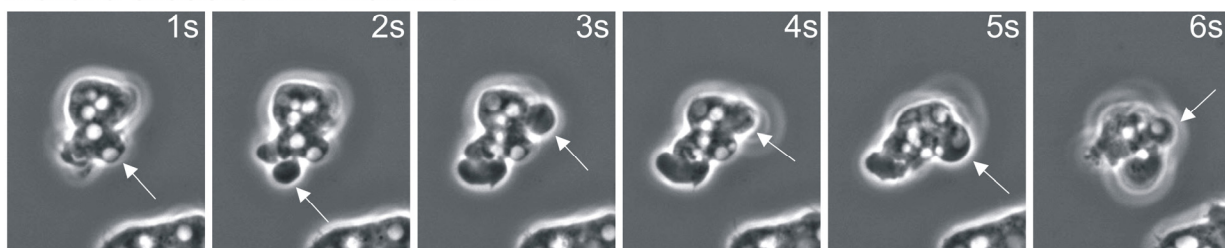
Figure 40: Overexpression of ForA results in membrane blebbing as well. An ectopic expression of GFP-ForA failed to rescue the blebbing phenotype of the null mutant, so the constitutively active ForA (GFP-ForA Δ DAD) was expressed in wild type background to make sure that the resultant blebbing is due to ForA overexpression. Also an overexpression of GFP-ForA Δ DAD in both wild type (A) and null mutant (B) background induced plasma membrane blebbing. Scale bars represent 10 μ m.

It should be mentioned, however, that the exact conditions for inducing membrane blebbing are still not known. The phenotype is dramatic, but it is very difficult to reproduce. Currently studies are underway to change buffers, temperatures, osmolarity, developmental stage, real time gene expression, number of passages, and transformation methods. This is important because it would be the first example for the requirement of an exactly balanced formin level in a cell. So far we can not exclude that an yet unknown equilibrium machinery causes the poor reproducibility of the phenomenon.

3.2.10 ForA induced blebbing is myosin II dependent

Blebbistatin is an inhibitor of myosin II and can prevent membrane blebbing. This is also the case in blebbing ForA null cells that were recorded live in Soerensen buffer. After addition of 10 μ M blebbistatin blebbing was abolished in a matter of seconds (Figure 41).

Before blebbistatin treatment



After 10 μ M blebbistatin treatment

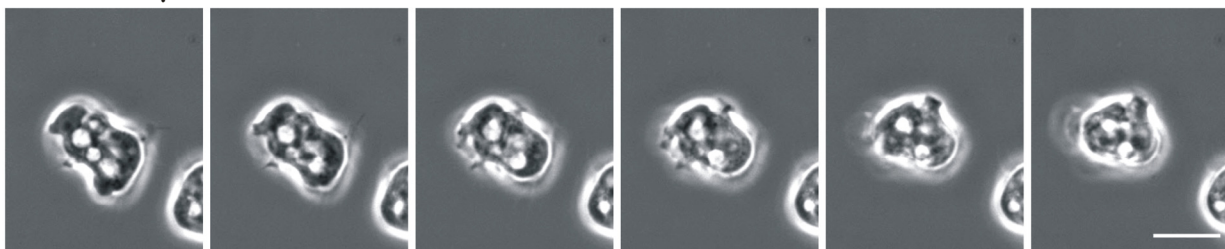


Figure 41: Blebbistatin treated ForA null mutant cells do not bleb.

ForA null mutant cells were seeded onto a glass bottom dish washed thoroughly in phosphate buffer and then imaged for 2 minutes every second (upper panel). After addition of blebbistatin, blebbing was arrested (lower panel). Arrows indicate membrane blebs. The scale bar represents 10 μ m.

In order to prove that the observed inhibition by blebbistatin was not a secondary effect of the drug itself, a genetic approach was carried out. A myosin II/ForA double null mutant was generated by disrupting the *forA* gene under blasticidin selection in the strain HS2205 that lacks myosin II heavy chain (Manstein et al., 1989) using the same strategy that was previously employed for knocking out *forA* in wild type (Figure 42A).

As expected, the myosin II/ForA double null mutant did not exhibit membrane blebbing (Figure 42B). Likewise, cells overexpressing constitutively active GFP-ForA Δ DAD in myosin II null mutant cells were also found to be devoid of membrane blebs (Figure 42C). Taken together, the results not only indicate that myosin II is a negative regulator of blebbing in the

ForA null mutant or overexpressor cells but also suggest that there is a cooperation between myosin II and ForA in maintaining the integrity of the cortical actin cytoskeleton.

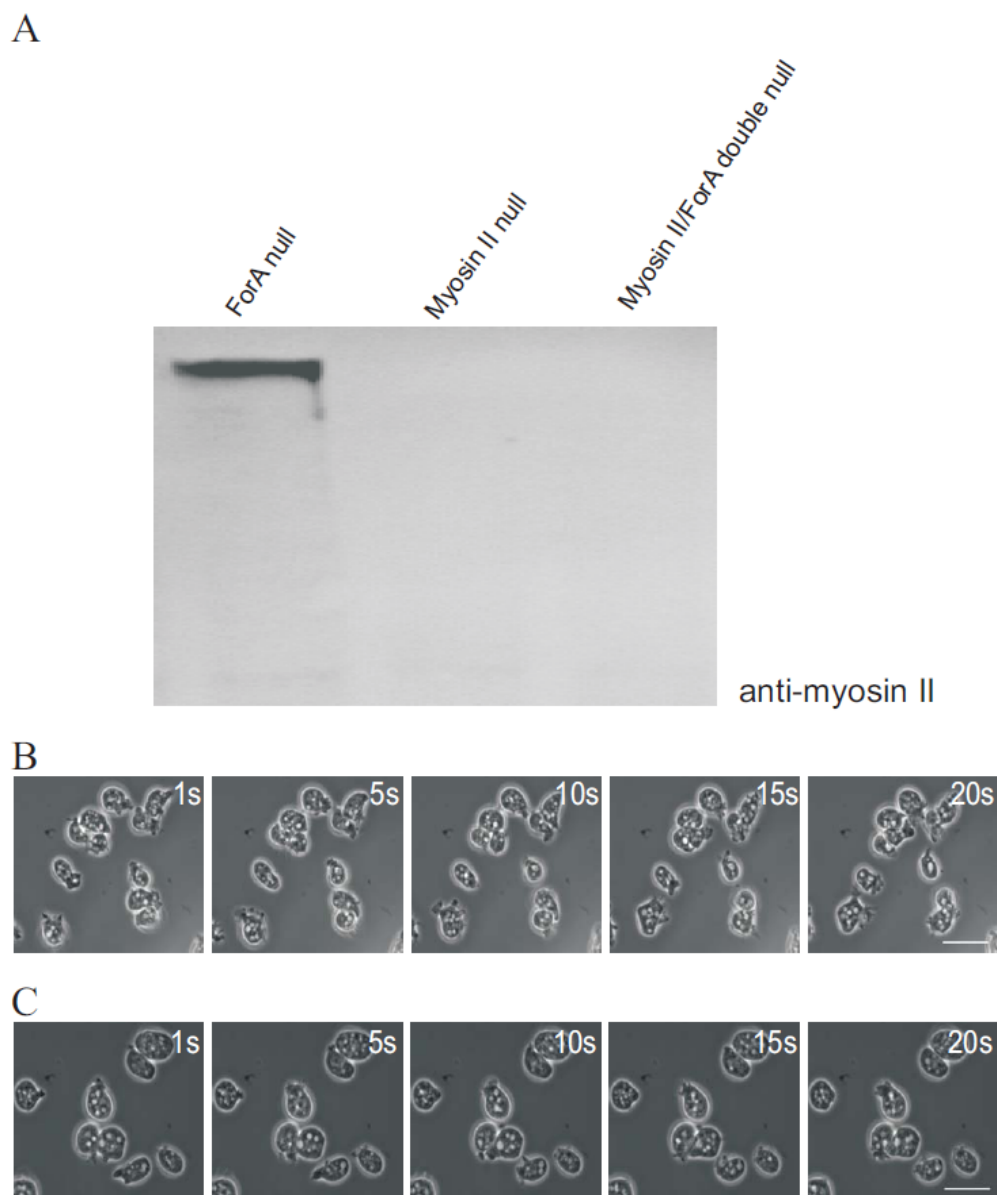


Figure 42: ForA blebbing is myosin II dependent.

(A) Myosin II heavy chain null cells are transformed with the ForA knockout construct to isolate myosin II/ForA double null mutant. At first the absence of ForA protein was confirmed by western blot using polyclonal antiserum generated against the N-terminal region of ForA. Later, ForA null, myosin II null and myosin II/ForA double null cells were probed with the monoclonal antibody (56-396-5) against myosin II heavy chain. Myosin II is expressed only in ForA null. The requirement of myosin II for blebbing was confirmed by genetic approaches. Firstly, myosin II/ForA cells were found to be devoid of plasma membrane blebbing (B). Secondly, overexpression of ForA in myosin II null cells did not induce plasma membrane blebbing (C). Scale bars represent 10 μ m.

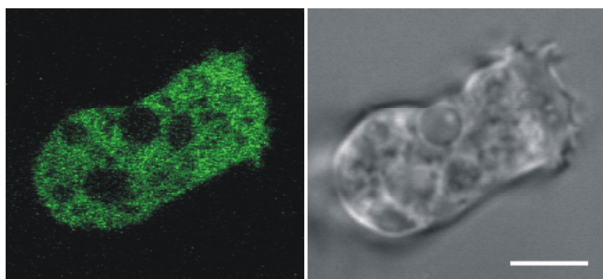
3.2.11 Subcellular localization of GFP-ForA and GFP-ForA Δ C2

Subcellular localization of the formin was studied with GFP-ForA. Assuming that the C2 domain might possess the localization signal of ForA, another construct lacking this lipid-binding domain was also generated simultaneously and expressed in both wild type and ForA null mutant cells. Neither of the constructs revealed specific subcellular distribution. This suggested that the C2 domain did not contain a localization signal, at least in an auto-inhibited full-length formin (Figure 43).

A



B



C

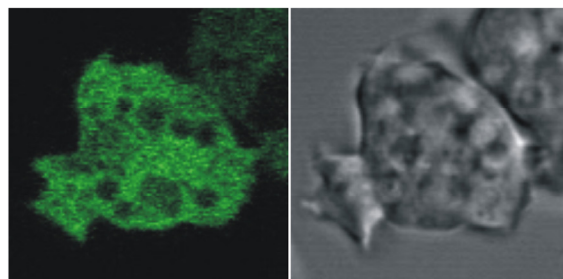


Figure 43: Localization of ForA.

(A) Schematic representation of GFP-ForA (top) and Δ C2 ForA (bottom) constructs used to study the localization. Both GFP-ForA (B) and GFP-ForA Δ C2 (C) fusion proteins are cytoplasmic. GFP fluorescence (left panels), phase contrast images (right panels). The scale bar represents 5 μ m.

3.2.12 Subcellular localization of constitutively active ForA

To address the hypothesis that a distinctly localized formin has to be constitutively active, a GFP-ForA Δ DAD construct was made and expressed in *D. discoideum* cells. Interestingly, under these conditions the formin was found to be localized to the trailing end of the motile cell (Figure 44B).

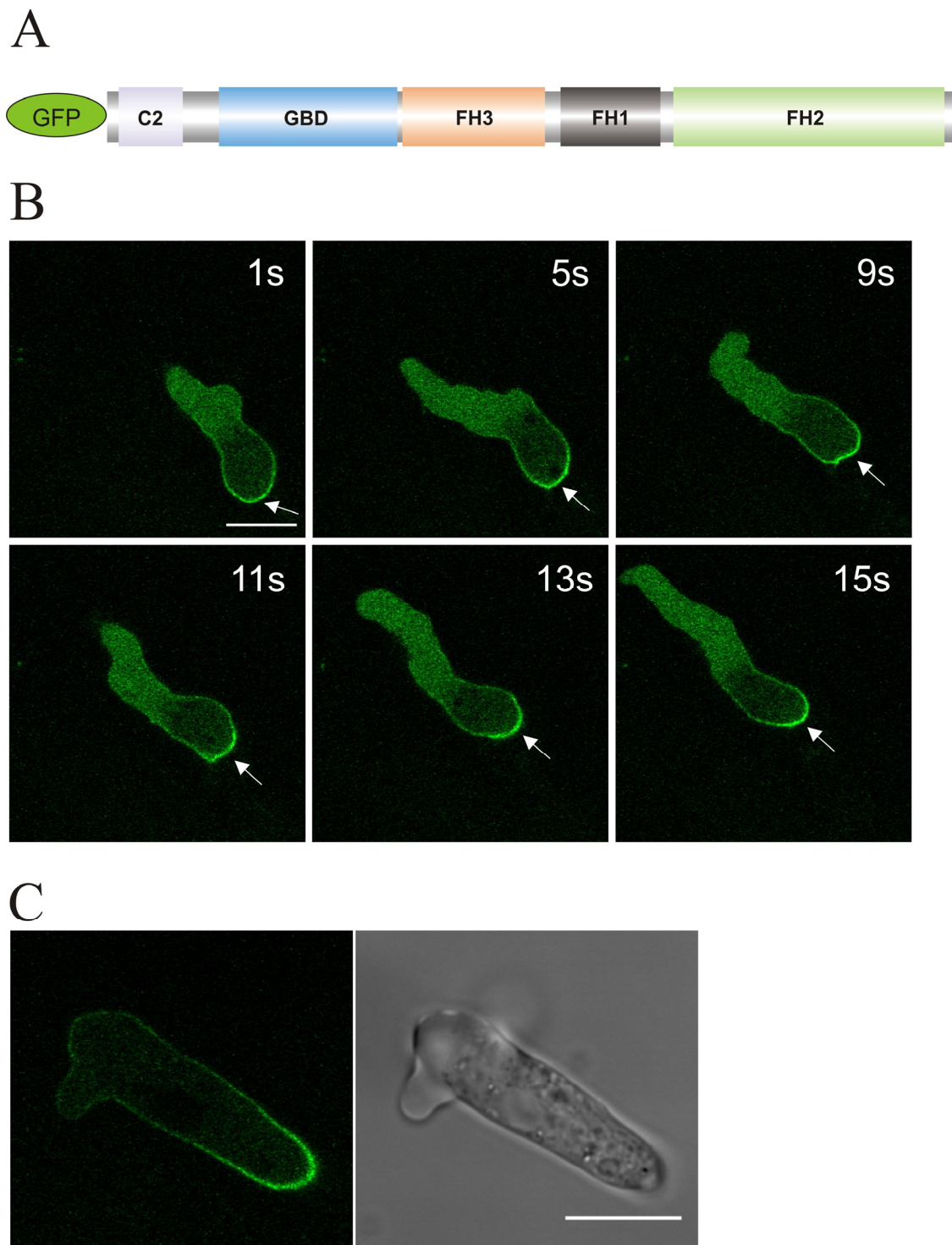


Figure 44: Localization of constitutively active ForA.

Schematic representation of the GFP-ForA Δ DAD construct (A). Expression of GFP-ForA Δ DAD in both wild type and ForA null mutant exhibited similar staining. GFP-ForA is enriched at the trailing end of motile vegetative cell (B) and developed cell (C). Arrows indicate that GFP-ForA Δ DAD is accumulated in the uropod. Scale bars represent 10 μ m.

A closer look at the localization revealed indeed the GFP-ForA Δ DAD staining was strongly accumulated at the trailing end of the t6 cell (Figure 44C). It was evident from the immunostaining of vegetative cells with anti-GFP antibodies (green) and phalloidin, an F-actin marker that ForA accumulation did not simply overlap with F-actin.

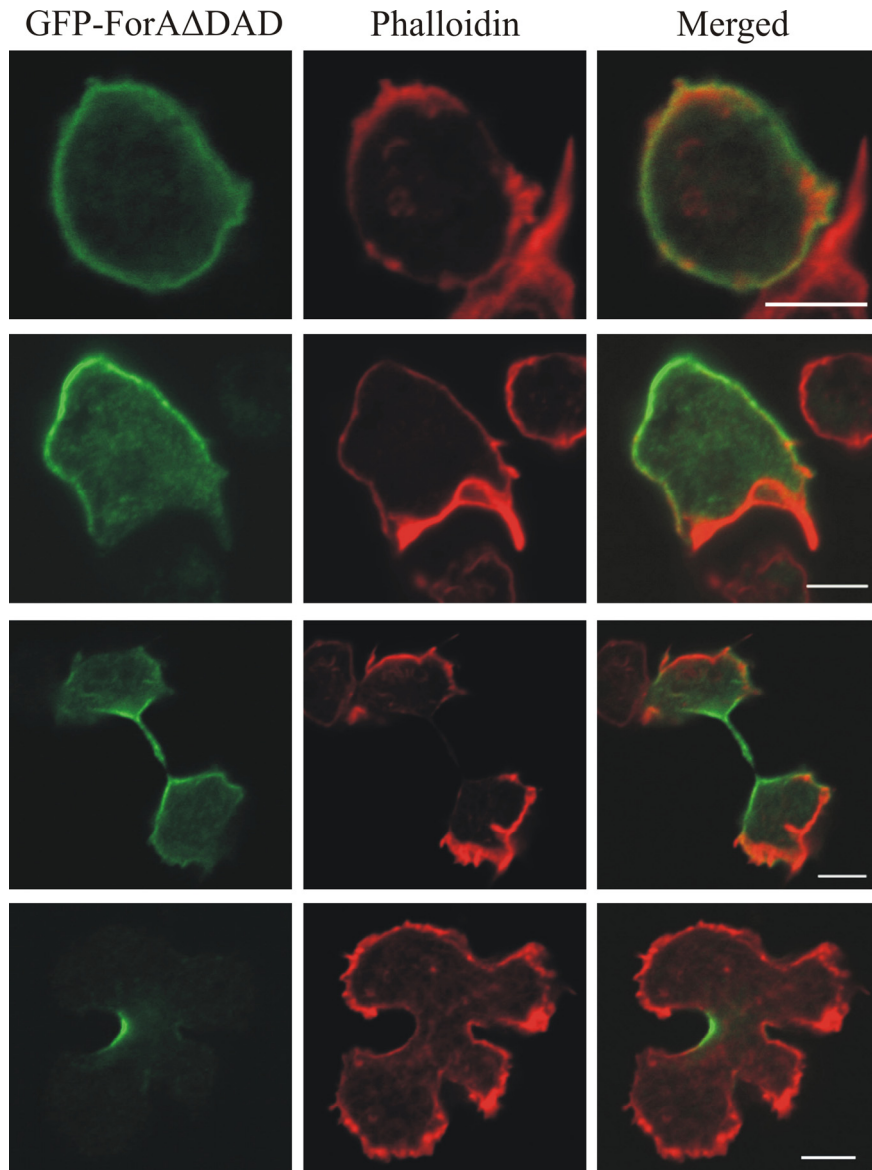


Figure 45: Localization of ForA Δ DAD in fixed cells.

The GFP signal is found uniformly throughout the cell periphery (first row) in resting and non-polarized cells but accumulated at the trailing end in a cell with a clearly distinguishable front and rear area (second row). During cytokinesis ForA prominently accumulated in cleavage furrows; (third row) normal cytokinesis and (fourth row) asymmetric cell division. Left - GFP-ForA Δ DAD, middle - actin and right - merged. The scale bars represents 5 μ m (Courtesy of Dr. Jan Faix)

It was also interesting to notice GFP-ForA Δ DAD staining the cleavage furrow during normal cytokinesis and asymmetric cell divisions (Figure 45).

3.2.13 The C2 domain is also not required for localizing constitutively active ForA

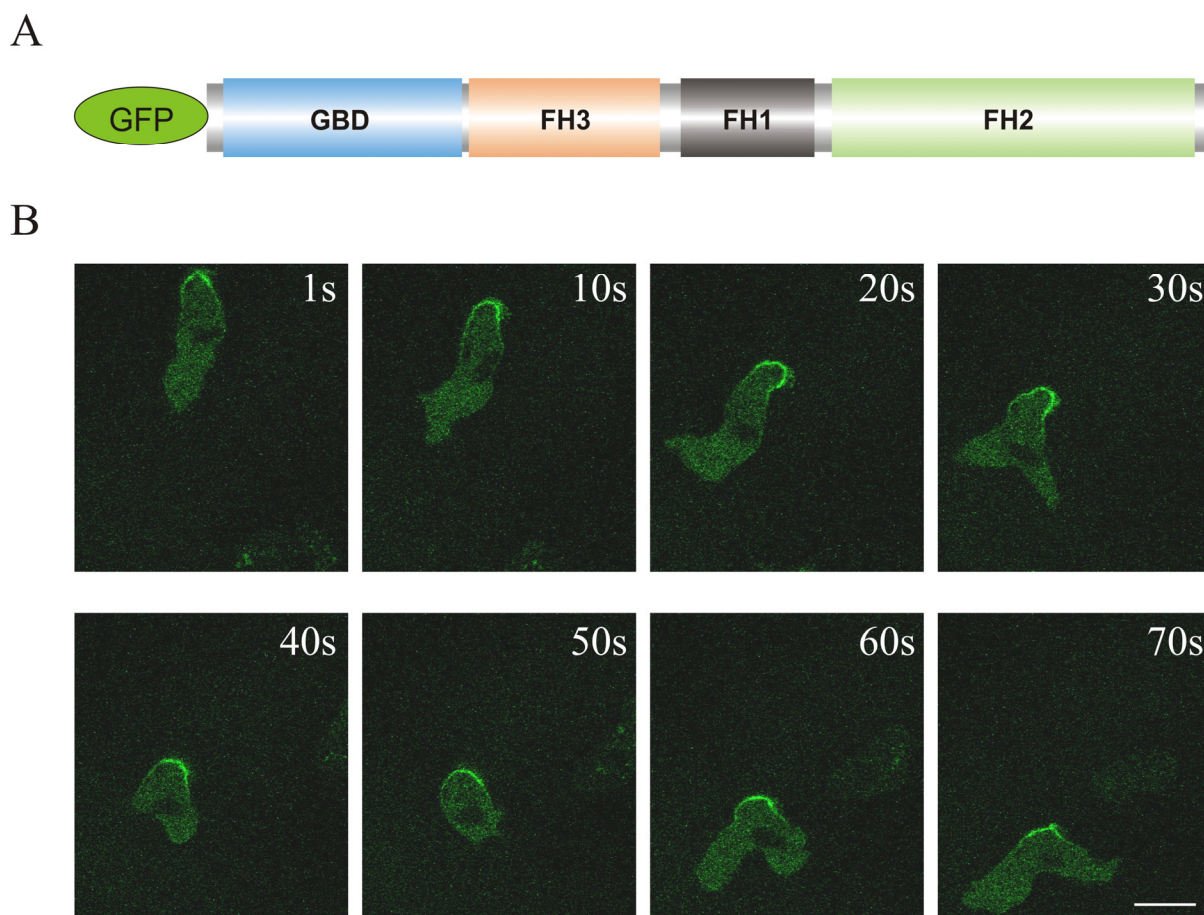


Figure 46: The C2 domain is dispensable for ForA accumulation at the rear.

(A) Schematic diagram of the constitutively active GFP-ForA Δ C2 Δ DAD. (B) Time lapse images of cells expressing GFP-ForA Δ C2 Δ DAD. The scale bar represents 10 μ m.

Since the constitutively active ForA prominently accumulated at the trailing ends of motile cells, it was tempting to see if the C2 domain of ForA is important for the localization. So a constitutively active GFP-ForA lacking the C2 domain was made and found to stain the rear as well (Figure 46). The results were surprising especially as the C2 domain of ForA (as a GST fusion protein fragment) interacted with multilamellar PIP₂ vesicles in vitro (Figure 47B) in a spin-down assay. Further analysis using a PIP strip revealed that indeed the GST-ForAC2

domain interacted with various phospholipids including PIP₂ and PIP₃ (Figure 47C). This suggests that the lipid-binding domain plays if any then a minor role for subcellular localization, and that ForA binds to the rear end with a protein region after the C2-domain and before the DAD.

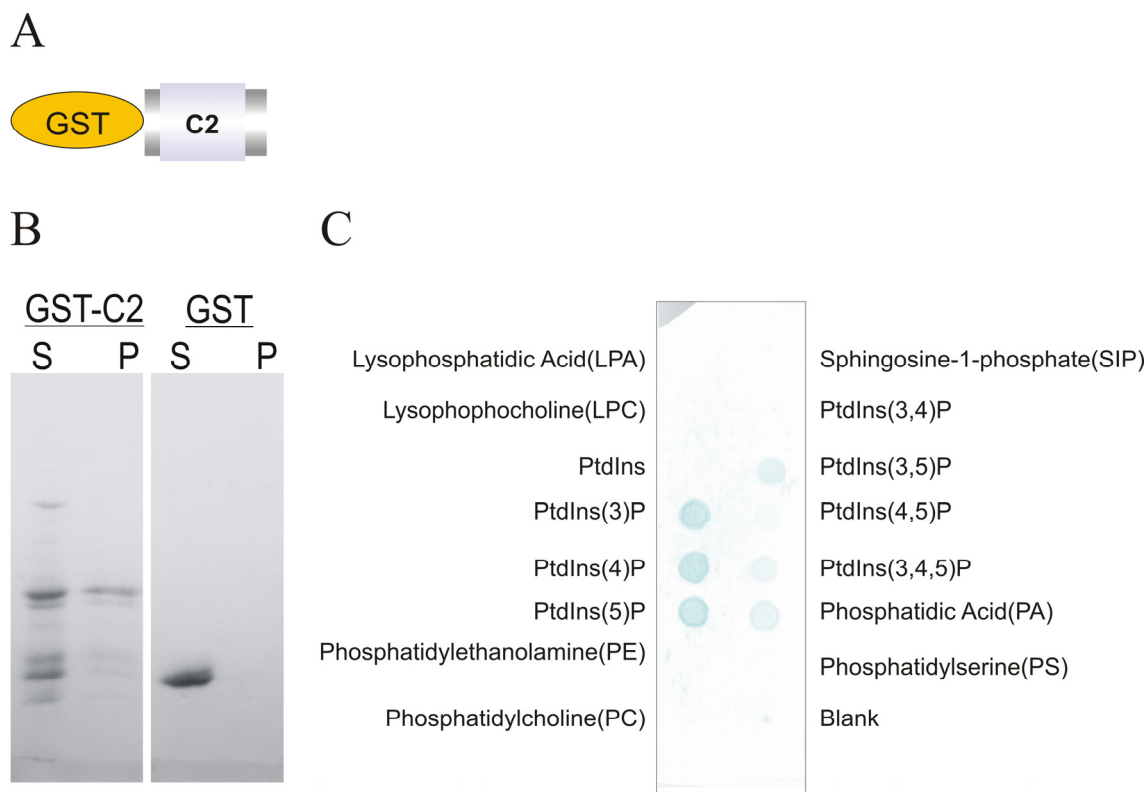


Figure 47: The C2 domain of ForA interacts with phospholipids.

(A) Schematic representation of GST-ForAC2 used in *in vitro* lipid-binding assays. (B) The GST-ForAC2 was incubated with mixed multilamellar PIP₂ vesicles for 60 min at room temperature. After centrifugation at 12,000 g for 20 min, the proteins in supernatant (S) and pellet (P) were normalized and analyzed by SDS-PAGE. About 40% of GST-ForAC2 is sedimented along with lipids. The GST-ForAC2 alone (without lipids) remained in the supernatant (not shown). GST alone served as a negative control (as in Figure 9). (C) A PIP strip membrane (Echelon) was incubated with GST-ForAC2 and the lipid-bound protein was blotted with anti-GST polyclonal antibody. Along with PtdIns(3)P, PtdIns(4)P and PtdIns(5)P - the C2 domain of ForA interacted also with PIP₂ and PIP₃.

3.2.14 GBD-FH3 harbors the localization signal

In order to dissect the localization signal within ForA further, selected C-terminal and N-terminal truncations were fused to GFP and expressed. The entire C-terminal construct spanning the FH1, FH2 domains and the DAD was found to be predominantly cytoplasmic

(Figure 48 B), but the N-terminal region of ForA comprised of the C2 domain, GBD and FH3 domain localized to the cortical region of the cell (Figure 48 C). Since, as shown above, the C2 domain was dispensable, the ForA localization signal could be mapped to GBD-FH3.

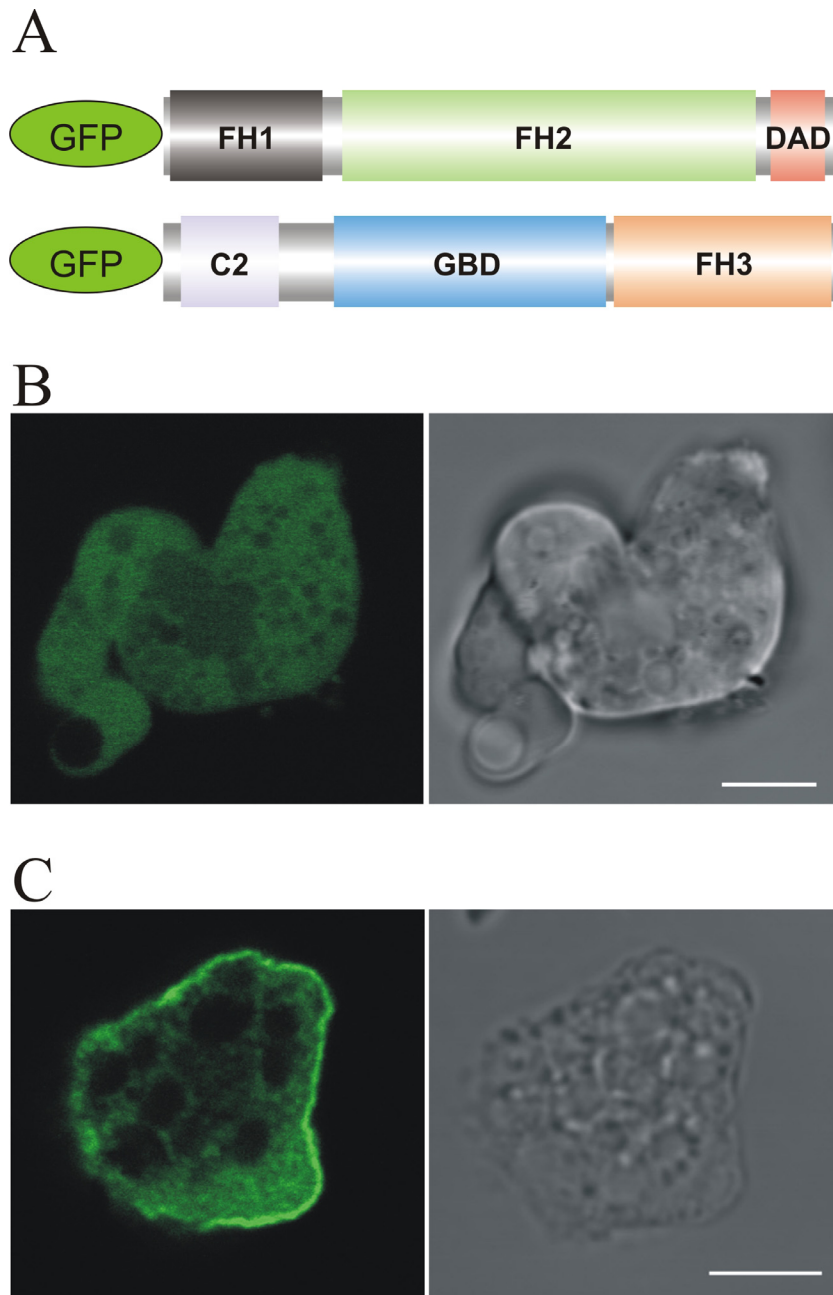


Figure 48: GBD-FH3 is essential for ForA localization.

(A) Schematic representations of truncated constructs used to map the localization signal. (B) The C-terminal region of ForA is dispensable for localization, whereas the N-terminal region the GBD-FH3 is required for ForA localization. Scale bars in B and C represent 10 and 5 μm respectively.

3.2.15 GFP-ForA N-terminus overexpression leads to an altered phenotype

Overexpression of the GFP-ForA N-terminus in ForA null mutant cells induced abnormal actin based structures. It is also to be noted that overexpression of the ForA N-terminus resulted in a variety of cell populations. Considering the fact that the N-terminal ForA region lacks the actin nucleation/elongation function, the observed phenotypes could be independent of the usual formin activities but the role of formin-binding partners in the resultant phenotype can not be completely ignored (Figure 49).

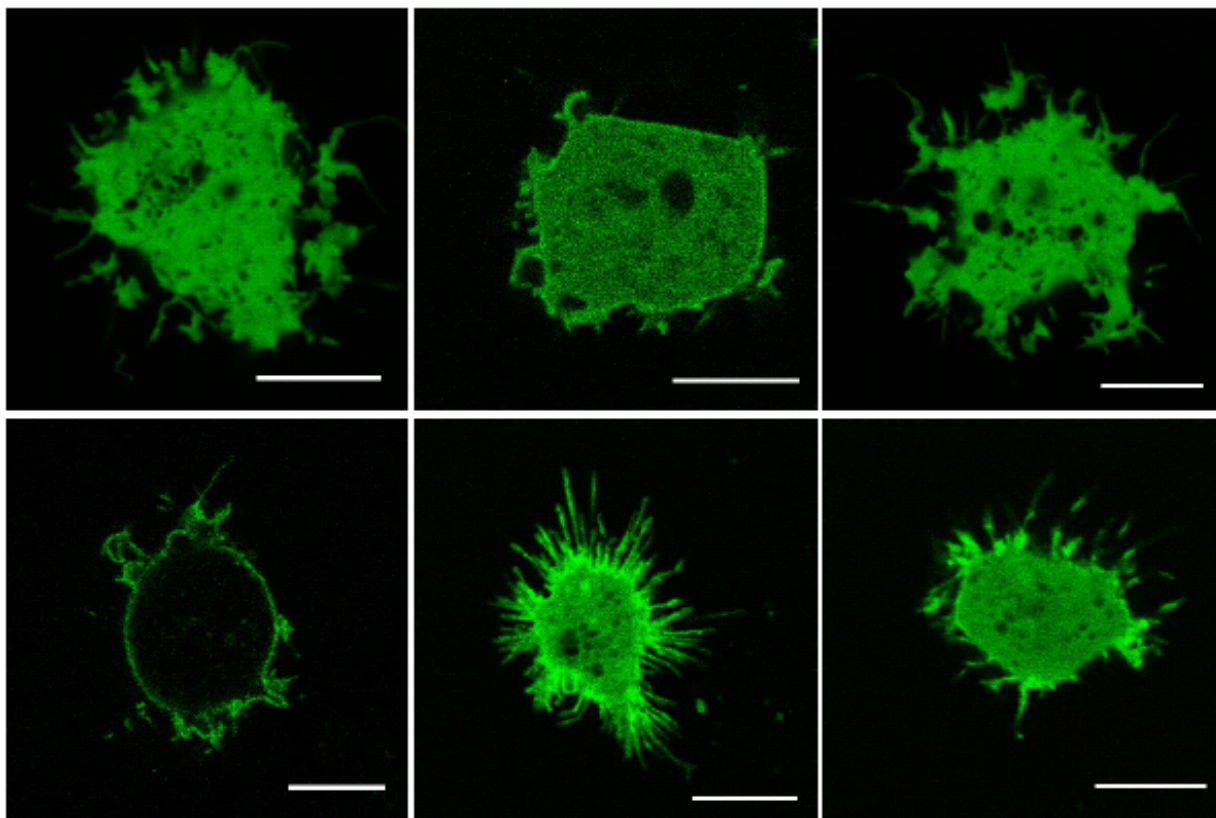


Figure 49: Variable phenotypes of GFP-ForA N-terminus overexpressing cells. ForA null cells overexpressing the N-terminus of ForA fused to GFP resulted in distinct cell populations including cells with obvious cortical or diffuse cytoplasmic staining. Abnormal actin structures are also observed. Scale bars represent 5 μ m.

3.2.16 ForA localization is myosin II independent

The localization to the rear end of a polarized cell was described for several proteins. Myosin II is one of the key actin-binding proteins was found to be localized also to the trailing end of the cell. Since ForA null mutant blebbing was myosin II dependent and ForA shared localization features with this motor protein, it was tempting to look at the staining of GFP-ForA Δ DAD in

a myosin II heavy chain null mutant. Interestingly, ForA localization was myosin II independent (Figure 50). A few attempts to transform clathrin heavy chain null mutant, PTEN null mutant, and cortexillin I/II double null mutant cells with GFP-ForA Δ DAD failed because of poor transformation efficiency, incompatible selection markers or both.

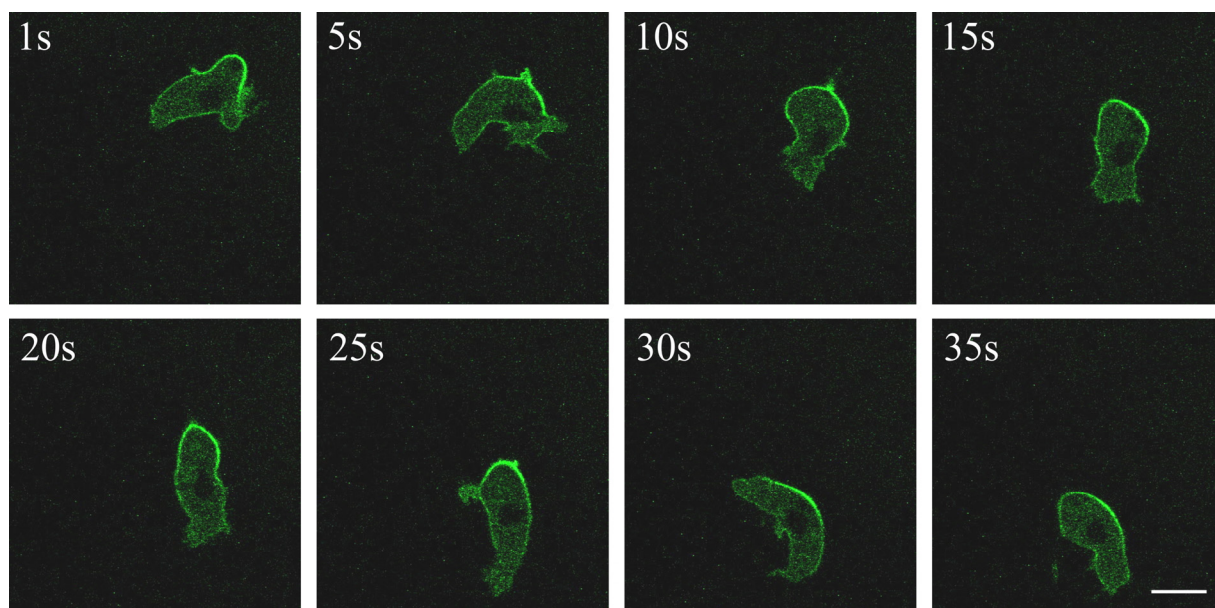


Figure 50: Myosin II is not required for ForA localization.

Time lapse images of myosin II heavy chain null mutant cells expressing GFP-ForA Δ DAD reveals that enrichment of ForA at the rear is independent of myosin II. The scale bar represents 10 μ m.

3.2.17 Putative binding partners of ForA

Identifying putative partners of the formin might provide a clue about the protein that is responsible for ForA localization. In a crude first attempt that could not be completed due to time restrictions, a GST pull down assay was carried out. A purified fragment encompassing the C2, GBD and FH3 as GST fusion (GST alone served as a negative control) was incubated with total lysates from cells overexpressing the constitutively active GFP-ForA Δ DAD in myosin II heavy chain null background. The myosin null mutant was used to avoid actomyosin contaminations.

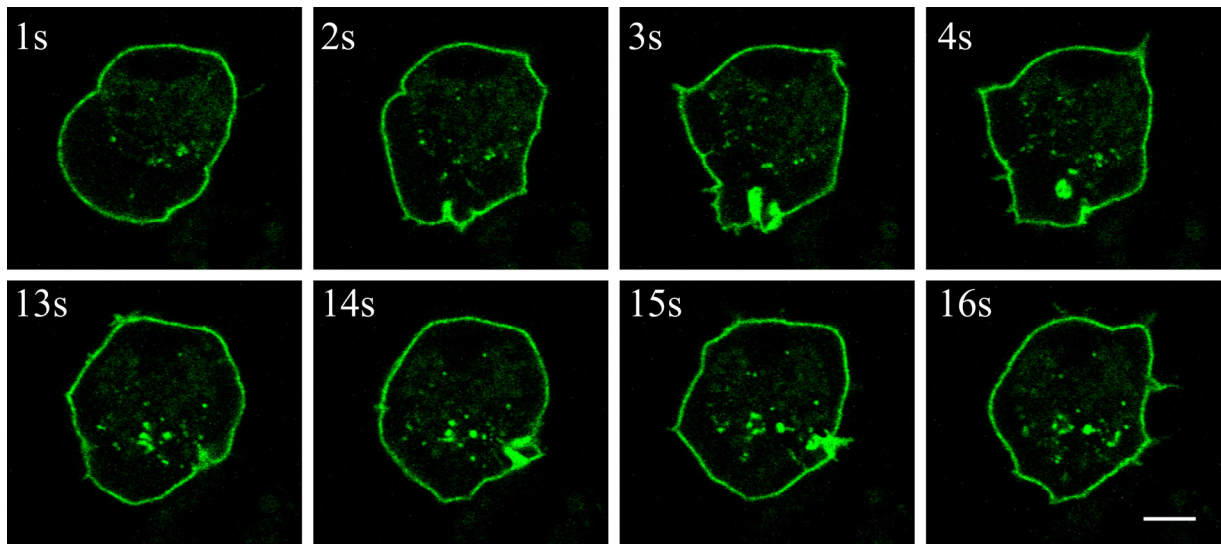


Figure 51: ForA localization is independent of IQGAP-related proteins. Expression of GFP-ForA Δ DAD in cells lacking IQGAP-related proteins (DGAP1/GAPA) implies that the cortical localization of ForA is independent of IQGAP-related proteins. Note that the actin dynamics in the form of endocytosis are prominent in time lapse images. Scale bar represents 5 μ m.

As a putative binding partner of ForA cortexillin (Faix et al., 1996) was picked up during the western blot analysis with polyclonal antibody generated against cortexillin (not shown). Since it was not possible to transform cortexillin I/II double null cells with GFP-ForA Δ DAD, the construct was used to transform DGAP1/GAPA double null mutant cells that harbor only non-functional cortexillin I/II (Faix et al., 2001). Initial transient transformation results showed that the peripheral cortical localization of ForA was not altered (Figure 51).

3.3 Characterization of dDia3

3.3.1 dDia3 is a DRF from *Dictyostelium discoideum*

dDia3 (or ForE) is with a molecular mass of about 175 kDa (Accession number: AJ812236, Dictybase ID - DDB0190413) one of the largest DRFs in *D. discoideum*. This DRF is encoded by a single exon comprised of 4686 bp in chromosome 1. Expression was confirmed by a RT-PCR approach (not shown). Subsequently, real time-PCR results (Rivero et al., 2005) confirmed that dDia3 is expressed throughout *D. discoideum* development.

The presence of the GBD-FH3 and DAD implies that dDia3 is a genuine DRF, suggesting that the endogenous formin will exist in its auto-inhibited state (Figure 52). As mentioned above, dDia3 is also a rather special formin because it contains at its N-terminus a C1 domain which is classified as protein kinase C - conserved region 1, also known as 'cysteine rich domain'. Originally, either the C1 domain-diacylglycerol interaction and/or the C1 domain-phorbol ester interaction seem to be crucial for the allosteric activation of protein kinase C enzymes. dDia3 is not the only non-protein kinase C protein that harbors the C1 domain. A number of cytoskeletal proteins including a Ras guanylyl nucleotide-releasing protein contain a C1 domain (Lemmon, 2008).

The sequence analysis of dDia3 revealed that unlike mDia1 and other related formins in lower and higher eukaryotes, the N-terminal region of dDia3 is mainly composed of acidic residues in addition to multiple S, Q, N, T and P repeats. Such amino acid sequence indeed pushes the GBD-FH3 farther from the N-terminus. This N-terminal amino acid composition, in particular the intriguing proline repeats and the position of the GBD-FH3 makes dDia3 a unique formin (Figure 53A). A multiple sequence alignment of the dDia3 C1 domain with the classical protein kinase C isoforms indicated that all six highly conserved cysteine residues are indeed present in dDia3 (Figure 53B).



Figure 52: Domain structure and protein sequence of dDia3.

dDia3 is a special multi-domain DRF with characteristic FH domains and an additional protein kinase C conserved region 1 (C1 domain).

A

```

1 MDNHSSSSNP SSLSSSSSSS SSSSSFLSDH VKKEEQNGLD TIKEEIEENKI
51 ENEEEEEKIE EKPIEKVEEE KIIIVQKEEEE KIEEEPIEKE EEKKVEEEKF
101 EQDNINTTVE AKTLETSTEP IATEVVDEKS ITSNNENLEE QQKEDVISIP
151 PPQQEQQQEQ EQQEKQKEET KPSIREEVKE KIKGKLSEIK EEIKDIKEEI
201 KHVIREEVTE PIIVVENNNS PPKPPPPPSI TVQSSSPVSS QISSPVSSPV
251 SSPKPSVTFN EDGRKRKEGG ITASISSEDI MALSSSTSTN NKGIPKENKR
301 TASTILRSKS SPNPGANNPN HNKDGNNSSS SSSSNNSDN NNSDNNSNN
351 NNINNNSSS NNLNYDSSDI DTEAIPKFYH DFKIHRGTSS CVYCGENTRL
401 WSTSYKCFFC GVVCHKKCLD SMNTIPCSSA IHNIGKGNRS QTISGYAPPN
451 SLALQAPPYI SVAKPSSITN SSSKSTPSLL SAPPQSNSN NSSPNISSKS
501 NPNSPITSA TTTTTTATIS SLSPTSISSP PIASEQPPSP LLQQQQQQQQ
551 QQQQQQQQQQ QQQQQQQQIS TTQLQDLNNT SEKPDDDMIN LMFDTLMVDL
601 DLNLPASKLS TTQKWLLEQ KFCLKKDELL PEYFINALKE QPSKSIQSL
651 VVILRTNVTK NWMCSFVQLN GVEILFEILS KSKRKDYKDD CLSCIGKMS
701 NPIGLNSVAQ LPMAPKTITK VLRKQYCIK SKAMAIELLT VMLLDKYVPG
751 GCSLVLKALT KTKEKKRFSF FVRFIKDNES LELKTKALCF INVLI FEMED
801 MNVRVNIRSE FLRLGLYTYL REIKKTI THE KTLFTQIEIF EEMNEDTQE
851 LDLRLEDLKR QLGIDIDDDVD QVFKALKNTT SKSGLNRQLL NILQNLIVIK
901 ACDPTDGVKY FILCDTLVKQ ISLHKGGFED PSNFDFRGLM VGLESATAEV
951 TLNRKLGELE KQNIKAMKI QEQDINIKSL LDLLKQLKDG GTAPDASMIK
1001 KIEEMIKQME PPPPISVKS PDDPNNAAPI VVAPIPPPPP PISGAPPPP
1051 PPPPPMKGA GPPPPPPPG KLGAKKPPAG VQCRPPPKVP KPSHPLKAYQ
1101 WVKLAPVKVN DSLFDKLGPM NDINLPWNQI EEEFAAKVIV REKKAIVKPK
1151 GPTQVIDPKL GQNISIFLSQ FKGVEPKQLI TYIQSMDESK MSRDQVKQIS
1201 KLLPSREDLA ALKEFLQAE RSKLSIADQY CIDIGAFPFA SEKISMFLK
1251 SELKSRLDEV KPQIAAVSVA CDEVYKSKKL IRIIEIILVL GNFINYGTPR
1301 GDISGYKLDL LIKLSDTKSS DLSSNLINTF VKYCQEKEPN LLTFADLPS
1351 LTTARKTIWS GVVADVSSIG RDVHSVQIV ETLQKSNEPF NQSIIDFLAT
1401 ASTEVEKLRK LLESTQENFK KLCKYFAEEE GKSQPEEFFD IFGRFITLFE
1451 NATTLQLOQK EEQLKEEKRL QQKQORQERA VRKLTTSNES ASASPNHAKS
1501 TDDKSEDEDD IVNDLLMAVR DGDAFRQAKG RRRTHQIAT SKMISNNLDP
1551 SKILPTSPNK N

```

B

```

dDia3 HDF--KIHRG TSSCVYCGEN T-RLWSTSYK CFFCGVVCHK KCLDSMNTIP C
PKCα HKFIARFFKQ PTFCSHCTDF IWGFGKQGFQ CQVCCFVVHK RCHEFV-TFS C
PKCβ HKFTARFFKQ PTFCSHCTDF IWGFGKQGFQ CQVCCFVVHK RCHEFV-TFS C
PKCγ HKFTARFFKQ PTFCSHCTDF IWGIGKQGLQ CQVCSFVVHR RCHEFV-TFE C

```

Figure 53: Amino acid sequence of dDia3.

(A) Formin domains are highlighted by colour codes: C1 domain [390-427 aa], GBD [582-740 aa], FH3 [750-933 aa], FH1 [991-1069 aa], FH2 [1070-1449 aa] and DAD [1501-1550 aa]. Please note there is a proline-rich region at the N-terminus [221-228 aa]. (B) C1 domain of dDia3. The C1 domain of dDia3 is aligned with the respective regions of conventional protein kinases. Conserved residues are highlighted by gray shades.

3.3.2 Recombinant dDia3 nucleates and caps actin filaments

Recombinant dDia3 FH2DAD was tested for its ability to nucleate actin polymerization. The recombinant fragment nucleated and assembled actin filaments in a dose-dependent manner (Figure 54A). Nanomolar amounts of the recombinant dDia3 FH2DAD also capped the filament barbed ends thus preventing the depolymerization of actin filaments that are diluted below the critical concentration of the barbed ends (Figure 54B). It is to be noted that the barbed end capping of dDia3 FH2DAD is at least 5 times stronger than that of the ForA-FH2DAD.

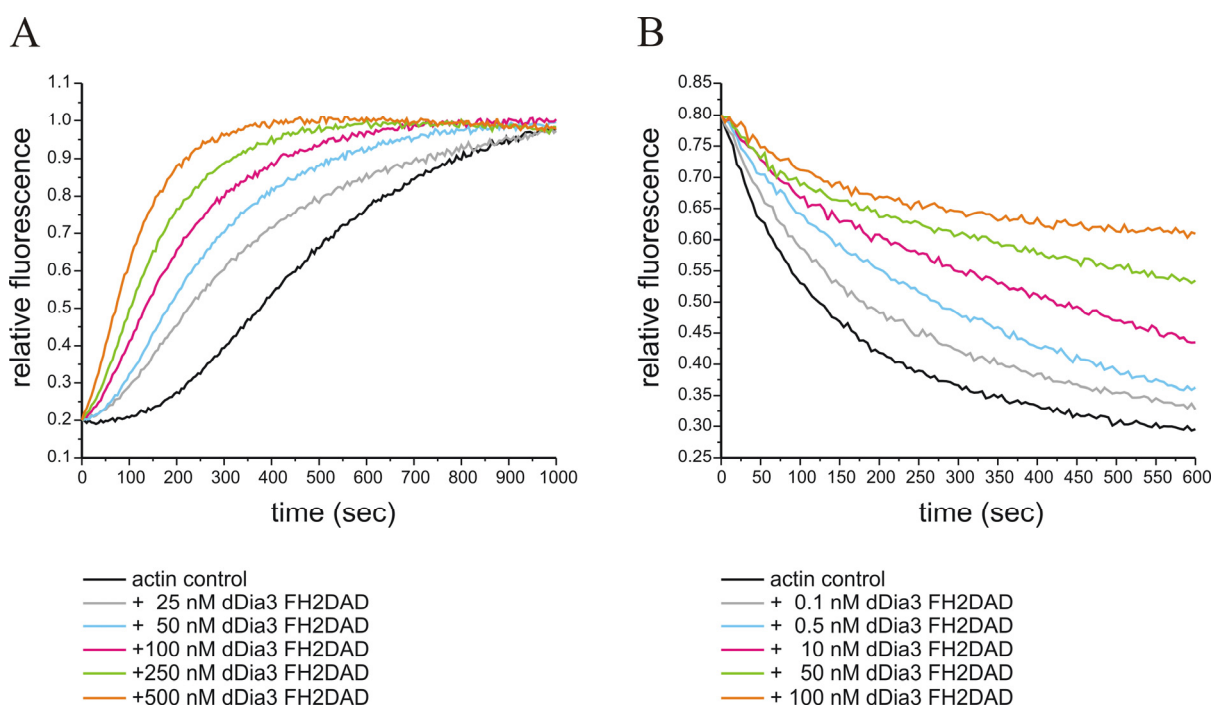


Figure 54: Recombinant dDia3 interacts with actin.

GST-dDia3 FH2DAD stimulated nucleation and assembly of actin filaments in a dose-dependent manner (A); it also significantly inhibited the depolymerization of the F-actin that has been diluted below the critical concentration of the barbed end (B).

3.3.3 dDia3 interacts with all three profilin isoforms

The yeast-two hybrid results indicated that the proline-rich FH1 domain of dDia3 did not show any preference for a profilin as it interacted with all three profilin isoforms present in *D. discoideum* (Figure 55). Nevertheless, these data need to be further tested at single molecule

level to find if there are any isoform-dependent changes of filament elongation. Also it will be interesting to see if the single proline repeat at the very N-terminus mediates the profilin-formin interaction.

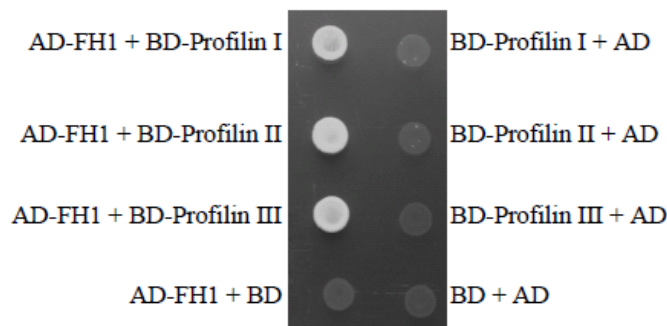


Figure 55: dDia3 interacts with all three profilin isoforms in *D. discoideum*.

Yeast cells were transformed with the indicated constructs and tested for potential interaction on conditional media lacking leucine, tryptophan, histidine and adenine. AD: activation domain, BD: binding domain. The result indicates that dDia3 interacts with all three profilin isoforms.

3.3.4 Characterization of dDia3 null mutant cells

Dr. Jan Faix isolated the dDia3 null mutant. In comparison to the wild type AX2 strain dDia3 null mutant cells did not exhibit any striking differences at least in routine assays including random motility of single vegetative cells, chemotaxis of streaming t6 cells, slug migration in response to light (phototaxis), endocytosis (phagocytosis and pinocytosis), exocytosis, growth in shaking culture and on *K. aerogenes* lawns; also the development of the dDia3 mutant cells was largely unaffected (not shown). The question of redundancy is quite apt for dDia3 as well.

3.3.5 Subcellular localization of GFP-dDia3

Despite the efforts to identify the loss of function of dDia3 using routine techniques the in vivo role of dDia3 remains unresolved. So to understand if dDia3 functions in a unique, yet uncharacterized pathway it was important to learn where the formin is localized? Subsequently, a GFP-dDia3 full-length construct was made for this purpose.

Both wild type and the dDia3 null mutant cells were transformed by a construct carrying the full-length dDia3 gene fused N-terminally to GFP. Microscopic examination of both cell lines expressing GFP-labelled dDia3 revealed that the formin was distributed uniformly on the

plasma membrane, which might be the result of the lipid-binding C1 domain at the N-terminus (Figure 56B).

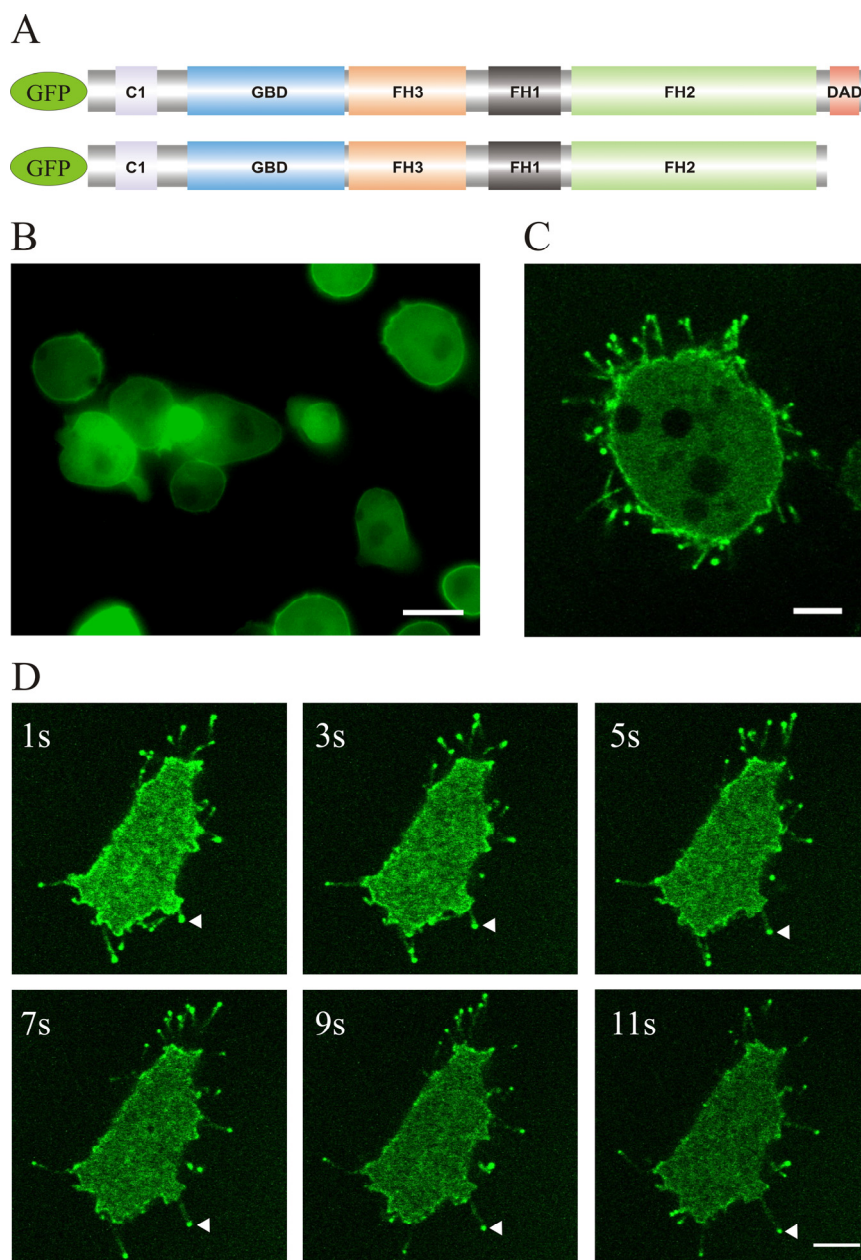


Figure 56: dDia3 is localized to the plasma membrane and filopodial tips in AX2 cells. (A) Schematic representation of the GFP constructs used; full-length dDia3 above and the constitutively active dDia3 below. GFP-Dia3 uniformly stained the plasma membrane (A), whereas the constitutively active GFP-dDia3 Δ DAD accumulated on tips of filopodia in addition to the plasma membrane (B). Time lapse images (1 frame/sec) of wild type cells expressing GFP-dDia3 Δ DAD (C). Arrow heads indicate growing filopodia. Scale bars represent 5 μ m.

The data suggest that dDia3 might link the cytoskeleton to the plasma membrane through DAG, facilitated by the C1 domain. The dDia3 C1 domain shares significant homology (signature motif - $HX_{11}CX_2CX_{12}CX_2CX_4HX_2CX_8C$, where H is histidine, X any amino acid and C is cysteine) with the C1 domains of classical protein kinase C isoforms (Hurley and Misra, 2000). To address its in vivo relevance one has to test a. construct lacking the C1 domain in vivo.

3.3.6 Subcellular localization of constitutively active dDia3

To better understand the in vivo function of dDia3, a constitutively active version missing the C-terminal Diaphanous-autoregulatory domain (DAD) was constructed for expression of a GFP fusion protein. Both the wild type and the dDia3 null mutant cells were transformed with the GFP-dDia3 Δ DAD construct. Interestingly, the constitutively active GFP-dDia3 Δ DAD construct decorated not only the plasma membrane but also the filopodial tips (Figure 56C and D) indicating that both dDia2 (Schirenbeck et al., 2005) and dDia3 are, in contrast to ForA, indeed filopodial formins.

Overexpression of GFP-dDia3 Δ DAD also resulted in abnormal club shaped filopodial tips as observed in mammalian cells overexpressing EGFP-mDia2 Δ DAD (Block et al., 2008) which implied there is no difference in filopodial structure induced by constitutively active formins from lower and higher eukaryotes.

Although the filopodial dynamics were largely unaltered in the dDia3 null mutant, intriguingly, a double knock out *D. discoideum* cell line lacking both dDia2 and dDia3 displayed a reduced number of filopodia and in addition showed severe defects in cell adhesion. The data strongly suggest that functions of both dDia2 and dDia3 overlap (not shown).

4 Discussion

The major goal of the thesis was to understand the regulation of mouse and *D. discoideum* formins, both in vitro and in vivo. The studies on the mouse formin mDia1 led to a discovery of a novel regulatory mechanism through phospholipids. The work on *D. discoideum* formins resulted in the very surprising observation that a formin can distinctly accumulate at the rear of a migrating cell, despite its nucleating activity which is usually required at the moving front and in filopodia tips.

4.1 mDia1

An important feature of actin polymerization in migrating cells is the need of filament elongation directly at the plasma membrane. Consequently, the majority of the filaments is not distributed randomly but rather in a polarized fashion with the fast growing barbed ends pointing towards the membrane and in parallel to the direction of movement. It is, therefore, a frequent question how a cell can organize such an arrangement and which factors are necessary for a biased orientation of filaments. Since many years a continuous search is underway whether proteins can hook a filament with its barbed end to the inner leaflet of the plasma membrane, and at the same time allows or even enhance elongation at this very end. The mechanics of such a process were puzzling. How can a membrane associated protein grab the barbed end of a filament, release the end for adding monomers without losing the filament. One of the first scientists asking these questions was Albrecht Wegner who studied a protein 'insertin' that bound to the membrane, allowed filament elongation and kept the filament end at the membrane. Insertin functioned as a dimer which guaranteed a hand-over-hand elongation of alternating hold of the filament and addition of an actin monomer (Gaertner and Wegner, 1991; Ruhnau et al., 1989). At that time it was not possible to unequivocally determine the biochemical nature of this membrane anchor. Capping proteins, profilins and more specific factors came into focus because they were regulated by membrane lipids (Yin and Janmey, 2003). But also these studies did not lead to clear-cut results.

Only since the discovery of the formins our understanding might move into the right direction. Formins are dimers, they are connected to the barbed end, add hand-over-hand actin monomers and, if they harbor the appropriate domain, stay bound to the inner leaflet of a biomembrane. In a previous report, Rosen and coworkers showed that the complete N-terminus of mDia1

(amino acids 1-570) was localized at the plasma membrane (Seth et al., 2006). However, this was a large portion of the protein and the finding that the inactivation of GBD by a point mutation abolished membrane attachment only partially suggested a more sophisticated mechanism and a membrane binding activity beyond the GBD.

The discovery of an N-terminal region rich in basic residues ('BR', see also mDia1 topology in Figure 5A) indicated the importance of BR-phospholipid interactions not only for plasma membrane recruitment but also for membrane insertion of active mDia1. Since the four independent constructs EGFP-mDia1BR, EGFP-mDia1GBD, EGFP-mDia1BR-GBD and EGFP-mDia1 Δ BR Δ DAD failed to localize to the plasma membrane (Figure 12B) an involvement of multiple signals for mDia1 localization was obvious.

The results of this thesis in relation to published data indicate the following cooperation between GBD, BR and DID (Figure 57).

- (1) a membrane-bound GTPase opens the closed formin conformation by interaction with GBD (Li and Higgs, 2005; Rose et al., 2005).
- (2) BR accomplishes the actual interaction with the phospholipids PS/PIP₂ in the plasma membrane.
- (3) The contact of DID to the scaffolding protein IQGAP strengthens the interaction between plasma membrane and the N-terminus of formin (Brandt et al., 2007).

Thus a failure in any one of the signals will result in mislocalized mDia1. A very interesting byproduct of these experiments is the distribution of the EGFP-mDia1 Δ BR Δ DAD construct to filopodia tips. EGFP-mDia1 Δ BR Δ DAD does not bind to membranes because the appropriate domains are missing. Consequently, if this construct accumulates at the barbed ends of filopodial actin filaments then - in contrast to the general opinion - it might be anchored in the tip complex and not in the membrane. This opens a completely new view of formins in concert with yet unidentified proteins from the filopodial tip complex. It is an important feature for a cell that the activity of potent actin nucleators is regulated differentially at independent levels. The inhibition of an active full-length mDia1 by PIP₂ occurs obviously after the protein has been activated by the GTP-bound RhoA upon a stimulus at the plasma membrane. Consequently, a removal of an active Rho at this stage would prevent refolding to the inactive hairpin structure. So the working hypothesis is that binding and the subsequent clustering of PIP₂ by the DAD and the FH2 domain presumably reduces the accessibility of actin to the

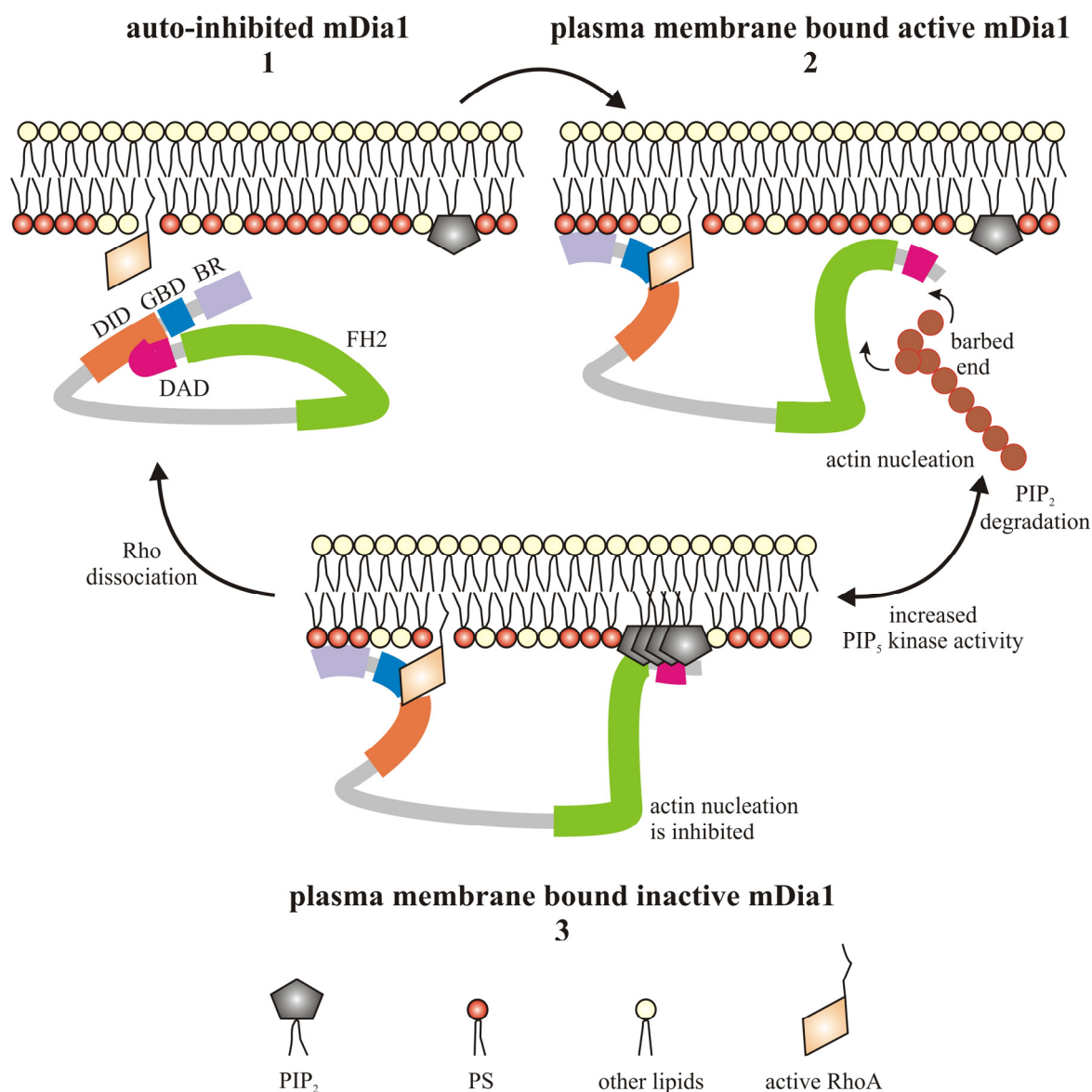


Figure 57: Schematic summary of mDia1 regulation.

Auto-inhibition of cytoplasmic formin occurs by the interaction of DID and DAD (step 1). Upon signal transduction GTP-bound RhoA binds to GBD, thus unfolds the protein and enables the FH2 domain to nucleate actin polymerization; at the same time the N-terminal phosphatidylserine-binding region BR establishes the contact of the active formin at the plasma membrane (step 2) which will be further strengthened by the IQGAP-DID interaction (not shown). For reversible fine tuning of formin-driven actin polymerization PIP₂ clusters are generated e.g. by an increased activity of PIP₅ kinase in response to a stimulus, and negatively regulate formin activity by binding to the DAD and the FH2 domain (step 3). This keeps the formin in a transiently inactive conformation, and GTPase-independent re-activation relies on the degradation of PIP₂. Eventually, membrane-bound formin returns to its auto-inhibited stage after GTP hydrolysis and dissociation from the membrane. GBD: GTPase-binding domain, DID: Diaphanous-inhibitory domain, FH: formin homology, DAD: Diaphanous-auto-regulatory domain, BR: basic region.

FH2 domain and thus resulting in actin assembly arrest. Furthermore, the data imply that mDia1 can remain at the plasma membrane even during a brief period of inhibition, i.e. localization and activity are distinct phenomena (Figure 57). It is somewhat puzzling that clustering of PIP₂ is diminished after the C-terminal basic residues have been stepwise replaced by alanines, but that there is still considerable PIP₂-dependent inhibition of the point mutations. Therefore, one can not exclude that it is the membrane insertion which reduces the activity. Under those presumptions the C-terminal interaction with PIP₂ might also rather function as a localization signal.

The most prominent and best studied machineries driving the nucleation of actin filaments in vertebrate cells are formins and the Arp2/3-complex (Mattila and Lappalainen, 2008). The latter requires activation by so-called nucleation promoting factors such as neuronal Wiskott-Aldrich syndrome protein (N-WASp) (Stradal et al., 2004). Like formins, N-WASp or WASp are folded in an auto-inhibited conformation (Kim et al., 2000; Seth et al., 2006). The simultaneous binding of active Cdc42 and PIP₂ to the GTPase-binding domain (GBD) and to a basic region, respectively, relieves auto-inhibition of N-WASp or WASp completely and allows subsequent activation of the Arp2/3 complex and increased actin nucleation synergistically (Higgs and Pollard, 2000; Prehoda et al., 2000).

The multi-domain architecture, auto-inhibition, the small GTPase and phospholipid signalling are all reminiscent of the DRF regulation. It is intriguing that the two key nucleators in the actin system are conversely regulated. In this scenario local changes of PIP₂ concentrations upon signal transduction could therefore trigger either the formation of lamellipodial actin networks by Arp2/3 or the generation of linear actin structures by formins.

Through this first formin-phospholipid study an unexplored area is now revealed which will have to deal with the following major questions in the future:

- (1) Relying on the unilamellar liposome fluorescence spectroscopy data, how can PIP₂ regulate both the localization and activity of mDia1? Does PIP₂ regulate mDia1 in a spatial-temporal manner?
- (2) PIP₂ clustering by the C-terminus of mDia1 is independent of its membrane insertion ability. How? Which residues are important for membrane insertion?

- (3) What is the structural basis of the PIP₂ mediated inhibition of mDia1 activity? Is it possible to obtain and to analyze this structure by crystallography and NMR techniques?
- (4) Is the negative regulation of mDia and related formins by PIP₂ embedded in distinct signal transduction cascades?

4.2 ForA

All 10 *D. discoideum* formin genes are reported to express the respective mRNA products as shown by a Real Time PCR approach (Rivero et al., 2005). Characterization of the ForA-actin interaction in vitro indicated that ForA is a typical DRF whose activity is likely to be regulated by one or more RacGTPases in agreement with other reports (Brandt et al., 2007; Li and Higgs, 2003; Seth et al., 2006). Attempts to identify the GTPase that relieves the auto-inhibition of ForA failed so far.

Interestingly, the presence of a structurally and functionally specialized lipid-binding C2 domain was found to play a crucial role in the auto-inhibition of ForA in vitro. This was further substantiated in vivo by ForA null mutant rescue experiments: ectopically expressed GFP-ForA Δ C2 restored the directed and coordinated cell migration defect during slug phototaxis completely, in contrast to the partial rescue of the phenotype displayed by the inactive full-length GFP-ForA. Why the full-length regulatable ForA does not rescue the migration defect is only poorly understood after ruling out an overexpression induced damage, as expression of the same construct in wild type did not alter the phototactic behaviour of slugs. Our current working hypothesis assumes an additional regulatory activity of the C2 domain in vivo. If the removal of the C2 domain which is located right in front of the GBD favors Rac-binding and consequently activation of ForA, then the Δ C2 construct could rescue the aberrant phenotype by an overall increased formin activity.

The role of formin in the induction of non-apoptotic plasma membrane blebbing seems to be a hot topic in recent times (Fackler and Grosse, 2008). Such membrane blebs are observed not only in amoeboid cells during movement (Langridge and Kay, 2006) but also after disturbance of cortical tension (Charras et al., 2006). Previously, the presence of mDia2 was reported to be important for promoting membrane blebs (Eisenmann et al., 2007). But in contrast a recent

report (Di Vizio et al., 2009) suggested that mDia2 knock down cells exhibited plasma membrane blebbing.

Also, ForA null mutant and ForA overexpressing cells were observed to stimulate membrane blebs in a myosin II dependent manner. These data are in agreement with a previous micro array report suggesting that ForA expression is regulated by osmotic stress (Na et al., 2007). Osmotic stress potentially can influence the cortical tension which in turn eventually stimulates the formation membrane blebs. We conclude from our data that the endogenous ForA level needs to be tightly controlled. As soon as the balance is tilted either way (ForA null, ForA overexpression) cortical tension would be disturbed and plasma membrane blebs are inevitable (Figure 58).

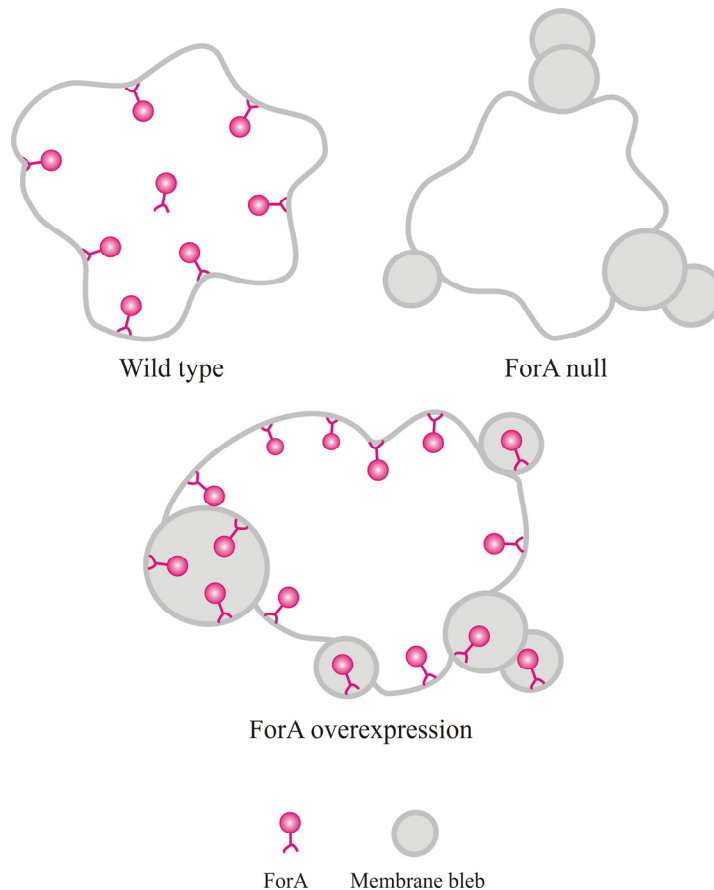


Figure 58: ForA regulates the integrity of the cortical actin cytoskeleton.

Both depletion (ForA null) and overexpression of ForA result in myosin II dependent membrane blebs. A finely regulated cellular concentration of ForA needs to be maintained to avoid a breakdown of the cortical cytoskeleton.

In addition to cortical defects the ForA null mutant displayed coordinated cell migration defects. Despite the fact that ForA null mutant slugs were phototactically defective, exhibited reduced single cell random motility and induced non-apoptotic membrane blebs, the phenotype of the null mutant is considered to be subtle. GFP-ForA Δ DAD is in the cleavage furrow during both normal and asymmetric cell division but the ForA null mutant does not display a strong cytokinesis defect. GFP-ForA Δ DAD accumulates at trailing ends of motile cells but there are no severe defects in cell migration, endocytosis and development. This strongly implies that the ForA signalling pathway is redundant. Redundancy, at least under laboratory conditions, is a frequent phenomenon especially in the cytoskeleton (Witke et al., 1992). Hence, identification of a second formin that might complement ForA functions is of paramount importance. This triggered studies on dDia3 which might compensate with its C1 lipid-binding domain C2-specific functions in ForA. However, ForA/dDia3 double null mutant cells were normal in cell division, chemotaxis and development (not shown) which strongly argues against dDia3 as functionally redundant component in the regulatory cascade.

The most peculiar feature of ForA is its accumulation at the rear and not in the moving front where de novo actin filaments are essential. This raises the question whether ForA nucleates actin filaments just for myosin II which is also at the rear end. Would an enhanced formation of an acto-myosin complex at rear help the motor protein to continuously retract the uropod during migration? Are cortexillins/IQGAP-related proteins (Faix et al., 2001) required for myosin II independent localization of ForA? In other words, how is ForA recruited to the trailing ends of motile cells? The answers are still open.

One of the interesting facts about formin regulation in general is the effective heterodimer formation between endogenous formins (Copeland et al., 2007). Overexpression of the N-terminal region of ForA spanning C2-GBD-FH3 as a GFP fusion protein in ForA null mutant cells induced abnormal actin structures. At first this was puzzling because the construct lacks the FH1 and FH2 domains which are responsible for formin/actin interactions. Presumably, the overexpressed GFP-ForA N-terminus dimerized with an endogenous full-length subunit(s), via a DID/DAD interaction and activated auto-inhibited formin(s) in a GTPase-independent manner. Such a plethora of possible heterodimers suggests a rather unsettling complexity in formin research.

5 References

- Ahuja, R., Pinyol, R., Reichenbach, N., Custer, L., Klingensmith, J., Kessels, M.M. and Qualmann, B. (2007) Cordon-bleu is an actin nucleation factor and controls neuronal morphology. *Cell*, **131**, 337-350.
- Alberts, A.S. (2002) Diaphanous-related Formin homology proteins. *Curr Biol*, **12**, R796.
- Applewhite, D.A., Barzik, M., Kojima, S., Svitkina, T.M., Gertler, F.B. and Borisy, G.G. (2007) Ena/VASP proteins have an anti-capping independent function in filopodia formation. *Mol Biol Cell*, **18**, 2579-2591.
- Arasada, R., Gloss, A., Tunggal, B., Joseph, J.M., Rieger, D., Mondal, S., Faix, J., Schleicher, M. and Noegel, A.A. (2007) Profilin isoforms in Dictyostelium discoideum. *Biochim Biophys Acta*, **1773**, 631-641.
- Arasada, R., Son, H., Ramalingam, N., Eichinger, L., Schleicher, M. and Rohlfs, M. (2006) Characterization of the Ste20-like kinase Krs1 of Dictyostelium discoideum. *Eur J Cell Biol*, **85**, 1059-1068.
- Bai, R., Covell, D.G., Liu, C., Ghosh, A.K. and Hamel, E. (2002) (-)-Doliculide, a new macrocyclic depsipeptide enhancer of actin assembly. *J Biol Chem*, **277**, 32165-32171.
- Block, J., Stradal, T.E., Hanisch, J., Geffers, R., Kostler, S.A., Urban, E., Small, J.V., Rottner, K. and Faix, J. (2008) Filopodia formation induced by active mDia2/Drf3. *J Microsc*, **231**, 506-517.
- Bradford, M.M. (1976) A rapid and sensitive method for the quantitation of microgram quantities of protein utilizing the principle of protein-dye binding. *Anal Biochem*, **72**, 248-254.
- Brandt, D.T., Marion, S., Griffiths, G., Watanabe, T., Kaibuchi, K. and Grosse, R. (2007) Dia1 and IQGAP1 interact in cell migration and phagocytic cup formation. *J Cell Biol*, **178**, 193-200.
- Breitsprecher, D., Kiesewetter, A.K., Linkner, J., Urbanke, C., Resch, G.P., Small, J.V. and Faix, J. (2008) Clustering of VASP actively drives processive, WH2 domain-mediated actin filament elongation. *Embo J*, **27**, 2943-2954.
- Bubb, M.R., Senderowicz, A.M., Sausville, E.A., Duncan, K.L. and Korn, E.D. (1994) Jasplakinolide, a cytotoxic natural product, induces actin polymerization and

- competitively inhibits the binding of phalloidin to F-actin. *J Biol Chem*, **269**, 14869-14871.
- Carrier, M.F., Pantaloni, D. and Korn, E.D. (1984) Evidence for an ATP cap at the ends of actin filaments and its regulation of the F-actin steady state. *J Biol Chem*, **259**, 9983-9986.
- Charras, G.T., Hu, C.K., Coughlin, M. and Mitchison, T.J. (2006) Reassembly of contractile actin cortex in cell blebs. *J Cell Biol*, **175**, 477-490.
- Chereau, D., Boczkowska, M., Skwarek-Maruszewska, A., Fujiwara, I., Hayes, D.B., Rebowski, G., Lappalainen, P., Pollard, T.D. and Dominguez, R. (2008) Leiomodin is an actin filament nucleator in muscle cells. *Science*, **320**, 239-243.
- Chesarone, M.A. and Goode, B.L. (2009) Actin nucleation and elongation factors: mechanisms and interplay. *Curr Opin Cell Biol*, **21**, 28-37.
- Chhabra, E.S. and Higgs, H.N. (2007) The many faces of actin: matching assembly factors with cellular structures. *Nat Cell Biol*, **9**, 1110-1121.
- Chisholm, R.L. and Firtel, R.A. (2004) Insights into morphogenesis from a simple developmental system. *Nat Rev Mol Cell Biol*, **5**, 531-541.
- Cooper, J.A. (1987) Effects of cytochalasin and phalloidin on actin. *J Cell Biol*, **105**, 1473-1478.
- Cooper, J.A., Blum, J.D. and Pollard, T.D. (1984) Acanthamoeba castellanii capping protein: properties, mechanism of action, immunologic cross-reactivity, and localization. *J Cell Biol*, **99**, 217-225.
- Cooper, J.A. and Sept, D. (2008) New insights into mechanism and regulation of actin capping protein. *Int Rev Cell Mol Biol*, **267**, 183-206.
- Copeland, S.J., Green, B.J., Burchat, S., Papalia, G.A., Banner, D. and Copeland, J.W. (2007) The diaphanous inhibitory domain/diaphanous autoregulatory domain interaction is able to mediate heterodimerization between mDia1 and mDia2. *J Biol Chem*, **282**, 30120-30130.
- Coue, M., Brenner, S.L., Spector, I. and Korn, E.D. (1987) Inhibition of actin polymerization by latrunculin A. *FEBS Lett*, **213**, 316-318.
- Dagert, M. and Ehrlich, S.D. (1979) Prolonged incubation in calcium chloride improves the competence of Escherichia coli cells. *Gene*, **6**, 23-28.

- De La Cruz, E.M., Mandinova, A., Steinmetz, M.O., Stoffler, D., Aebi, U. and Pollard, T.D. (2000) Polymerization and structure of nucleotide-free actin filaments. *J Mol Biol*, **295**, 517-526.
- Devreotes, P.N. and Zigmond, S.H. (1988) Chemotaxis in eukaryotic cells: a focus on leukocytes and Dictyostelium. *Annu Rev Cell Biol*, **4**, 649-686.
- Di Vizio, D., Kim, J., Hager, M.H., Morello, M., Yang, W., Lafargue, C.J., True, L.D., Rubin, M.A., Adam, R.M., Beroukhi, R., Demichelis, F. and Freeman, M.R. (2009) Oncosome Formation in Prostate Cancer: Association with a Region of Frequent Chromosomal Deletion in Metastatic Disease. *Cancer Res*.
- Didry, D., Carlier, M.F. and Pantaloni, D. (1998) Synergy between actin depolymerizing factor/cofilin and profilin in increasing actin filament turnover. *J Biol Chem*, **273**, 25602-25611.
- Dumontier, M., Hocht, P., Mintert, U. and Faix, J. (2000) Rac1 GTPases control filopodia formation, cell motility, endocytosis, cytokinesis and development in Dictyostelium. *J Cell Sci*, **113 (Pt 12)**, 2253-2265.
- Edwards, R.A. and Bryan, J. (1995) Fascins, a family of actin bundling proteins. *Cell Motil Cytoskeleton*, **32**, 1-9.
- Eichinger, L. and Schleicher, M. (1992) Characterization of actin- and lipid-binding domains in severin, a Ca(2+)-dependent F-actin fragmenting protein. *Biochemistry*, **31**, 4779-4787.
- Eisenmann, K.M., Harris, E.S., Kitchen, S.M., Holman, H.A., Higgs, H.N. and Alberts, A.S. (2007) Dia-interacting protein modulates formin-mediated actin assembly at the cell cortex. *Curr Biol*, **17**, 579-591.
- Fackler, O.T. and Grosse, R. (2008) Cell motility through plasma membrane blebbing. *J Cell Biol*, **181**, 879-884.
- Faix, J., Gerisch, G. and Noegel, A.A. (1992) Overexpression of the csA cell adhesion molecule under its own cAMP-regulated promoter impairs morphogenesis in Dictyostelium. *J Cell Sci*, **102 (Pt 2)**, 203-214.
- Faix, J. and Grosse, R. (2006) Staying in shape with formins. *Dev Cell*, **10**, 693-706.

- Faix, J., Kreppel, L., Shaulsky, G., Schleicher, M. and Kimmel, A.R. (2004) A rapid and efficient method to generate multiple gene disruptions in *Dictyostelium discoideum* using a single selectable marker and the Cre-loxP system. *Nucleic Acids Res*, **32**, e143.
- Faix, J., Steinmetz, M., Boves, H., Kammerer, R.A., Lottspeich, F., Mintert, U., Murphy, J., Stock, A., Aebi, U. and Gerisch, G. (1996) Cortexillins, major determinants of cell shape and size, are actin-bundling proteins with a parallel coiled-coil tail. *Cell*, **86**, 631-642.
- Faix, J., Weber, I., Mintert, U., Kohler, J., Lottspeich, F. and Marriott, G. (2001) Recruitment of cortexillin into the cleavage furrow is controlled by Rac1 and IQGAP-related proteins. *Embo J*, **20**, 3705-3715.
- Fowler, V.M., Sussmann, M.A., Miller, P.G., Flucher, B.E. and Daniels, M.P. (1993) Tropomodulin is associated with the free (pointed) ends of the thin filaments in rat skeletal muscle. *J Cell Biol*, **120**, 411-420.
- Fullner, K.J. and Mekalanos, J.J. (2000) In vivo covalent cross-linking of cellular actin by the *Vibrio cholerae* RTX toxin. *Embo J*, **19**, 5315-5323.
- Gaertner, A. and Wegner, A. (1991) Mechanism of the insertion of actin monomers between the barbed ends of actin filaments and barbed end-bound insertin. *J Muscle Res Cell Motil*, **12**, 27-36.
- Goode, B.L. and Eck, M.J. (2007) Mechanism and function of formins in the control of actin assembly. *Annu Rev Biochem*, **76**, 593-627.
- Halliburton, W.D. (1887) On Muscle-Plasma. *J Physiol*, **8**, 133-202.
- Hama, H., Kasai, M., Maruyama, K. and Noda, H. (1969) Natural F-actin. IV. Length distribution and its change studied by electron microscopy. *Biochim Biophys Acta*, **194**, 470-477.
- Haus, U., Hartmann, H., Trommler, P., Noegel, A.A. and Schleicher, M. (1991) F-actin capping by cap32/34 requires heterodimeric conformation and can be inhibited with PIP2. *Biochem Biophys Res Commun*, **181**, 833-839.
- Heiss, S.G. and Cooper, J.A. (1991) Regulation of CapZ, an actin capping protein of chicken muscle, by anionic phospholipids. *Biochemistry*, **30**, 8753-8758.
- Higgs, H.N. and Peterson, K.J. (2005) Phylogenetic analysis of the formin homology 2 domain. *Mol Biol Cell*, **16**, 1-13.

- Higgs, H.N. and Pollard, T.D. (2000) Activation by Cdc42 and PIP(2) of Wiskott-Aldrich syndrome protein (WASp) stimulates actin nucleation by Arp2/3 complex. *J Cell Biol*, **150**, 1311-1320.
- Hurley, J.H. and Misra, S. (2000) Signaling and subcellular targeting by membrane-binding domains. *Annu Rev Biophys Biomol Struct*, **29**, 49-79.
- Isenberg, G., Aebi, U. and Pollard, T.D. (1980) An actin-binding protein from *Acanthamoeba* regulates actin filament polymerization and interactions. *Nature*, **288**, 455-459.
- Janmey, P.A., Chaponnier, C., Lind, S.E., Zaner, K.S., Stossel, T.P. and Yin, H.L. (1985) Interactions of gelsolin and gelsolin-actin complexes with actin. Effects of calcium on actin nucleation, filament severing, and end blocking. *Biochemistry*, **24**, 3714-3723.
- Jockusch, B.M., Murk, K. and Rothkegel, M. (2007) The profile of profilins. *Rev Physiol Biochem Pharmacol*, **159**, 131-149.
- Joseph, J.M., Fey, P., Ramalingam, N., Liu, X.I., Rohlf, M., Noegel, A.A., Muller-Taubenberger, A., Glockner, G. and Schleicher, M. (2008) The actinome of *Dictyostelium discoideum* in comparison to actins and actin-related proteins from other organisms. *PLoS One*, **3**, e2654.
- Kasai, M. (1969) Thermodynamical aspect of G-F transformations of actin. *Biochim Biophys Acta*, **180**, 399-409.
- Kasai, M. and Hama, H. (1969) Natural F-actin. 3. Natural F-actin as inactive polymer. *Biochim Biophys Acta*, **180**, 550-561.
- Khaire, N., Muller, R., Blau-Wasser, R., Eichinger, L., Schleicher, M., Rief, M., Holak, T.A. and Noegel, A.A. (2007) Filamin-regulated F-actin assembly is essential for morphogenesis and controls phototaxis in *Dictyostelium*. *J Biol Chem*, **282**, 1948-1955.
- Kim, A.S., Kakalis, L.T., Abdul-Manan, N., Liu, G.A. and Rosen, M.K. (2000) Autoinhibition and activation mechanisms of the Wiskott-Aldrich syndrome protein. *Nature*, **404**, 151-158.
- Kitayama, C. and Uyeda, T.Q. (2003) ForC, a novel type of formin family protein lacking an FH1 domain, is involved in multicellular development in *Dictyostelium discoideum*. *J Cell Sci*, **116**, 711-723.

- Kouyama, T. and Mihashi, K. (1981) Fluorimetry study of N-(1-pyrenyl)iodoacetamide-labelled F-actin. Local structural change of actin protomer both on polymerization and on binding of heavy meromyosin. *Eur J Biochem*, **114**, 33-38.
- Kovar, D.R. (2006) Molecular details of formin-mediated actin assembly. *Curr Opin Cell Biol*, **18**, 11-17.
- Kovar, D.R., Harris, E.S., Mahaffy, R., Higgs, H.N. and Pollard, T.D. (2006) Control of the assembly of ATP- and ADP-actin by formins and profilin. *Cell*, **124**, 423-435.
- Kovar, D.R., Kuhn, J.R., Tichy, A.L. and Pollard, T.D. (2003) The fission yeast cytokinesis formin Cdc12p is a barbed end actin filament capping protein gated by profilin. *J Cell Biol*, **161**, 875-887.
- Kriebel, P.W., Barr, V.A., Rericha, E.C., Zhang, G. and Parent, C.A. (2008) Collective cell migration requires vesicular trafficking for chemoattractant delivery at the trailing edge. *J Cell Biol*, **183**, 949-961.
- Laemmli, U.K. (1970) Cleavage of structural proteins during the assembly of the head of bacteriophage T4. *Nature*, **227**, 680-685.
- Lakshmi, R., Baskar, V. and Ranga, U. (1999) Extraction of superior-quality plasmid DNA by a combination of modified alkaline lysis and silica matrix. *Anal Biochem*, **272**, 109-112.
- Lammers, M., Meyer, S., Kuhlmann, D. and Wittinghofer, A. (2008) Specificity of interactions between mDia isoforms and Rho proteins. *J Biol Chem*, **283**, 35236-35246.
- Lammers, M., Rose, R., Scrima, A. and Wittinghofer, A. (2005) The regulation of mDia1 by autoinhibition and its release by Rho*GTP. *Embo J*, **24**, 4176-4187.
- Langridge, P.D. and Kay, R.R. (2006) Blebbing of Dictyostelium cells in response to chemoattractant. *Exp Cell Res*, **312**, 2009-2017.
- Lappalainen, P. and Drubin, D.G. (1997) Cofilin promotes rapid actin filament turnover in vivo. *Nature*, **388**, 78-82.
- Lassing, I. and Lindberg, U. (1985) Specific interaction between phosphatidylinositol 4,5-bisphosphate and profilactin. *Nature*, **314**, 472-474.
- Lemmon, M.A. (2008) Membrane recognition by phospholipid-binding domains. *Nat Rev Mol Cell Biol*, **9**, 99-111.

- Lengsfeld, A.M., Low, I., Wieland, T., Dancker, P. and Hasselbach, W. (1974) Interaction of phalloidin with actin. *Proc Natl Acad Sci U S A*, **71**, 2803-2807.
- Li, F. and Higgs, H.N. (2003) The mouse Formin mDia1 is a potent actin nucleation factor regulated by autoinhibition. *Curr Biol*, **13**, 1335-1340.
- Li, F. and Higgs, H.N. (2005) Dissecting requirements for auto-inhibition of actin nucleation by the formin, mDia1. *J Biol Chem*, **280**, 6986-6992.
- Lizarraga, F., Poincloux, R., Romao, M., Montagnac, G., Le Dez, G., Bonne, I., Rigail, G., Raposo, G. and Chavrier, P. (2009) Diaphanous-related formins are required for invadopodia formation and invasion of breast tumor cells. *Cancer Res*, **69**, 2792-2800.
- Maas, R.L., Jepeal, L.I., Elfering, S.L., Holcombe, R.F., Morton, C.C., Eddy, R.L., Byers, M.G., Shows, T.B. and Leder, P. (1991) A human gene homologous to the formin gene residing at the murine limb deformity locus: chromosomal location and RFLPs. *Am J Hum Genet*, **48**, 687-695.
- Manstein, D.J., Titus, M.A., De Lozanne, A. and Spudich, J.A. (1989) Gene replacement in Dictyostelium: generation of myosin null mutants. *Embo J*, **8**, 923-932.
- Marquez, B.L., Watts, K.S., Yokochi, A., Roberts, M.A., Verdier-Pinard, P., Jimenez, J.I., Hamel, E., Scheuer, P.J. and Gerwick, W.H. (2002) Structure and absolute stereochemistry of hectochlorin, a potent stimulator of actin assembly. *J Nat Prod*, **65**, 866-871.
- Mattila, P.K. and Lappalainen, P. (2008) Filopodia: molecular architecture and cellular functions. *Nat Rev Mol Cell Biol*, **9**, 446-454.
- Mockrin, S.C. and Korn, E.D. (1980) Acanthamoeba profilin interacts with G-actin to increase the rate of exchange of actin-bound adenosine 5'-triphosphate. *Biochemistry*, **19**, 5359-5362.
- Na, J., Tunggal, B. and Eichinger, L. (2007) STATc is a key regulator of the transcriptional response to hyperosmotic shock. *BMC Genomics*, **8**, 123.
- Nachmias, V.T. (1993) Small actin-binding proteins: the beta-thymosin family. *Curr Opin Cell Biol*, **5**, 56-62.
- Nakaoka, Y. and Kasai, M. (1969) Behaviour of sonicated actin polymers: adenosine triphosphate splitting and polymerization. *J Mol Biol*, **44**, 319-332.

- Neuhaus, J.M., Wanger, M., Keiser, T. and Wegner, A. (1983) Treadmilling of actin. *J Muscle Res Cell Motil*, **4**, 507-527.
- Nezami, A.G., Poy, F. and Eck, M.J. (2006) Structure of the autoinhibitory switch in formin mDia1. *Structure*, **14**, 257-263.
- Noegel, A., Witke, W. and Schleicher, M. (1987) Calcium-sensitive non-muscle alpha-actinin contains EF-hand structures and highly conserved regions. *FEBS Lett*, **221**, 391-396.
- Otto, J.J., Kane, R.E. and Bryan, J. (1979) Formation of filopodia in coelomocytes: localization of fascin, a 58,000 dalton actin cross-linking protein. *Cell*, **17**, 285-293.
- Pollard, T.D. and Borisy, G.G. (2003) Cellular motility driven by assembly and disassembly of actin filaments. *Cell*, **112**, 453-465.
- Pollard, T.D. and Cooper, J.A. (1986) Actin and actin-binding proteins. A critical evaluation of mechanisms and functions. *Annu Rev Biochem*, **55**, 987-1035.
- Popowicz, G.M., Schleicher, M., Noegel, A.A. and Holak, T.A. (2006) Filamins: promiscuous organizers of the cytoskeleton. *Trends Biochem Sci*, **31**, 411-419.
- Prehoda, K.E., Scott, J.A., Mullins, R.D. and Lim, W.A. (2000) Integration of multiple signals through cooperative regulation of the N-WASP-Arp2/3 complex. *Science*, **290**, 801-806.
- Quinlan, M.E., Heuser, J.E., Kerkhoff, E. and Mullins, R.D. (2005) Drosophila Spire is an actin nucleation factor. *Nature*, **433**, 382-388.
- Raper, K.B. (1935) Dictyostelium discoideum, a new species of slime mold from decaying forest leaves. *J. Agric. Res.*, **50**, 135-147.
- Rivero, F., Muramoto, T., Meyer, A.K., Urushihara, H., Uyeda, T.Q. and Kitayama, C. (2005) A comparative sequence analysis reveals a common GBD/FH3-FH1-FH2-DAD architecture in formins from Dictyostelium, fungi and metazoa. *BMC Genomics*, **6**, 28.
- Rose, R., Weyand, M., Lammers, M., Ishizaki, T., Ahmadian, M.R. and Wittinghofer, A. (2005) Structural and mechanistic insights into the interaction between Rho and mammalian Dia. *Nature*, **435**, 513-518.
- Ruhnau, K., Gaertner, A. and Wegner, A. (1989) Kinetic evidence for insertion of actin monomers between the barbed ends of actin filaments and barbed end-bound insertin, a protein purified from smooth muscle. *J Mol Biol*, **210**, 141-148.

- Saito, S., Watabe, S., Ozaki, H., Fusetani, N. and Karaki, H. (1994) Mycalolide B, a novel actin depolymerizing agent. *J Biol Chem*, **269**, 29710-29714.
- Schirenbeck, A., Arasada, R., Bretschneider, T., Schleicher, M. and Faix, J. (2005) Formins and VASPs may co-operate in the formation of filopodia. *Biochem Soc Trans*, **33**, 1256-1259.
- Schirenbeck, A., Arasada, R., Bretschneider, T., Stradal, T.E., Schleicher, M. and Faix, J. (2006) The bundling activity of vasodilator-stimulated phosphoprotein is required for filopodium formation. *Proc Natl Acad Sci U S A*, **103**, 7694-7699.
- Schirenbeck, A., Bretschneider, T., Arasada, R., Schleicher, M. and Faix, J. (2005) The Diaphanous-related formin dDia2 is required for the formation and maintenance of filopodia. *Nat Cell Biol*, **7**, 619-625.
- Schleicher, M., Andre, B., Andreoli, C., Eichinger, L., Haugwitz, M., Hofmann, A., Karakesisoglou, J., Stockelhuber, M. and Noegel, A.A. (1995) Structure/function studies on cytoskeletal proteins in Dictyostelium amoebae as a paradigm. *FEBS Lett*, **369**, 38-42.
- Schleicher, M., Gerisch, G. and Isenberg, G. (1984) New actin-binding proteins from Dictyostelium discoideum. *Embo J*, **3**, 2095-2100.
- Schleicher, M. and Jockusch, B.M. (2008) Actin: its cumbersome pilgrimage through cellular compartments. *Histochem Cell Biol*, **129**, 695-704.
- Seth, A., Otomo, C. and Rosen, M.K. (2006) Autoinhibition regulates cellular localization and actin assembly activity of the diaphanous-related formins FRLalpha and mDia1. *J Cell Biol*, **174**, 701-713.
- Shimada, A., Nyitrai, M., Vetter, I.R., Kuhlmann, D., Bugyi, B., Narumiya, S., Geeves, M.A. and Wittinghofer, A. (2004) The core FH2 domain of diaphanous-related formins is an elongated actin binding protein that inhibits polymerization. *Mol Cell*, **13**, 511-522.
- Shortle, D., Haber, J.E. and Botstein, D. (1982) Lethal disruption of the yeast actin gene by integrative DNA transformation. *Science*, **217**, 371-373.
- Spudich, J.A. and Watt, S. (1971) The regulation of rabbit skeletal muscle contraction. I. Biochemical studies of the interaction of the tropomyosin-troponin complex with actin and the proteolytic fragments of myosin. *J Biol Chem*, **246**, 4866-4871.

- Stradal, T.E., Rottner, K., Disanza, A., Confalonieri, S., Innocenti, M. and Scita, G. (2004) Regulation of actin dynamics by WASP and WAVE family proteins. *Trends Cell Biol*, **14**, 303-311.
- Tempel, M., Goldmann, W.H., Isenberg, G. and Sackmann, E. (1995) Interaction of the 47-kDa talin fragment and the 32-kDa vinculin fragment with acidic phospholipids: a computer analysis. *Biophys J*, **69**, 228-241.
- Towbin, H., Staehelin, T. and Gordon, J. (1979) Electrophoretic transfer of proteins from polyacrylamide gels to nitrocellulose sheets: procedure and some applications. *Proc Natl Acad Sci U S A*, **76**, 4350-4354.
- Wegner, A. (1976) Head to tail polymerization of actin. *J Mol Biol*, **108**, 139-150.
- Wegner, A. and Isenberg, G. (1983) 12-fold difference between the critical monomer concentrations of the two ends of actin filaments in physiological salt conditions. *Proc Natl Acad Sci U S A*, **80**, 4922-4925.
- Witke, W., Schleicher, M. and Noegel, A.A. (1992) Redundancy in the microfilament system: abnormal development of Dictyostelium cells lacking two F-actin cross-linking proteins. *Cell*, **68**, 53-62.
- Xu, Y., Moseley, J.B., Sagot, I., Poy, F., Pellman, D., Goode, B.L. and Eck, M.J. (2004) Crystal structures of a Formin Homology-2 domain reveal a tethered dimer architecture. *Cell*, **116**, 711-723.
- Yin, H.L. and Janmey, P.A. (2003) Phosphoinositide regulation of the actin cytoskeleton. *Annu Rev Physiol*, **65**, 761-789.
- Yin, H.L., Janmey, P.A. and Schleicher, M. (1990) Severin is a gelsolin prototype. *FEBS Lett*, **264**, 78-80.
- Zallar, A. and Szabo, T. (1989) Habent sua fata libelli: the adventurous story of Albert Szent-Gyorgyi's book entitled Studies on Muscle (1945). *Acta Physiol Scand*, **135**, 423-424.
- Zhou, F., Leder, P., Zuniga, A. and Dettenhofer, M. (2009) Formin1 disruption confers oligodactylysm and alters Bmp signaling. *Hum Mol Genet*, **18**, 2472-2482.
- Zuniga, A., Michos, O., Spitz, F., Haramis, A.P., Panman, L., Galli, A., Vintersten, K., Klasen, C., Mansfield, W., Kuc, S., Duboule, D., Dono, R. and Zeller, R. (2004) Mouse limb deformity mutations disrupt a global control region within the large regulatory landscape required for Gremlin expression. *Genes Dev*, **18**, 1553-1564.

6 List of figures

Figure 1: Actin filaments are polar.	6
Figure 2: Schematic representation of mDia1 regulation.	10
Figure 3: <i>D. discoideum</i> life cycle.	11
Figure 4: <i>D. discoideum</i> is a phagocyte.	12
Figure 5: Domain structure of mDia1.	31
Figure 6: The N-terminal basic region of mDia1, mDia2 and DAAM proteins.	32
Figure 7: BR is essential for interaction with phospholipids.	33
Figure 8: The first two poly-basic clusters are important for interaction with phospholipids. ...	34
Figure 9: BR specifically interacts with multilamellar vesicles containing PS.	35
Figure 10: Quenching of lipid fluorescence upon interaction with the basic region of mDia1. 36	
Figure 11: The mDia1 N-terminus inserts into the membrane.	37
Figure 12: The basic region is essential for recruitment of mDia1 to the plasma membrane. ...	38
Figure 13: Percentage of cells with plasma membrane localization for each mutant is plotted as a bar chart.	39
Figure 14: mDia1 Δ DAD and Δ BR Δ DAD constructs are equally active in vitro.	39
Figure 15: PIP ₂ inhibits RhoA induced mDia1 activity.	40
Figure 16: Scheme of insertional assembly of monomers to a filament bound to GST-mDia1 and NEM-myosin II.	42
Figure 17: TIRF-microscopy of actin filaments assembled by full-length mDia1.	43
Figure 18: TIRF-microscopy of actin filaments assembled by mDia1FH1FH2DAD.	44
Figure 19: PIP ₂ inhibits the activities of mDia2 and mDia3 as well.	45
Figure 20: The poly-basic cluster in the DAD is conserved in most formins.	46
Figure 21: mDia1DAD relieves PIP ₂ -mediated inhibition of FH1FH2DAD activity.	47
Figure 22: Unilamellar PIP ₂ vesicles also inhibited mDia1-mediated actin assembly.	48
Figure 23: The C-terminus of mDia1 contains two potential PIP ₂ -binding regions (blue).	49
Figure 24: Differential sensitivity of the mDia1FH1FH2DAD variants to PIP ₂	50
Figure 25: Summary of the PIP ₂ -mDia1FH1FH2DAD interaction.	51
Figure 26: Clustering and membrane insertion of PIP ₂ induced by the mDia1FH1FH2DAD. .	52
Figure 27: Putative GBD of <i>D. discoideum</i> DRFs.	54

Figure 28: ForA expression profile.....	54
Figure 29: Domain structure and protein sequence of ForA.....	55
Figure 30: The C2 domain of ForA.	56
Figure 31: Recombinant ForA interacts with actin.....	57
Figure 32: ForA specifically interacts with profilin I.	57
Figure 33: Gene disruption strategy.....	58
Figure 34: Development of ForA null mutant cells.....	59
Figure 35: Null mutant spores are smaller.....	60
Figure 36: ForA slugs are phototaxis defective.....	62
Figure 37: Random motility of ForA null mutant cells.....	63
Figure 38: Blebbing ForA null mutant cells.....	64
Figure 39: YFP-ACA expression in ForA null cell.....	64
Figure 40: Overexpression of ForA results in membrane blebbing as well.....	65
Figure 41: Blebbistatin treated ForA null mutant cells do not bleb.....	66
Figure 42: ForA blebbing is myosin II dependent.....	67
Figure 43: Localization of ForA.....	68
Figure 44: Localization of constitutively active ForA.....	69
Figure 45: Localization of ForA Δ DAD in fixed cells.....	70
Figure 46: The C2 domain is dispensable for ForA accumulation at the rear.....	71
Figure 47: The C2 domain of ForA interacts with phospholipids.....	72
Figure 48: GBD-FH3 is essential for ForA localization.....	73
Figure 49: Variable phenotypes of GFP-ForA N-terminus overexpressing cells.....	74
Figure 50: Myosin II is not required for ForA localization.....	75
Figure 51: ForA localization is independent of IQGAP-related proteins.....	76
Figure 52: Domain structure and protein sequence of dDia3.....	77
Figure 53: Amino acid sequence of dDia3.....	78
Figure 54: Recombinant dDia3 interacts with actin.....	79
Figure 55: dDia3 interacts with all three profilin isoforms in <i>D. discoideum</i>	80
Figure 56: dDia3 is localized to the plasma membrane and filopodial tips in AX2 cells.....	81
Figure 57: Schematic summary of mDia1 regulation.....	85
Figure 58: ForA regulates the integrity of the cortical actin cytoskeleton.....	88

7 Abbreviations

DAAM	dishevelled-associated activator of morphogenesis
EGFP	enhanced green fluorescent protein
FHOD	formin homology domain containing protein
g	ground acceleration; gram(s)
GFP	green fluorescent protein
h	hour(s)
INF2	inverted formin 2
IPTG	isopropyl- β -thiogalactopyranoside
kDa	kilodalton
l	liter(s)
min	minute(s)
ml	milliliter(s)
mM	millimolar
μ M	micromolar
μ m	micrometer(s)
μ l	microliter(s)
nM	nanomolar
nm	nanometer
OD	optical density
PBS	phosphate buffered saline
PMSF	phenylmethylsulfonyl fluoride
PTEN	phosphatase and tensin homolog
sec	second(s)
TRITC	tetramethyl rhodamine isothiocyanate
V	volt
v/v	volume per volume
w/v	weight per volume

Acknowledgements

I am very grateful to *Prof. Dr. Michael Schleicher* for providing me an excellent working environment. He is not only an outstanding advisor but also a great friend and a colleague who took care of my scientific career and personal life. He made my stay in Munich a memorable one. It would give me an immeasurable satisfaction if I could thank him adequately, but it is impossible.

I would like to place on record my sincere thanks to *Dr. Jan Faix* for inspiring guidance and continuous encouragement during the thesis. He is a wonderful person to work with.

I express my gratitude to *Prof. Dr. Angelika Noegel* for her generosity in supporting my research and sharing precious reagents. Many heartfelt thanks to *Prof. Dr. Manfred Schliwa* for his valuable advice and kindness in sharing lab space and equipment.

I thank *Dr. Rajesh Arasada* for teaching me *Dictyostelium* techniques and making sure that I am comfortable in Munich. I had many exciting scientific discussions with him.

I cherish the generous intellectual help received from *Dr. Meino Rohlfs*. He patiently taught me not only how to use the confocal microscope but also how to eat meat with ‘Gabel und Messer’. He and his wife helped me a lot in breaking the cultural barrier.

A special thanks to the lab encyclopedia, the pillar and my honey! *Daniela Rieger*. There is no fun in the lab without her. Actin does not polymerize in her absence. I am indebted to *Dr. Annette Müller-Tauberberger* for her advice and sharing valuable reagents.

Working with colleagues in the Schleicher lab is like working with family members, friends and well wishers. I sincerely thank *Marlis Fürbringer, Maria Beer, Petros Batsios, Peter Kastner, Gergana Gateva, Annette Vogel, Marc Borath* and *Andreas Batsios* for their admirable scientific and moral support. I also thank *the Schliwa lab members* and *the Elite Network Bavaria colleagues* for their generous support.

I express my deep sense of gratitude to *Dr. Pekka Lappalainen, Dr. Ludwig Eichinger, Dr. Hongxia Zhao, Dennis Breitsprecher, Alexander Pyrkowski* and *Simone Köhler* for their eminent suggestions and assistance during the execution of experiments. I also extend my thanks to *Bobby Cherian* and *Petros Batsios* for proof reading the thesis.

My life in Munich would have not been easy without my friends *Rajesh, Meino, Petros, Geri, Marta, Rahul, Anji, Dilip, Vignesh, Sufyan, Onkar, Sathish* and *Madhu*.

This thesis was financially supported by the *Deutsche Forschungsgemeinschaft*, the *Ludwig-Maximilians University*, the *University of Cologne*, the Graduate College ‘*Infektion und Immunität*’ and the *Elite Network Bavaria*.

Finally, I bow my head to my beloved parents *Ramalingam and Late Vijaya*; and brothers *Rajkumar and Vijaychandran* for showering me with blessings to finish this dissertation.

Curriculum Vitae

Nagendran Ramalingam

Date of Birth: 29.06.1977

Nationality: Indian

Education:

2003-2009 Ludwig-Maximilians-University, Munich, Germany

Ph.D., Cell Biology

2000-2003 Jawaharlal Nehru Centre for Advanced Scientific Research,
Bangalore, India

Junior Research Fellow

1997-1999 Bharathidasan University, Trichy, India

M.Sc., Biochemistry

1994-1997 Bharathidasan University, Trichy, India

B.Sc., Botany

Memberships: German Society for Cell Biology

American Society for Cell Biology

Elite Network Bavaria